POLITECNICO DI TORINO

Department of Mechanical and Aerospace Engineering

Master Degree in Biomedical Engineering

Body Area Network Synchronization for Pulse Transit Time Estimation

Supervisor
Prof. Gabriella Olmo

Co-supervisor
Ing. Alessandro Gumiero

Candidate
Miriam Zinnanti

Academic Year 2018-2019

Summary

Cardiovascular disease is the leading cause of death. For the prevention and treatment of such phatologies, continuous patient monitoring is necessary. The development of miniaturized, minimally invasive and wearable devices within a Body Area Network is the breakthrough of the state-of-the-art technologies.

Accurate and continuous monitoring allows pathological subjects to live in safe conditions, without restrictions of lifestyle.

As blood pressure plays a key role among many factors affecting the cardiovascular system, increasingly accurate techniques, such as the photopletismography, allow its monitoring. The Pulse Tranit Time is a physiological parameter derived from calculations on ECG and PPG signals.

The aim of this study is to develop an algorithm capable of accurately calculating the PTT, using two wearable devices with BLE connection within a BAN. One device was used to acquire the single channel ECG signal, the other one on the wrist to acquire the PPG signal with a green LED. Through an algorithm of motion and noise detection, the study of the PTT was carried out only in absence of motion contributions. To ensure the synchronization of BAN devices, a simple and innovative synchronization algorithm based on the study of the accelerometric signals morphology was proposed. The PTT was calculated on the synchronized signals using three PPG different references points, such as the foot, the peak and the maximum slope point.

The results were compared with the ones obtained from a single device capable of acquire the ECG signal and the finger PPG one, at the same time.

The results show that, despite the PTT computation algorithm providing positive results, it is necessary to increase the level of accuracy of the synchronization algorithm and device to ensure a proper evaluation of the PTT within the BAN.

Contents

List of acronyms

ABP	Arterial Blood Pressure
AC	Alternate Current
ACC	Accuracy
AV	Atrioventricular
ADC	Analog (to) Digital Converter)
AV	Atrioventricular
B2BNM	Bio2Bit New Move
BA	Bland-Altman
BAN	Body Area Network
BLE	Bluetooth Low Energy
BP	Blood Pressure
CVD	Cardiovascular Disease
DAC	Digital (to) Analog Converter
DC	Direct Current
DBP	Diastolic Blood Pressure
ECG	Electrocardiogram
FDA	Food and Drug Administration
FIR	Finite Impulse Response
FN	False Negative

FP	False positive
GUI	Graphical Interface
HR	Heart rate
IBP	Invasive Blood Pressure
ICG	Cardiographic Impedence
ICT	Information and Communication Technologies
IIR	Infinite Impulse Response
IPA	Point Area
ISDN	Integrated Services Digital Network
K	Kurtosis
LED	Light-Emitting Diodes
LTI	Time-Invariant System
MAE	Mean Absolute Error
MAP	Mean Arterial Pressure
MBP	Mean Blood Pressure
NTP	Network Time Protocol
OFDM	Orthogonal Frequency-Division Multiplexing
PEP	Pre-Ejection Period
PCG	Phonocardiogram
PDT	Pulse Transit Distance
PNV	Predictive Negative Value
POTN	Plain Old Telephone Network
PPG	Photoplethysmogram
PP	Pulse Pressure
PPV	Predictive Positive Value

PTT	Pulse Transit Time
PW	Pulse Wave
PWV	Pulse Wave Velocity
QoS	Quality-of-service
RAM	Random Access Memory
RMS	Root mean square
RF	Radio frequency
RRI	R-R Iterval
S	Skewness
SA	Sinoatrial
SBP	Systolic Blood Pressure
SDPPT	Systolic-Diastolic Peak to Peak Time
Se	Shannon Entropy
SE	Sensitivity
SNR	Signal-to-Noise Ratio
SP	Specificity
TN	True Negative
TP	True Positive
V	Variance
WLAN	Wireless Local Area Network
WMAN	Wireless Metropolitan Area Network
WPAN	Wireless Personal Area Network

List of Figures

List of Tables

Part I

Introduction

Chapter 1

Aim of the project

The evolution of demographic dynamics and the variation in the health needs of the population require an organizational redesign services network. Given the growing number of elderly and chronic diseases, it needs to provide increasingly advanced devices, able to monitor patients constantly, without hinder or limit their normal lifestyle [24].

Chronic diseases are becoming the most common cause of disability and death. A chronic disorder is a psychological or physical health condition that causes functional restrictions with a negative impact on the quality of life. Examples include hypertension, cancer, stroke, diabetes, respiratory diseases, arthritis, heart and oral disease [25].

Hypertension plays an influential role in this area and in the formation of ischemic heart and cerebrovascular disease, like renal and cardiac failure [26]. Treating hypertension allows to reduce the strokes of 40% and the possibility of heart attacks of 15%. Even if there are different strategies for treating the problem of hypertension, which aim to prevent cardiovascular disease (CVD), hypertension remains a problem even now [27].

For this reason, in recent decades, biomedical engineering has encouraged the development of simple and reliable devices.

Great interest has been shown in wearable systems to monitor the risk of acute events. By continuously monitoring, wearable devices allow to detect chronic diseases characterised by large latency. These devices permit over longer periods of time, several weeks or months, to monitor patients: detects signals, interpret the data and every medical condition that will benefit in some shape, way or form the person's health.

Using multiple sensors, one can control several aspects of the patient by means of wireless connections and send the information to a personal server [28]. Technological innovation can contribute to the reorganization of health care, in particular by supporting the shift of the focus of health care from the hospital to the entire territory. This is possible through innovative care models focused on the citizen and facilitating access to services in the territory. The objective is to assure assistance by ensuring the continuity of

care. Telemedicine aims to bring the service of the doctor directly to the patient's home, without the doctor leaving his office and without the patient himself being forced to move. The treatment of chronic diseases through wearable devices and remote monitoring can be a priority area for the application of Telemedicine models [24].

The aim of this project is to use wearable and synchronized devices in order to calculate the Pulse Transit Time (PTT), i.e. the time needed for the Pulse Pressure (PP) wave to propagate through an arterial vessel [29].

Results obtained using only one device are compared with those obtained by two devices synchronized among them.

It has been demonstrated that PTT is one of the most promising parameters for calculating blood pressure (BP), as measured with a catheter implanted in the artery [30]. The future objective will be to obtain reliable blood pressure results: the proposed method, using wearable devices, supplies a promising alternative for a continuous measure of blood pressure.

1.1 Telemedicine

Telemedicine is a way of providing health care services using Information and Communication Technologies (ICT), related to wired and wireless integrated telecommunications systems.

In non ambulatory situations, where the patient live far from the medicine, telemedicine involves the secure transmission of medical information and data in form of images, texts, sounds.

It promotes the prevention, the diagnosis and the treatment of patients. However, these systems do not replace the traditional healthcare service in the doctor-patient relationship, but improve their effectiveness and efficiency.

Telemedicine may be used for several purposes. The problem of people classified at risk is that they must undergo constant monitoring of certain vital parameters in order to reduce the risk of complication onset. Telemedicine systems provide the management of their vital parameter allowing to conduct a normal life.

The patients can acquire their data and then record and transmit them by telephone to a computer/modem system. Alternatively, this option can be replaced by an automated acquisition: continuous data can be submitted in real time or in store-and-forward mode, in which the delay between the acquisition of the data and the advice is planned without impairing the treatment [31].

In addition, it offers services that aim to transfer diagnostic information without any commitment by the patient. A complete diagnostic process is difficult to perform through

the exclusive use of the telemedicine tools, but it can be a complement for the process of diagnosis and treatment.

Furthermore, telemedicine is also used for teleconsultation. The patient can be treated through services aimed at making therapeutic choices and assessing the prognostic progress [24].

Telesurgery is another application: it consists of giving the assistance by specialists in a surgical procedure. Normally, audio and video connection are used to provide assistance. Another option is Telepresence Surgery, which guides robotic arms to perform remote surgical procedures [31].

1.1.1 Components of telemedicine systems

Telecommunications infrastructures play a fundamental role in Telemedicine services. They transmit data and ensure the communication between the User, the Medical Center and the Service center. The *Medical Center* receives health information from the User and transmits the service results. The *Service Centre* cover the function of managing the information system like telephones, computers or tablets, maintaining of biomedical devices in remote sites like patient's home for acquiring, processing signals and communication between patients and doctors or other health professionals [24].

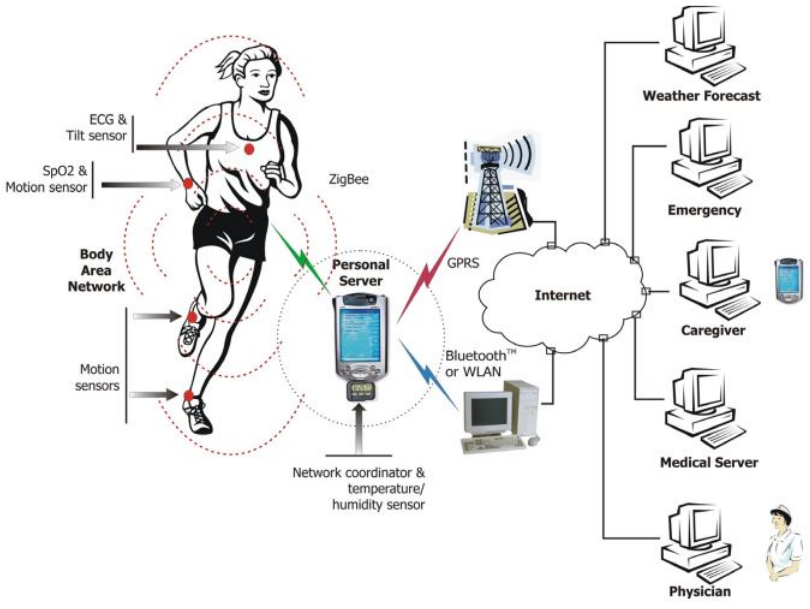

Figure 1.1: Components of a telemedicine system [1]

When the telemedicine service was used for the first time, its applications needed of

wired communications technologies. An exemple are the integrated services digital network (ISDN) or plain old telephone network (POTN) .

Normally, wireless telemedicine systems consist of:

- wearable/implantable medical devices;
- wireless communications networks.

The proliferation of radio frequency (RF) and microwave techniques over the last decades has given new wireless and broadband solutions [32]. Some examples are given below:

- **Wireless personal area networks** (WPAN) allows a last metre connection by the introduction of IrDA, RFID, Bluetooth, ZigBee and ultra-wide band [33];
- **Wireless local area networks** (WLANs) is the standard to provide moderate-to high-speed data communications within a medium range (30m to 100m). They are commonly used in their 802.11a, 802.11b, and 802.11g versions to provide wireless connectivity for local telemedicine services.

  IEEE 802.11b operates in the 2.4 GHz band and accommodates data rates of up to 11 Mb/s, whereas 802.11g, based on orthogonal frequency-division multiplexing (OFDM), uses frequencies in the same band of the previous case but is characterized by a data rates of up to 54 Mb/s.

  IEEE 802.11a operates in the 5 GHz band with data rates of up to 54 Mb/s.

  Limitations of WLANs are his coverage area and mobility;

- **Wireless metropolitan area networks** (WMANs) is the standard to provide Internet access over a long range outdoor environment. The success of open-standard-based Wi-Fi WLANs has enebled to develop IEEE802.16 and IEEE802.20, which are capable of cover longer distances with better quality-of-service (QoS) support than Wi-Fi.

  IEEE802.16, more commonly known as WiMAX, is a WMAN technology able to provide backhaul connection to WLAN hotspots [33].

  The IEEE 802.16/WiMAX is the standard to provide broadband wireless services requiring high-rate transmission and strict QoS requirements in both indoor and outdoor environments. The integrated network of IEEE 802.11/WLAN and IEEE 802.16/WiMAX can bring a synergetic improvement to the telemedicine services on coverage, data rates, and QoS provisioning to mobile users.

  To increase the coverage area of a WLAN network, it can be integrated with the WiMAX one. This can improve the availability of the health services.

However, to integrated the WiMAX network in the WLAN one, many challenging problems such as QoS support, radio resource management, scheduling, connection admission control, and handover management have to be addressed [32];

- **third-generation** (3G) cellular networks allow the provision of faster data transfer rates thus enabling the development of telemedicine systems that require high data transfer rates and are currently only feasible on wired communication networks [33].

Chapter 2

Physiological background

2.1 Heart physiology

The heart is a muscle organ placed on the inspiratory diaphragm muscle. Anatomically and functionally, the heart is divided into right and left portions, separated by a longitudinal wall called *septum*. Within these two areas, a further wall divides the upper and lower portions, forming a total of four cavities with different sizes, the atria and ventricles. They are separated respectively by the interatrial and interventricular septa. The atria have the function of collecting blood, but also to perform a modest pumping action. This facilitates the blood moving into the left ventricle from the left atrium, which distributes blood into the rest of the body [34].

The myocardium consists of striated muscle cells. The contact between nearby cells with very low electrical resistance allows the passage of ions, so that the electrical impulse can propagate from fiber to fiber, enabling muscle contraction of the atria and ventricles. The heart works as two intermittent pumps that support the circulation of the blood. To do this, the two pumps must remain synchronised [34]. Cardiac contraction is called *systole*, while the release phase is called *diastole*.

The **action potential** is an event supported by ionic currents that depolarize and repolarize the cell [34]:

- the **repolarization phase** is generated by a progressive reduction of the passage inside the cell of Sodium and Calcium ions and by an output current of positive charges (K^+ ions) that make the inside of the cell negative. This generates the formation of the *resting potential*, in which the amount of K^+ ions inside the cell is lower than that of Na^+ ions outside;
- the **depolarization phase** is characterized by an inversion of polarization and therefore by a massive entry of positive charges inside the cell. Calcium ions go into the cell generating an action potential.

The impulse from the sinoatrial node (SA), located on the outer wall of the right atrium, reaches the atrioventricular node (AV) located above the plane of the tricuspid valve, where conduction slows down. The contraction of the atria occurs before the ventricular one and it allows the atrium to fill the left ventricular chamber. From the AV node, the His beam originates running along the wall of the interventricular septum. Reaching the distal portions, it gives rise to two branches, the right branch and the left one. These branches spread into the peripheral system of conduction (Purkinje fibers) which allows the almost simultaneous transmission of the pulse (depolarization waves) to the endocardium of the two ventricles [34].

The *heart cycle* is the period defining the time interval between a systole and the next one. It consists of four phases [34]:

- **ventricular filling**: the blood reaches the ventricles because the Atrioventricular valves between the atria and the ventricles are open. Since the heart is relaxed, the diastolic phase occurs. The increase of the ventricular volume at the end of the filling phase determines the closure of the valves, marking the beginning of the systolic phase;
- **isovolumetric contraction**: in this phase all the valves are closed. The pressure inside the ventricle rises rapidly due to isometric contraction. When the value of the ventricular pressure exceeds that of the aorta, the semi-moon valves open;
- **ejection**: with the opening of the semi-moon valves, the blood is expelled from the contracting ventricle. Ventricular pressure continues to rise (because it continues to contract) while volume decreases rapidly;
- **iso-volumetric release**: once the aortic valve is closed, the pressure inside the ventricular chamber decreases.

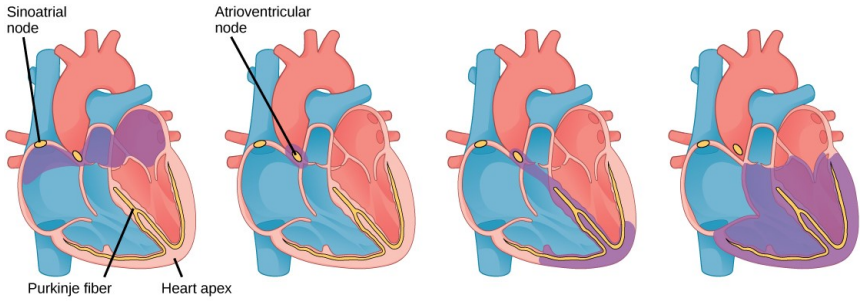

Figure 2.1: Representation of heart cycle [2]

The cardiovascular system, consisting of the heart and blood vessels, is in charge of releasing nutrients and oxygen to the body cells. Body vessels con be distinguished in [35]:

- **arteries**: vessels that transport nutrients from the heart to the tissues;
- **veins**: vessels that transport nutrients from the tissues to the heart.

There are two types of blood circulation [35]:

- **the systemic circulation** connects the heart to all tissues of the body. The blood moves along the arteries, according to decreasing diameters. In the capillary network, it gives oxygen and nutrients to the tissues. Recharging itself with waste substances and carbon dioxide, the blood reach the right ventricle through the veins;

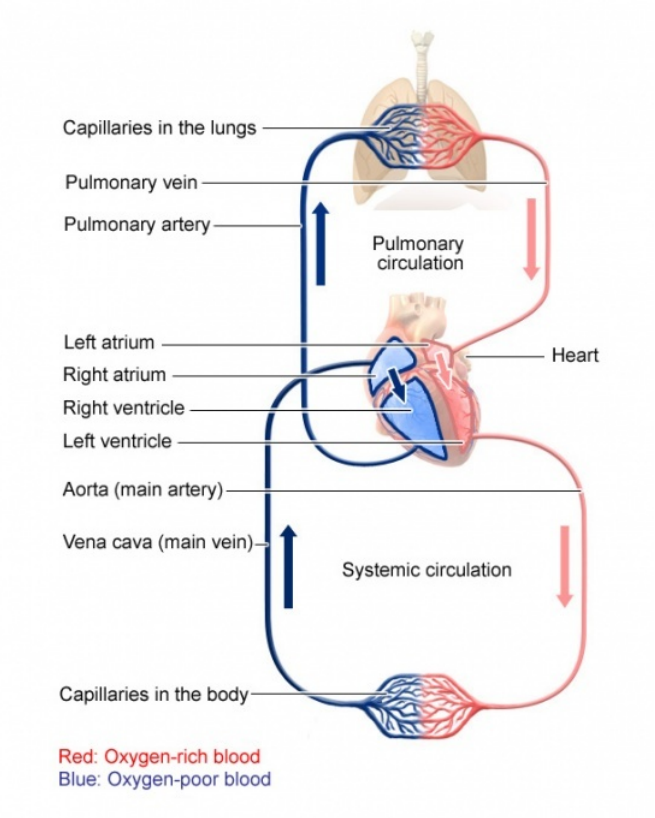

Figure 2.2: Circulatory system [3]

- The **pulmonary circulation** connects the heart to the lungs. The blood rich in carbon dioxide moves from the right ventricle to the pulmonary artery. Latter branches out into smaller vessels to form a network around the pulmonary vesicles. Here, the blood recharges with oxygen, releasing carbon dioxide.

2.1.1 Electrocardiogram

The electrocardiogram (ECG) is the recording and reproduction of the electrical and chemical activity of the cardiac muscle fibres. The electrical potential is transmitted around the body and can be detected on the skin [36]. This non-invasive measurement is obtained by using ten electrodes at specific points in the human body: six of these are placed on the chest, the rest on each limb. The obtained recording represents the various phases of depolarization and repolarization of the heart muscle fibers during the cardiac cycle [37].

The ECG can provide information useful to establish the condition of the patient, based on the analysis on the intervals it is composed of. Specifically, it is formed by the following waves and segments [38]:

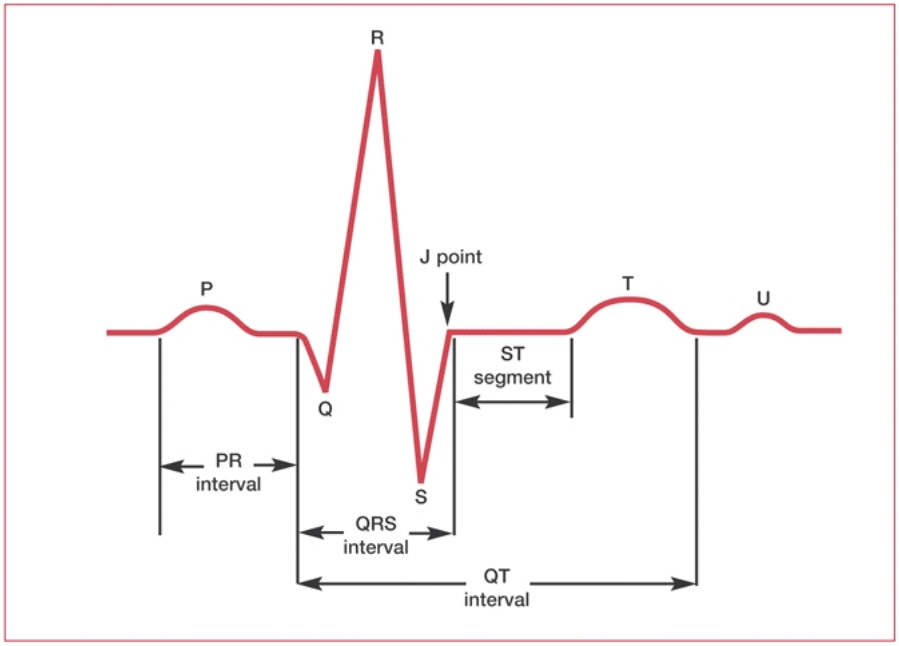

Figure 2.3: Pattern of electrical activity in the heart [4]

- the **P wave** is a deflection wave that represents the depolarization phase of the atria;
- the **QRS complex** is generated after atrial depolarization and consists of 3 waves constituting the ventricular depolarization;
  - the **Q wave** is usually thin and small and is related both to the depolarization of the interventricular septum and to the respiration. They give information about the myocardial infarction;

  - the **R wave** is the largest because it reflects the depolarization activity of a large portion of the ventricle;
  - the **S wave** is generated by the final action of ventricle depolarization [36].

- the **T wave** represents the repolarization of the ventricle, from the epicardium to the endocardium [34];
- the **PR interval** is the time measured between the first deflection of the P wave and those of the QRS complex;
- the **ST segment** is the portion between the end of the QRS complex and the beginning of T wave. It defines the interval between the ventricular depolarization and the repolarization [36].

2.1.2 Cardiovascular variability

The variability of the time period between consecutive heartbeats reflects the healthy functioning of the heart activity. Its fluctuations are not purely random episodes, but they are related to several influencing factors that may be external or internal to the subject (i.e diseases or stress).

Factors influencing the spontaneous cardiac variability are the activity of the sympathetic and parasympathetic nervous system in addition to the pressure interactions of respiratory activity. Chronotropy, namely the variation in the regular heart rate coming from the nervous system, can be evaluated in two different ways [5]:

- **heart rate** (HR) measured in beats per minute (bpm). This is an estimate normalized over time, i.e in 60 seconds. By using several heart rate values, it is possible to obtain a final value defined in a specific time interval. It is a measure easily feasible as it occurs through the palpation of an artery;
- **R-R interval** (RRI), as the distance in milliseconds between two consecutive R-peaks of the cardiac cycle. The inverse of this measure corresponds to the HR, even if the changes in the R-R range do not correspond with those in the HR. In fact, the variability with which the interval of time between two heartbeats changes, is not known in the case of HR.

2.1.3 Blood pressure

The blood flowing inside their vessels generates a pressure on the walls proportional to the force that the heart uses to pump the blood into the vessels, which is called *blood*

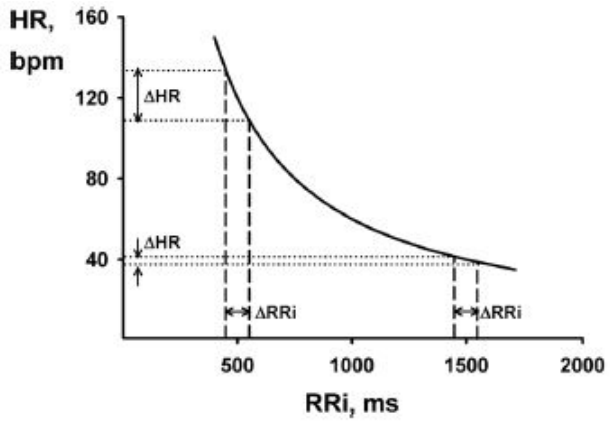

Figure 2.4: Relationship between HR and RRI [5]

pressure. Depending on the type of vessel in which it is measured, this is called *venous pressure* or *arterial pressure*. The tone of the venous pressure is lower than the arterial one, since in this tract the blood does not receive the cardiac thrust. For this reason, the measurement of venous pressure is carried out only in the case of particular pathologies [39].

Venous pressure

The measurement of the central venous pressure is generally performed in the vena cava. Its value fluctuates in the range of 8-12 mmHg.

Many factors influence the estimation of the venous pressure, such as the cardiac output, the variation of the position during the measurement, the transition from erect to supine position, renal failure or even dilation of the arteries.

This measurement can be used as an estimate of the pressure at the right atrium of the heart. It is influenced by the functioning of different organs and therefore is a reference of the hemodynamic state of the patient.

The central venous pressure is measured by means of a catheter which, through the jugular vein, is positioned inside the vena cava, near the atrium.

Pressure transducers and amplifiers are used to convert the signal. Alternatively, the ultrasound machine can also be used. By studying the response of the fluid with the ultrasound, it is possible to measure the diameter of the lower vena cava thus making an estimate of the pressure [40].

Arterial pressure

The blood pressure depends on the blood flow at a given time: an increase in blood volume causes an increase in blood pressure. Since the blood is introduced from the heart into the large arteries during systole, the arteries will contain more blood in the systolic period than in the diastolic one.

Therefore, four arterial pressure values can be distinguished, all resulting from the same periodic phenomenon. Each one, however, depends on specific hemodynamic parameters [41]:

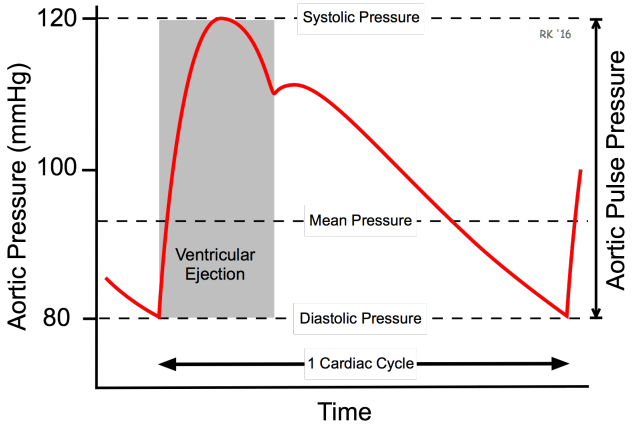

Figure 2.5: Representation in time of arterial blood pressure [6]

- **Mean pressure** (MBP), is the pressure that a continuous and non pulsatile flow system would have, to keep the blood flow constant. It depends on cardiac output and vascular resistance, which in turn are determined by vessel size and by the number of small arteries and arterioles.

- **Diastolic pressure** (DBP), also called minimum pressure. It is generated when the heart is not contracted but released. Its value is always lower than the systolic one [39]. The hemodynamic parameters that influence this measure are the peripheral resistance to the sliding generated by the small arterioles, the rigidity of the arteries and the duration of the diastolic phase [23].

- **Systolic pressure**, also called maximum pressure, is generated by the flow of oxygen-rich blood into the vessels during the contraction phase of the heart. It depends on the left ventricular ejection rate, vascular resistance, peripheral reflection waves. Indeed, if the cardiac output increases, the systolic blood pressure augments

contrary to the diastolic one, which does not undergo significant variations. An increase in peripheral resistance leads to an increase in the systolic pressure, but also to a more marked increase in the diastolic one. The decrease in arterial compliance increases systolic pressure due to two mechanisms: the decrease in the damping capacity of the systolic wave as a result of the more rigid arterial walls, and the earlier arrival of peripheral reflection waves that are added to the incident wave generated by the left ventricle. Changes in the characteristics of the reflected waves (amplitude of the reflected wave and location of the reflection site) cause some modifications of the arterial pressure, especially in the central arteries [23].

- **Pulse pressure** represents the aortic pressure pulse during systole. In fact, the aorta undergoes a great variation in pressure during the ejection phase, due to the high blood flow that passes through its vessel walls [42]. Pulsatory pressure, also called differential pressure, is defined as the variation of blood pressure values around the mean pressure value. It can be measured as the difference between systolic and diastolic pressures [43]. The pulse pressure is mainly influenced by the viscoelastic properties of the wall of arteries with more or less large diameters. When the blood flow is constant, there is a reduction in the viscoelastic properties of the wall of the large arteries, causing an increase in systolic pressure and a decrease in the diastolic one, so the non-variation of the mean pressure and the increase of the pulse pressure [23].

	Systolic (mmHg)	Diastolic (mmHg)
normal	below 120	below 80
elevated	120-129	below 80
high BP (stage 1)	130-139	80-89
high BP (stage 2)	140 or higher	90 or higher
hypertensive crisis	above 180	above 120

Table 2.1: Blood pressure categories defined by American Heart Association [23]

With the terms *hypertension* and *hypotension*, it refers to chronic medical conditions dictated by an abnormal variation in blood pressure. The problem of hypotension occurs with an excessive decrease in blood pressure. In contrast, hypertension is caused by an excessive increase in blood pressure, which in addition to encourage the appearance of certain risk factors such as heart attack, heart failure and stroke, causes a high decrease in life expectancy. Hypertension can only be diagnosed by repeated blood pressure measurements. Following diagnosis, medication and frequent blood pressure monitoring can help to prevent the insurgence of this type of episodes [44].

2.2 Photoplethysmography

The term Photoplethysmography was coined by the Hertzman team in 1930. It refers to an optical and non-invasive plethysmographic technique used to obtain measurements of blood volume fluctuations within the arterial vessels [45].

In fact, the volume of blood inside the tissues depends on the pulsatile nature of the circulatory system, influenced by the alternation of the four phases of the cardiac cycle. [15].

The study of arterial volumetric blood pulsations has great clinical potential. Recently, the PPG signal, thanks to its simplicity and non-invasiveness, is seen as a potential alternative for the measurement of BP. The versatility of the small PPG sensors make it easy to use for the detection of many cardiovascular diseases as well as for the study of peripheral microcirculation [13].

The PPG signal has a morphology apparently similar to the arterial pressure pulse wave but considering the two signals the same leads to errors, as explained below.

2.2.1 PPG sensor

The characteristics of the PPG signal are related to the mode of light diffusion into the tissues, as well as to the part of the body chosen to collect the signal [15].

The PPG sensor consists of two main components:

- **light source**. PPG devices use the semiconductor technology, such as LEDs (Light-Emitting Diodes). LEDs are electronic devices, or diodes, transforming electrical energy into light energy. Characterized by a narrow emission band, LEDs illuminate the tissues with a specific wavelength. They operate in long term, generally more than 10^5 hours. A low LED intensity and non-ionizing radiation is usually chosen, to minimize tissue heating, with subsequent cell death [9];

- **photodetector** to capture the light emitted by the irradiated tissues and to measure the variations in its intensity [45]. The photodetector converts light energy into electrical current. Its spectral characteristics are chosen in combination with those of the light source [9].

2.2.2 Physical principles

Generally, the light radiation interacts with the tissues in three different ways:

- **the reflection**, generated when the light wave interacts with a body characterized by a different refraction coefficient, so the wave will be re-emitted. There are different types of reflection:

- *the specular reflection* occurs if the wavelength of the radiation is smaller than the discontinuities of the surface and the reflected angle forms an angle with the normal to the surface equal to the incident one;
- *diffuse scattering* occurs when the beam is broken down and re-emitted in several directions.

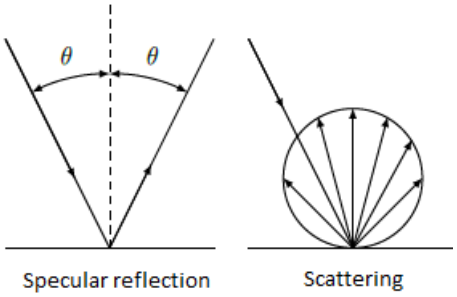

Figure 2.6: Types of reflection [7]

- **absorption** of incident wave energy. It generates an increase of the molecules kinetic and thermal energy. As a result, absorption depends on the frequency of the wave. In particular, each substance has specific absorption spectra that can be used quantitatively for analytical investigations of tissue composition.
- **refraction**, namely the deviation of the light wave path. It takes place when the light passes in one medium in which its propagation speed changes.

Depending on the arrangement of the light source and the detector, two possible device configurations can be chosen:

- transmission mode;
- reflectance mode.

In **transmission mode**, the light source is in the diametrically opposite position of the detector.

The LED light is emitted and cross the absorbent tissues with skin pigments, bones, venous and arterial blood. Subsequently, the detector captures the light transmitted through the tissues between the two devices, filters it and converts it [9].

This mode is susceptible to the presence of specific environmental factors, such as low ambient temperature [45].

Parts of the body suitable for this type of analysis are limited, because they must be as transparent as possible to allow the passage of the light. Usually fingertips, earlobes or

other areas with a reduced thickness are chosen [9]. However, the advantage of this mode is that a mathematical law enables to analyze the interaction between light and tissues, since the light path inside the medium is a known parameter [46].

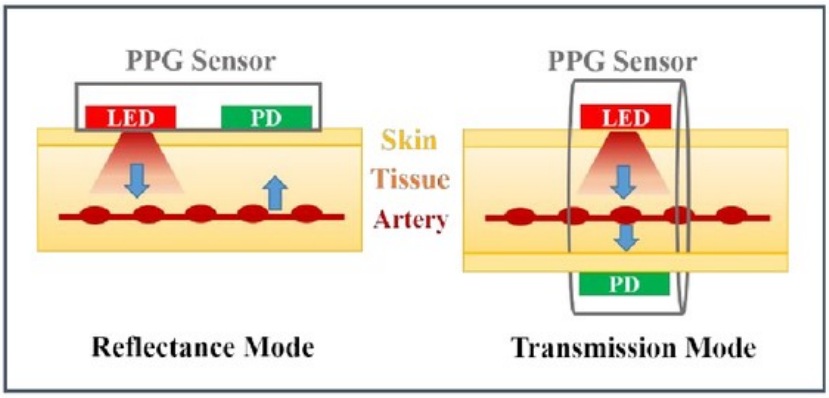

Figure 2.7: Disposition of the PPG sensor, according to the arrangement of detector and light source [7]

In **reflection mode** the detector and the LED are arranged side by side and the detected light is the one that has been reflected from the tissues and vessels. Also in this case, the light will be filtered and converted.

An opaque schield is generally placed between the two optoelectronic elements to avoid artifacts generated by the light emitted directly from the source [45]. This mode, unlike the first, can be applied to thicker areas of the body, such as wrist, forehead, limbs and chest [15].

Using a device that can be placed centrally on the body can be an advantage for people suffering from peripheral vasoconstriction. Some disadvantages are the high sensitivity to movement between the probe and the tissues in addition to the presence of detected light from ambient sources. Moreover, it is impossible to know the path of light inside the tissues, which makes it difficult to apply mathematical laws to interpret the results [46].

2.2.3 Influencing factors

Reflected or transmitted light provides information on the variation in the amount of blood in the microvascular tissue system, useful for studying the performance of the vascular system. The amount of light that is usually studied does not coincide with the incident one, but it oscillates between 1 and 5% of the initial radiation. It is difficult to distinguish the light absorption by blood from that caused by other anatomical components

such as skin and tissues [47]. Reflected or transmitted light is influenced by many factors such as [48]:

- properties of the skin: skin structure and composition, blood oxygen saturation, temperature and blood flow variation;
- number of red blood cells in circulation, orientation and agglomeration;
- speed of contraction and dilation of arterioles and their capillaries .

The structure of the skin can be represented through a medium divided into six layers. The first layer is the *epidermis*, which contains dead or dehydrated cells, without melanosomes and without blood. This layer produces a minimum dispersion of light, in fact it contributes for just 6% of the total reflectance: the epidermis acts mainly as an absorbent medium [49].It has a wide absorption band, around 275nm due to aromatic chromatophores.

The *dermis*, on the other hand, is the underlying layer which includes elastic collagen fibres and blood vessels of various sizes, sebaceous and sweat glands and hair follicles. It is divided into four layers, each of them with different blood concentration: the *capillary rings* with a thickness of $150 - 200\mu$m, the *upper plexus* with a thickness of 80μm, the *reticular dermis* with a thickness of $1400 - 3000\mu$m and the *deep plexus*. The dermis receives oxygenated blood from the arterial compartment, while the venules collect the returning deoxygenated blood. Its attenuation coefficients are typically lower and mainly influenced by collagen fibres that increase the scattering.

The deepest layer is the *subcutaneous* one, also called hypodermis, which includes fat, connective tissue and pulsating arteries [8].

The substances that influencing most the optical properties are water and melanin (i.e the pigment responsible for the colour of the skin). In fact, in presence of light, the transmittance of the dark sinks can vary by up to three orders of magnitude.

In addition to melanin and water, there are also other substances which affect the absorption spectrum of this layer, including hemoglobin, fibrous proteins, collagen, fat, bilirubin and carotene.

The measurement of non-absorbed light, i.e. reflected or transmitted light, can be used to estimate the amount of blood volume in the tissues, since they are inversely related to each other [50].

Due to the complicated structure of the skin, studying its behavior through mathematical laws implies making some simplifications: the thin layer of the epidermis is generally omitted. The skin, in this case, is considered as a single homogeneous layer and therefore the behavior can be studied with the theory of photon diffusion on a one-dimensional model [49].

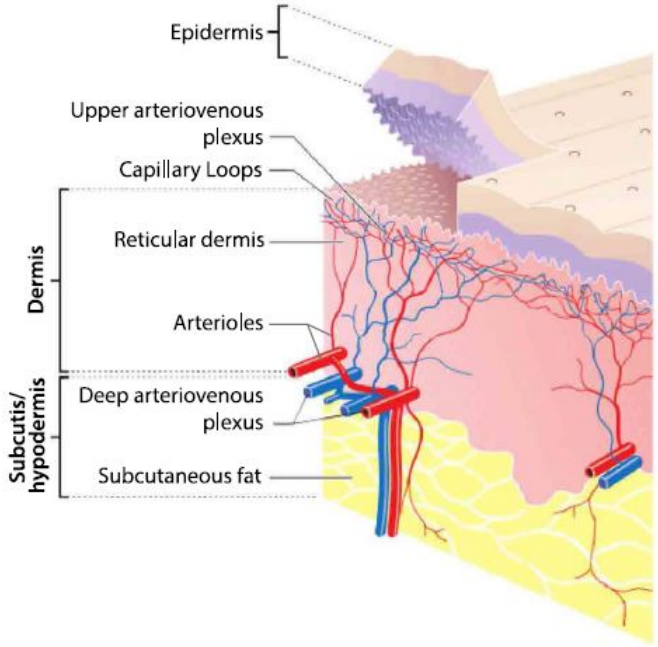

Figure 2.8: Schematic representation of skin structure [8]

Beer-Lambert's law correlates biological behaviour with physical results and can be employed to explain the theory of diffusion of light radiation [47]. This law relates the intensity of the incident light beam with the emitted one by the material, which decreases exponentially increasing its thickness. The result is influenced in the first analysis by the wavelength of the incident light; other influencing factors are the path travelled by the light and the composition of the tissues. As explained in (2.1), considering λ as the wavelength of the light, by increasing the light emitted by the photo-emitter $I_{in}(\lambda)$, the light transmitted $I_{out}(\lambda)$ by the tissue and the reflected light will increase [9]:

$$I_{out}(\lambda) = I_{in}(\lambda)e^{-\mu_a d} \tag{2.1}$$

where μ is the absorbtion coefficient of the tissue. In addition to the common elements present in the skin, the transmitted light is influenced by the properties of the blood in the vessels. Oxygen and glucose, for example, greatly influence the response to irradiation. The presence of glucose decreases the refractive coefficient of the tissue, causing the reduction of the light absorption and an increment in the amount of light that passes through the tissue [9]. Oxygenated or deoxygenated haemoglobin in the blood influences the absorption of light according to the wavelength that is used.

Consequently, the absorption spectrum of the tissues has a fundamental influence on

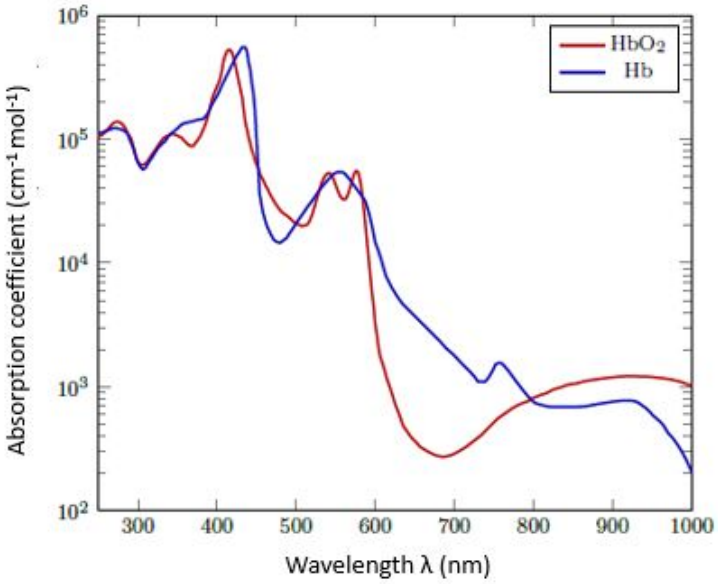

Figure 2.9: Absorption spectrum of the oxygenated and deoxygenated hemoglobin [9]

the choice of the wavelength of the light source [9].

The chosen wavelength of the light must be within the so-called *optical windows* of the skin, i.e. in the frequency band in which the various pigments of the tissue absorb a small amount of light and in contrast, most of it is absorbed by the blood. This promotes the penetration of the radiation in depth, allowing to accurately monitor changes in the volume of blood.

Light with long wavelength, such as *infrared* or *red*, is absorbed in small quantities by the tissues and can penetrate deep. In contrast, short wavelengths such as *blue* or *green* one are easily absorbed, especially by melanin, so they cannot penetrate deep into the tissue, but they are mainly used for surface tissue analysis.

The light that goes deep into the tissues is more affected by artifacts such as movement. It has been shown that the signal obtained with blue light has SNR comparable to the green light one. Additionally, since blue light manages to penetrate into the tissues less than the green one, it reflects the characteristics only of small and superficial vessels [51].

Water, which is the most abundant element in human tissues, absorbs mainly in ultraviolet. In its absorption spectrum there is a window that allows the passage of light with wavelengths in red and infrared [9]. Also for this reason, red and infrared are used in many applications.

Recently, new applications using green light have been explored. The wavelength of green light is absorbed abundantly, more than the red one, by both oxygenated and

deoxygenated hemoglobin, improving the quality of the acquired signal. Moreover, its low penetrating capacity into the tissues reduces the presence of motion artifacts in the signal acquisition, increasing its SNR [9].

Both photon diffusion theory and in vivo results show an increase in modulation using green light compared to the red or infrared one. The improvement is greater when the fractional volume of blood into the skin is smaller. The signal obtained with green light, due to reduced penetration into the tissues, represents the blood pulsation in the dermis layer. The red and infrared light, on the other hand, are also affected by the pulsation of the blood found in the subcutaneous tissue, as well as in the dermis, and the two contributions are not even separable [49].

2.2.4 PPG signal morphology

The waveform of the PPG signal consists of two components: AC and DC.

The AC component is attributed to the pulsatile behavior of the cardiovascular system and synchronous cardiac variations in blood volume at each heartbeat [47]. This compo-

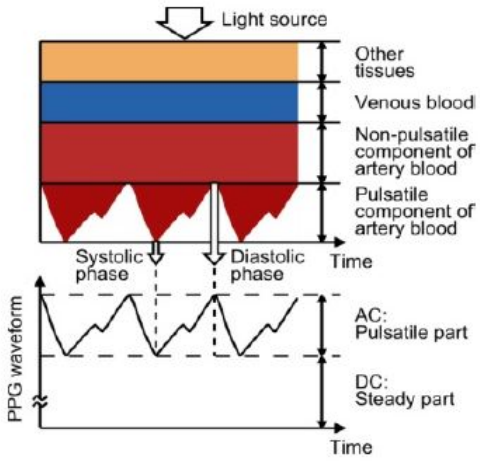

Figure 2.10: Components of PPG signal [10]

nent is superimposed to the DC one, which represents the continuous component linked to the average volume of blood. The latter changes slowly over time and is influenced by breathing, vasomotor activity, sympathetic nervous system activity, vasoconstrictor waves as well as thermoregulation [9].

The first part of the waveform is called **anacrotic phase** or **systolic tract** and is obtained by the passage of blood from the aortic root to the peripheral site on which the sensor is placed. The second part, the **catacrotic phase**, includes the diastolic tract and

is obtained by the transmission of pressure from the ventricle, along the aorta, to the lower part of the body [50]. The features of the signal are:

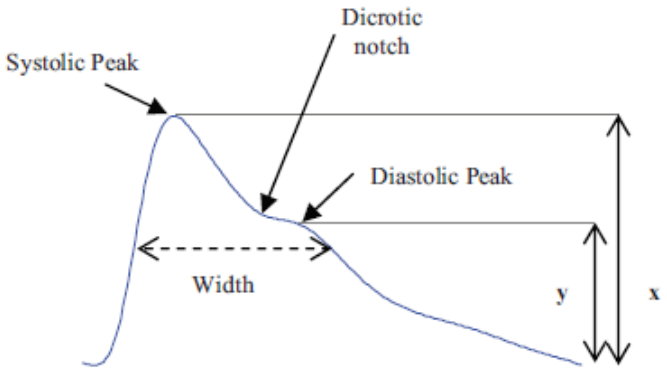

Figure 2.11: Typical waveform of PPG signal [11]

- **systolic peak**: obtained when the pressure pulse reaches the peripheral site from the left ventricle;
- **diastolic peak**: generated when the pressure wave through the arteries and reaches the lower part of the body;
- **systolic-diastolic peak-to-peak time** (SDPPT): measured as the interval time between the systolic peak and the diastolic one [52];
- **dicrotic notch**: located at the diastolic tract, it is generated in the instant of closing of the aortic valve [47]. This episode causes a retrograde flow and an increase of the blood volume in the arteries for a short time [11]. Its amplitude varies with the elasticity of the arterial vessels and depends on the pressure wave that is reflected in the peripheral arteries [15];
- **pulse width**: defined like the width of the signal obtained considering the time distance of the two points of the PPG signal with a value equal to half of the systolic peak. This point relates more precisely the PPG signal with the resistance of the vascular system than the peak reached in the systolic phase;
- **pulse area**: defined as the total area underlying the PPG signal curve. The Inflection Point area (IPA) is an indicator of the resistance of peripheral vessels and is obtained by the ratio of the two areas underlying the curve separated by the dichrotic notch;

- **peak to peak interval**: time interval between two systolic peaks of the PPG signal. This value corresponds to the duration of the cardiac cycle and is comparable to the RRI of the ECG signal;
- **pulse interval**: measures the distance between the start and end point of the PPG signal. This is a time interval related to some parameters of the heart system but the precise relationship is not yet known [11].

2.2.5 Comparison with ABP signal

Since the ABP and PPG signals are generated from the same source, i.e. the heart, it is expected that the two signals have the same morphology.

A first difference is related to the site where the signal is acquired. In fact there are differences between the arterial pulse pressure wave acquired distally or in proximity to the heart.

The waveform of arterial pressure is influenced by multiple contributions such as ventricular contraction, velocity of flow and reflection [12].

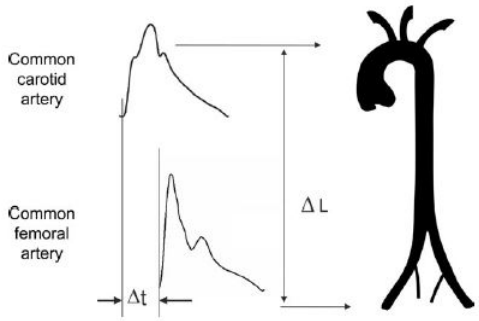

Figure 2.12: Comparison between two different gathering sites of BP wave [12]

The velocity at which blood flow changes along the vessels is influenced by their elasticity. The vessels are very elastic in correspondence of the proximal zone to the heart, becoming more rigid distally. This heterogeneity is caused by the different histological structure of the wall as well as by the different molecules and cells.

The reflection of the wave, on the other hand, is generated when the blood flow reaches the branch points of the vessels. A pressure wave is progressively attenuated as it spreads along the viscoelastic tube, with an exponential decay along the tube, caused by the variation of the velocity. On the other hand, the pressure in a viscoelastic tube with numerous branches, is affected by the reflection and it undergoes amplifications.

In elastic vessels, since the velocity of the blood flow is lower, the pressure wave undergoes a slow reflection and goes back to the aortic root, in the diastolic phase. If, on

the other hand, the arteries have greater rigidity, the blood flow velocity is higher and the reflected wave returns to the central arteries more quickly, causing an increase in systolic pressure.

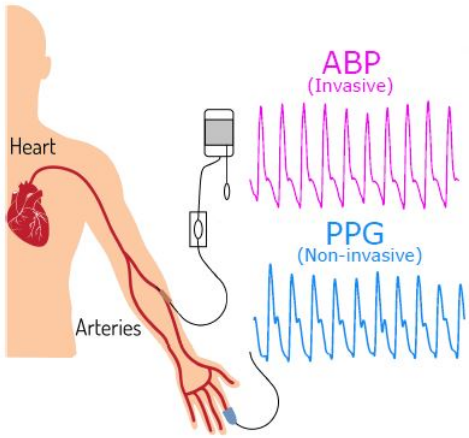

Figure 2.13: Comparison between ABP and PPG signal [13]

The contribution of reflection changes the morphology of the signal collected at the arteries from the recorded near the heart. In the aorta for example, the reflection is negligible as it is less rigid.

Aortic pressure can also be measured at the radial artery using a transfer function, or in carotid artery.

The difference between ABP and PPG is related also to the different technique used to acquire the signal. The aortic pressure wave can be acquired using a non-invasive technique, which uses a pencil type probe with a built-in transducer [12]. The acquisition of the PPG signal is different, as already explained. The contribution of absorption and reflection of the light generated by the different tissues is added.

2.2.6 Applications

The photopletimographic signal is one of the most valuable signals for physiological and health monitoring.

In fact, it is used in various clinical fields [53]:

- **monitoring** of certain parameters. It is advantageous not only for routine health monitoring but also to support the clinical diagnosis of certain conditions, e.g. cardiorespiratory problems. Applications such as heart rate, blood pressure, cardiac output and pulse oximeter are listed below;

- **vascular assessments** e.g. (arterial compliance and disease, endothelial function, vasospastic conditions, venous assessment);
- **autonomic function** e.g. (thermoregulation and vasomotor function, orthostatic intolerance, neurology assessments, heart rate variability and blood pressure).

Heart rate

The PPG signal can be used to gather heart rate information. The intensity of the light, detected and converted into an electrical signal to obtain the PPG signal, changes with the variation of blood in the tissues whom depends by the frequency coinciding with that of the heartbeats. Since the AC pulsatile component of the PPG signal has the periodicity of the heart rhythm, the heart rate can be estimated precisely through the PPG signal [53].

The estimation of this parameter can be used to evaluate an numerous set of useful information in the clinical field [9]. Heart rate monitoring through photopletismographic techniques can be an advantageous solution to replace the common techniques that employ the ECG signal, thanks to the versatility of the devices used. This allows monitoring even during physical activity, helpful for example to adjust the training load of the exercises [53]. Robust algorithms are needed to detect and remove noise, otherwise the reliability of heart rate estimation will be worsened [9].

Cardiac output

The cardiac output refers to the amount of oxygenated blood that is pumped in one minute from the heart. It is a parameter that greatly influences one person's health, as it impacts the distribution of nutrients in the body through systemic circulation and the removal of waste nutrients.

Generally, mean values are $5L/min$ for healthy people, 30 L/min for athletes after training and about $2L/min$ with heart problems [48].

Mathematically, it is defined as [9]:

$$OC = SV \times HR \tag{2.2}$$

where HR is the heart rate, and SV is the stroke volume. The SV is related to the reflected waveform because of the pressure that can be measured by it:

$$SV = \frac{\int dP}{dt \times Z} \tag{2.3}$$

where dP is the pressure that goes from the end of the diastole to the end of the systole. The Z parameter corresponds to the impedance in the aorta.

Pulse oximetry

Pulse oximetry is one of the most significant applications of the PPG signal. The pulse oximeter provides information about the oxygen saturation level of arterial blood.

The device can work in both transmission and reflection mode.

More traditional techniques use red and infrared LEDs to illuminate the tissues [4]: the AC amplitude of the detected signal varies as with oxygen level in the hemoglobin. Oxygenated (HbO2) and deoxygenated (Hb) hemoglobin behave differently. The oxygenated blood transmits red light and absorbs the infrared one, the deoxygenated one acts in the opposite way [53].

From the ratio of the AC and DC components, it is possible to estimate the level of oxygen saturation of the blood in the arteries [53].

2.3 Pulse transit time

The study of the pulse transit time is one of the most recent approaches to evaluate the arterial tree functionality [54]. The PTT measures the time required by the pressure pulse to spread into peripheral arterial blood vessels.

Therefore, it begin in the time point when the arterial pulse pressure wave is detected in the aortic valve, marking the beginning of the systolic phase. It ends when the pulse pressure wave is detected in the distal part of the vessel.

There are several ways to calculate the PTT:

- **I-PTT** denotes the time delay between the proximal BF waveform and the temporal BP [14];
- **PPG-PTT** measures the time interval between two characteristic points of two PPG signals. The time delay can be estimated by using two photopletismographs positioned on two different peripheral points, like wrist joint and little finger. It is calculated as the time interval between two peaks of the detected pressure waves [55];
- **PAT** is the time delay between the R-peak of the ECG signal and a characteristic point of the PPG signal taken distally to the heart [14]. An electrocardiograph and photopletismograph are required.

The third measure is the most common technique, although it requires an approximation of the estimated time. Measuring the PTT from the time point when the R peak appears in the ECG signal,includes a delay that causes variations of the PTT compared to the true value.

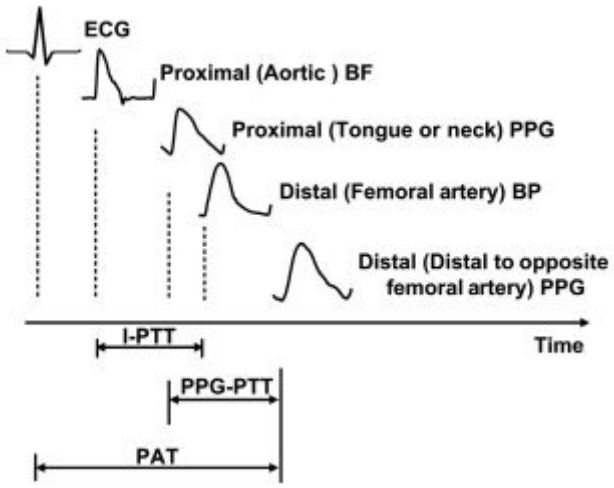

Figure 2.14: Representation of different PTT types [14]

This error is due to the *pre-ejection period* (PEP), which is the interval beginning with the onset of the QRS complex in the ECG signal and ending with the beginning of the blood ejection from the heart [56]. PEP is the time employed by the heart to convert the electrical signal into a mechanical contraction that open the aortic valve. This delay varies from subject to subject and is influenced by age, stress and physical activity. The measurement of the PEP can be done by acquiring an additional signal. Usually cardiographic impedance (ICG) or phonocardiogram (PCG) are used [57].

In order to measure the true PTT, a first acquisition should be made at the radix of aorta although this requires sophisticated instruments such as phonocardiograph, ultrasounds or MRI [58].

This is one of the reasons why PEP is usually included in the calculation of PTT, considering the PAT and the PTT values to be equal.

The influence of the error in the PTT calculation is related to different factors:

- distance between the heart and the arterial site where the signal is acquired. The error decreases if the distance is large [59];
- heart rate. The error increases among patients with low HR [15].

Some studies show that the MAP, SBP and DBP values are less related to the PAC value than to the PTT one, while others state that the PAC value is well connected to the SBP value because it depends on both ventricular contraction and vascular functions [59]. Three different points can be taken as reference in the PPG signal, so three different PTT values can be obtained [15]:

- **PTT-peak**: distance between the R-peak of the ECG signal and the peak of the PPG signal in the same beat;
- **PTT-middle**: distance between the R-peak of the ECG signal and the maximum slope point of the PPG signal in the same beat;
- **PTT-foot**: distance between the R-peak of the ECG signal and the minimum of the PPG signal in the same beat.

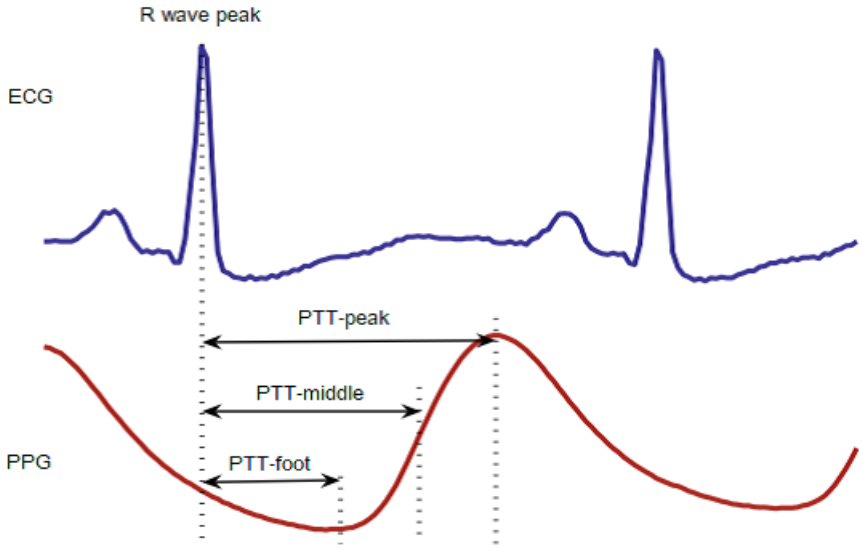

Figure 2.15: Representation of the PTT different references [15]

The reliability of the estimate varies with the reference point taken on the PPG signal. Although the peak of the PPG signal is a theoretically good indicator of the SBP, in real cases this correlation leads to errors, due to the different instrumentation used to detect the ECG and the PPG signals. PPG peaks are distorted compared to the real ones, due to the reflection that the pressure wave undergoes in the arteries [59].

The distance between the two point in which the signal is acquired is called **pulse transit distance** (PTD) [55]. Instead, the velocity of the blood flow covering the PTD in a time interval equal to the PTT is the **pulse wave velocity** (PWV):

$$PWV = \frac{PTD}{PTT} \tag{2.4}$$

In common ambulatory techniques, it is preferable to replace the PWV with the PTT, as the first one depends on the unknown distance, varying from one person to another [58].

The pulse transmission time depends on several parameters [15]:

- rigidity of the arterial wall;
- age of the subject;
- vascular remodeling and arteriosclerosis;
- ambient temperature;
- posture and stress.

2.3.1 Blood pressure computing

Recenlty, great attention to the PTT has been devoted due to the positive result achieved in many applications calculating the BP. The relationship between PTT and BP can be demonstrated by the *Moens-Korteweg* and *Bramwell-Hills* laws, which correlate the PWV, and therefore the PTT, with the elasticity of the vessels.

It is assumed that a volume V of blood subjected to a pressure P, generates a flow Q. The volume of the arteries in which the blood flow moves has an internal ray R, an area A and a wall thickness h, as shown in figure 2.16.

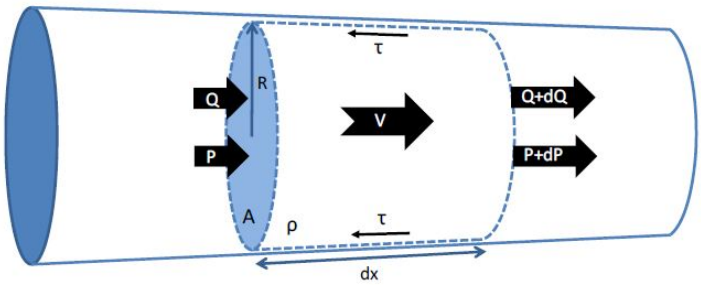

Figure 2.16: Geometrical representation of a blood volume moving along an artery [16]

Starting with the *Mass Conservation law*:

$$Q_{in} - Q_{out} = \frac{dV}{dt} \tag{2.5}$$

$$Q - (Q + dQ) = \frac{d(Adx)}{dt} \tag{2.6}$$

$$-dQ = \frac{dA}{dt}dx \tag{2.7}$$

$$\frac{dQ}{dx} + \frac{dA}{dt} = 0 \tag{2.8}$$

By imposing *Newton's law* on the conservation of the moment, considering the force applied

by the blood flow:

$$\sum F_x = ma_x \tag{2.9}$$

$$\big(P - (P + dP)\big)A - \tau 2\pi R dx = ma_x \tag{2.10}$$

$$\big(P - (P + dP)\big)A - \tau 2\pi R dx = \rho A dx \frac{dV}{dt} \tag{2.11}$$

$$-\frac{dP}{dx}A - \tau 2\pi R = \rho A \frac{dV}{dt} \tag{2.12}$$

where m and ρ are the mass and density of the blood flow respectively, a its acceleration. It is assumed that the cross section of the artery does not change and the wall shear stress is negligible:

$$-\frac{dP}{dx}A = \rho \frac{dAV}{dt} \tag{2.13}$$

$$-\frac{dP}{dx}A = \rho \frac{dQ}{dt} \tag{2.14}$$

$$\frac{dQ}{dt} = -\frac{A}{\rho}\frac{dP}{dx} \tag{2.15}$$

The arterial compliance C_A is given by the ratio between the variation of the area and the variation of the pressure. Considering that C_A does not change :

$$\frac{dA}{dt} + \frac{dQ}{dx} = 0 \tag{2.16}$$

$$\frac{dAdP}{dPdt} + \frac{dQ}{dx} = 0 \tag{2.17}$$

$$C_A\frac{dP}{dt} + \frac{dQ}{dx} = 0 \tag{2.18}$$

$$C_A\frac{\partial^2 P}{\partial^2 t} + \frac{\partial^2 Q}{\partial x \partial t} = 0 \tag{2.19}$$

Supposing that $\frac{\partial^2 Q}{\partial x \partial t}$= - $\frac{A\partial^2 P}{\rho \partial x^2}$ and replacing this expression in the previous one:

$$\frac{\partial^2 P}{\partial^2 t} = \frac{A\partial^2 P}{\rho C_A \partial x^2} \tag{2.20}$$

According to the proposed model, a pressure wave P(x,t) with speed $c = \sqrt{\frac{A}{\rho C_A}}$ cross the arterial vessel with the following equation:

$$\frac{\partial^2 P}{\partial^2 t} = c^2\frac{\partial^2 P}{\partial x^2} \tag{2.21}$$

The previous equation is called **Bramwell-Hill equation**.

The arterial compliance is defined as:

$$C_A \frac{dA}{dP} = \frac{\pi R^2}{dP} = 2\pi R \frac{dR}{dP} \tag{2.22}$$

The law of conservation of the moment is applied with the contribution of all tangential efforts, as shown in figure 2.17:

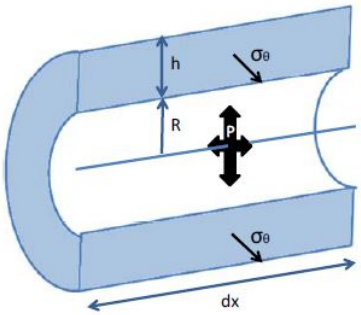

Figure 2.17: Biomechanical model of the arterial wall [16]

$$\sum F_\theta = 0 \tag{2.23}$$

$$P2Rdx - 2\sigma_\theta h dx = 0 \tag{2.24}$$

$$\sigma_\theta = \frac{PR}{h} \tag{2.25}$$

where σ_θ is the shear stress. The previous equation is the *Laplace law*. By differentiating:

$$\sum F_\theta = 0 \tag{2.26}$$

$$d\sigma_\theta = \frac{RdP}{h} + \frac{PdR}{h} - \frac{PRdh}{h^2} \tag{2.27}$$

Assuming the arterial wall does not change its size and that h is negligible compared to R:

$$\pi(R+h)^2 - \pi R^2 = \gamma \tag{2.28}$$

$$h(2R+h) = \gamma' \tag{2.29}$$

$$hR = \gamma'' \tag{2.30}$$

$$drh = -rdh \tag{2.31}$$

where γ is a costant value. It is possible to obtain the Laplace law in a differentiated form:

$$d\sigma_\theta = \frac{RdP}{h} + 2\frac{PdR}{h} \tag{2.32}$$

At this point, it can be inserted the Young's module E_{inc}, which describes the stress on the wall of the arteries in presence of the strain:

$$E_{inc} = \frac{d\sigma_{t\theta}}{d\epsilon} = \frac{d\sigma_\theta}{\frac{dR}{R}} \tag{2.33}$$

$$E_{inc} = \frac{R^2 dP}{hdR} + 2\frac{PR}{h} \tag{2.34}$$

$$E_{inc} = \frac{R^2 dP}{hdR} + 2\sigma_\theta \tag{2.35}$$

Assuming negligible the second term of the equation (2.35):

$$E_{inc} = \frac{R^2 dP}{hdR} \tag{2.36}$$

By inserting Young's modulus E_{inc} into the modified Bramwell-Hill equation, one obtains the **Moens-Korteweg equation** [16]:

$$c = PWV = \sqrt{\frac{hE_{inc}}{2\rho R}} \tag{2.37}$$

in which c or PWV is the *pulse wave velocity*. Blood pressure can be correlated to the PTT through different mathematical laws. Some of them are explained below.

Logarithmic model

In 2010 Shiram developed the logarithmic PTT-BP model based on the Moens-Korteweg equation [60]. He assumed that the elasticity of the vessels changes in function of the pressure with an exponential law:

$$E = E_0 e^{\gamma P} \tag{2.38}$$

where γ is a coefficient in the range $0.016 - 0.018$ mmHg^{-1}, E_0 is the elastic modulus when the pressure is zero. Considering d as the pulse wave distance:

$$c = PWV = \frac{d}{PTT} \tag{2.39}$$

The blood pressure measured in mmHg turns out to be:

$$BP = -\frac{2}{\gamma} \ln PTT + \frac{\ln \frac{2r\rho L^2}{hE_0}}{\alpha} \tag{2.40}$$

In order to evaluate the correlation between PTT and BP, it is assumed that all the variables in the equation are constant [61]:

$$BP = -A \ln PTT + B \tag{2.41}$$

The values of A and B are obtained experimentally through a regression analysis between the reference value of BP and the PTT one [59]. The calculated pressure in this case is the MBP.

Proportional linear model

Assuming small variations of the PTT in the range where BP can change, it is possible to relate the PTT and the blood pressure through a linear relationship [61]:

$$BP = A \cdot PTT + B \tag{2.42}$$

Some studies [62] state that the heart rate is a contribution to consider in addition to the stiffness index of the ASI arteries. It has been shown that the correlation with the heart rate is not always yields by an improvement: under normal conditions the correlation is positive, but when the pressure undergoes acute changes related to the activity of the baroreceptors then the HR is negatively correlated.

Arterial stiffness is considered constant in short time intervals, therefore it affects the frequency with which the calibration must be carried out, and can be estimated with the ASI [59].

Inverse square model

In this case it is assumed that the vessels are rigid pipes and their section A is constant. The algorithm has been elaborated by Fung et al. who demonstrated the relationship between PTT and BP studying the potential and kinetic energy of the pressure wave. Considering also the relationship between BP and force F exerted on the blood:

$$F \cdot d = \frac{1}{2} m v^2 + mgh \tag{2.43}$$

$$F = BP \cdot A \tag{2.44}$$

in which d the distance measured between the two sites on which the PTT is calculated, m the mass of the blood, A the cross section of the arteries and h the height difference between the two points. In this way, the pressure formula is [60]:

$$BP = \frac{A}{PTT^2} + B \tag{2.45}$$

where B is the coefficient estimated through the correlation between PTT and BP measured with cuff-based techniques, ρ is the blood density (1035 $\frac{kg}{m^3}$), A = $\frac{\rho}{1.4}(\frac{0.6h}{df})^2$, h the height and df the distance factor [61].

Chapter 3

State of the art

Several methods can be adopted for the evaluation of the blood pressure. Generally, they are divided into [44]:

- invasive methods;
- noninvasive methods.

3.1 Invasive methods

The BP monitoring with invasive techniques (IBP) is used only for patient in critical conditions or during surgery. Generally, it is avoided in case of chronic hypertension treatment. The goal of measuring intra-arterial blood pressure is to obtain a beat-to-beat record of the blood pressure of the patient, suffering from rapid changes in blood pressure which therefore be kept under control. The technique provides accurate measurements of BP at low pressures (e.g shocked patients) and in people not suitable for non-invasive monitoring of BP, for example obese patients.

The catheter is inserted into a suitable artery, generally the radial artery because it is superficial and easily accessible. The pressure wave is then displayed on the monitor and finally analyzed. An intra-arterial monitoring system is made up of:

- **measuring apparatus**, which encompasses a cannula placed into the artery and connected to tubing. The latter contains a column of saline which conducts the pressure wave to the transducer.

  A flushing system is connected at the other end of the arterial line, which supplies a slow but continuous flushing of the system. Furthermore, through the manual setting up of the flush valve, a quick flush can be provided;

- **the transducer**, that acquires a physical quantity at the input and yields an electrical quantity at the output. It must be calibrated to the atmospheric pressure. It

consists of a flexible diaphragm electrically charged;

- **the monitor** to show the input signal properly amplified and filtered. Moreover, allows to display the signal in real time as well as the calculation of the blood pressure [63].

The numerous disadvantages of the technique are listed below [63]:

- limited use due to the need of the electrical supply;
- infections generated by the arterial cannula;
- possible formation of thrombus which causes the occlusion of the arteries. This risk is limited if the arterial vessel is chosen appropriately and if the catheter is kept in contact with a saline solution.

3.2 Non-invasive methods

3.2.1 Auscultatory method

The auscultatory method for measuring blood pressure is the most common to date. Until now, two instruments are used to measure blood pressure:

- the sphygmomanometer;
- the stethoscope.

The first consists of an inflatable cuff connected both to the pressure gauge and to the pump regulated by a valve for inflating the cuff.

The brachial artery is occluded by the cuff positioned at the upper portion of the arm. This artery is easily accessible and it is located at the same level as the heart, eliminating the hydrostatic component of the pressure that would cause an altered detection.

The cuff is inflated until it reaches a pressure higher than the systolic one, stopping the blood flow downstream of the cuff [44]. The stethoscope is placed on the antecubital fossa of the elbow and then the pressure inside the cuff is reduced by means of the valve.

In this way, the pulsatile blood flow is restored and sounds are detected through the stethoscope. The sounds are generated by the combination of the turbulent blood flow and the oscillations of the arterial wall [44].

The physicist Korotkoff was the first one to study this method and he divided the detected sounds into five phases [64]:

- **step 1**: it corresponds to the appearance of a palpable pulse. Sounds are clear and repetitive. The pressure measured in correspondence of these sounds is the systolic one;

- **step 2**: the sounds become less intense and more durable, with the presence of slight noise;
- **step 3**: the sounds become louder and clearer. Together with step 2, this phase has no physiological significance;
- **step 4**: the sounds become softer and less distinct from each other;
- **step 5**: it corresponds to the last audible sound. The pressure that can be evaluated when this sound appears is the diastolic one.

Among the sphygmomanometers available, the most commonly used is mercury based. It is the most reliable instrument, although in recent years it has been replaced by other devices to limit the use of this toxic substance.

The *mercury sphygmomanometer* consists of a cloth cuff covering an air chamber connected to the pump and a mercury column. Next to the latter, a graduated scale shows the different pressure values expressed in mmHg [65].

Figure 3.1: Mercury sphygmomanometer [17]

The *aneroid sphygmomanometer* is another type of manual pressure measuring system. It is also equipped with a cuff that can be inflated by means of a pump.

The pressure measured is obtained through a mechanical system which expands as the pressure increases and a clock manometer with a mobile needle, instead of the mercury column. The latter has a graduated scale in mmHg and is connected by tubes to the pump used to inflate the cuff. These systems do not maintain stability over time, therefore they must be calibrated periodically [64].

New sphygmomanometers, called *hybrids*, combine the best features of classic auscultatory devices with those of electronic devices. An electronic pressure gauge replaces the mercury column. An observer listens the Korotkoff sounds when the cuff is deflated, through a button it unlocks the digital display to correlate the values of systolic and

diastolic pressure on the display to the pressure value corresponding to the time of the sound hearing. This system reduces the errors that can occur when reading with other auscultatory instruments [64].

3.2.2 Oscillometric method

The oscillometric method is performed in the same way as the auscultation one, with the advantage that it avoids the errors that can be made by reading the pressure data in the first method [66].

Instead of the stethoscope used to listen to the Korotkoff sounds, a pressure sensor inside the inflatable cuff is used to detect the pressure. The oscillations that the pressure undergoes are recorded over time. Then the signal is filtered and evaluated.

The cuff is wrapped around the patient's wrist or biceps and it is inflated to a pressure that exceeds the systolic one through a pump. This allows to transmit the cuff pressure to the wall of the arteries, causing a decrease in his lumen until the complete occlusion.

Subsequently, the cuff is deflated by decreasing the pressure until it reaches a pressure lower than the diastolic one. This causes an increase of the arterial lumen until it opens completely [67].

The method is based on the observation made in 1876 by Marey who showed that the point of maximum oscillation of the pressure wave, during the gradual insufflation, corresponds to the mean intra-arterial pressure.

The cuff pressure oscillations begin above systolic pressure and increase in amplitude as cuff pressure decreases to the mean blood pressure, which corresponds to the maximum oscillation [68]. So SBP and DBP can be estimated with appropriate derived algorithms.

Therefore, the pressure estimation is not a direct estimation, but it is the result of calculations made on the envelope of the oscillations [66]. The maximum amplitude algorithm is often used to estimate systolic and diastolic pressure values. The maximum oscillation point is used to divide the envelope into ascending and descending phases. Subsequently, experimentally processed fractions of the peak amplitude are used to find the points corresponding to the systolic pressure on the ascending phase of the envelope and the points corresponding to the diastolic one on the descending phase.

The characteristic ratios are obtained experimentally by measuring the cuff oscillation amplitude divided by the cuff's maximum oscillation amplitude [68].

An advantage of the method is the versatility with which the instruments can be inserted, replaced and removed on the body.

Unfavourable points are the influence of artifacts, as well as the rigidity of the arteries that causes a low-frequency vibration. Estimating pressure by means of the oscillometric method in elderly people, for example, with rigid arterial walls, can yield a significantly

underestimated pressure result.

3.2.3 Tonometric method

The technique of the tonometry is applied to superficial arteries located near bone structures, generally the radial or carotid arteries because they are easily accessible and with a large diameter [69].

When an artery is compressed on a surface and flattened, it is subject to pulsations that are proportional to those generated by blood pressure.

The tonometer is a device consisting of several pressure transducers with a frequency response larger than 50 Hz. The transducers consist of piezoresistive crystals [70]. This pressure sensor is placed near the right wrist, in correspondence with the superficial artery to be studied.

By applying a constant pressure to the inner tube, the sensor is pressed onto the artery to flatten it. The pressure exerted by the tonometer should be [71];

- limited, so as not to occlude the artery and not to change the intra-arterial pressure;
- intense, until it equals the pressure that the blood exerts on the wall, without the intervention of the tension forces of the wall .

The intra-arterial pressure measurement is made at the compressed section, because the circumferential tension in the flattened arterial wall acting transcutaneously at the transducer is negligible [69]. It is necessary to calibrate the sensor and the pressure measurement

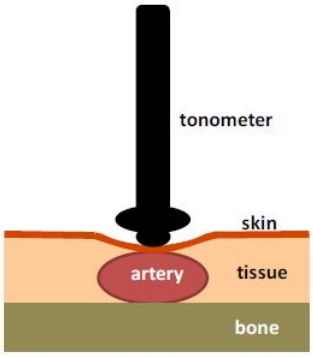

Figure 3.2: Principle of work of arterial applanation tonometry [16]

by means of a reference method, which is usually the oscillometric method referred to the pressure recorded on the arm [71]. Calibration must be done for each patient and this limits the use of the instrument which is generally avoided for routine patient analysis [70]. Calibration is usually done by estimating two coefficients: gain and offset. In this way

the SBP and DBP values will be comparable with those measured with the oscillometric technique of reference.

In addition to the problem of calibration, two other critical points of the technique are [69]:

- *the positioning of the sensor.* To have an accurate measurement of pressure is necessary to position the transducers accurately on the artery. For this reason, automatic positioning system of the sensor, which automatically determines the best position, is usually necessary;
- *sensitivity to movement.* The sensor must be fixed to the wrist and the immobility of the patient is required.

.

3.2.4 Volume clamp measurement

This method was introduced in 1969 by Penaz. A small headser, with a photoplethysmograph inside it, is placed on the finger of the hand [16]. The cuff surrounding the arteries of the finger generates back pressure which dynamically adapts to the entire cardiac cycle one so as to maintain a constant diameter. The technique consists of two distinct phases:

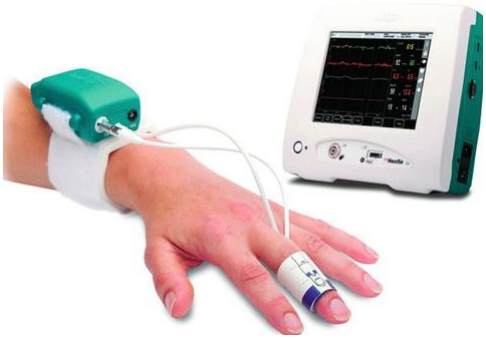

Figure 3.3: Volume clamp device [18]

- *calibration.* During this phase, the pressure that the cuff should exert at the beginning is defined, so as not to constrain the width of the PPG signal. In fact, if the pressure exerted exceeds the positive transmural pressure, then the artery would stretch too much, decreasing the amplitude of the true pulsations. On the other hand, if the pressure exerted by the cuff is lower than the negative transmural pressure, the artery collapses, thus reducing pulsatility [16].

  To calibrate the cuff and choose the correct pressure to be applied, the setpoint volume must be defined. Among the calibration software, the one that allows a

good estimate of pressure is *Physiocal*, developed by Wesseling et al. It consists of a software able to analyzes the trend of the plethysmographic signal in a short time interval where it is sure that the pressure is not affected by other factors. A set of criteria allows determining the ideal volume that should be guaranteed in the artery. In order to follow the alterations of the physiological states of the vascularization, the calibration is automatically repeated at regular intervals [72];

- *measurement*. The artery is clamped from the cuff to allow maximum pulsatility. The variation of blood volume on the finger, is detected by the photoplethysmograph. Latter is able to predict the increase in volume during the systolic phase, through the light detected. The detected signal is proportional to the diameter of the vessel, which expands in the systolic phase, allowing the passage of a larger volume of blood. The information is sent to a servo-controller system which regulates the pressure of the cuff. This prevents the variation in volume to which the artery is subjected, so as to constantly maintain the volume of blood inside. Only when the artery is maintained at its setpoint volume, there is no tension in the wall and the pressure inside the vessel is equal to the external pressure exerted. For this reason, the pressure on the cuff must vary in order to keep the volume in the artery at the setpoint value. During the vascular discharge state, the continuous pressure changes in the cuff to impede diameter variation correspond directly to the mean blood pressure [72].

3.2.5 Wearable devices

Wearable technology includes all miniature electronical devices, which can be worn or used as accessories for measuring constantly or frequently the arterial pressure.

In 2019, the use of wearable devices for health purposes was estimated among 15% of the adult population.

In addition to the minimal invasiveness of the device and its simple accessibility, using the Internet connection and low-consumption integrated circuits to download signals, data and parameters collected in sophisticated data processing platforms are further advantages of wearable technology [73].

Wearable devices are useful for both ambulatory and home monitoring. Among the forms of home monitoring, two are the most widely used:

- **tonometric technique**;
- **pulse wave velocity analysis**.

The tonometric one works according to the principles explained in section 4, but it proceeds autonomously. In addition, a monitor optionally connected to the watch, shows the data

obtained. Otherwise, the signal can be sent via Bluetooth connection to a smartphone, which processes it through a specific App.

A first example is the smartwatch of HealthSTATS Technologies, the **BPro**. It consists of a small piston positioned on the radial artery that works by exerting a constant pressure to obstruct the venous return and to compress the surrounding median nerve.

The smartwatch requires calibration prior to the analysis phase, by measuring the pressure with an already validated oscillometric technique [74].

The pulsing signal in the artery is sampled with a frequency of 60 to 200 Hz so that the original arterial waveform can be reconstructed. Each recording is saved to calculate its mean pressure as well as different coefficients and indices. Through these, by evaluating the variation of the pressure waveform compared to the first one, the new systolic and diastolic pressure [74] are estimated.

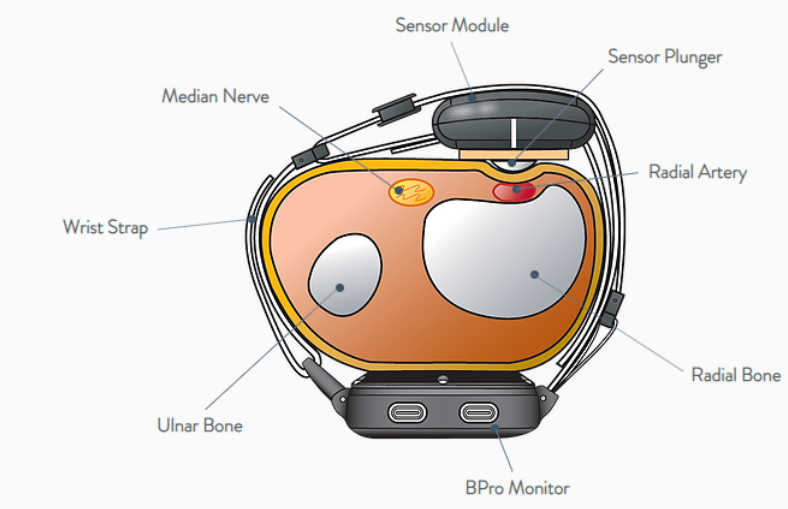

Figure 3.4: BPro smartwatch, HealthSTATS [19]

The smartwatch repeats pressure measurement frequently, about 96 times in 24 hours autonomously, about 15 minutes [73].

Tests have been made to compare the results obtained with the pressure limits set by the AAMI standards (Association for the Advancement of Medical Instrumentation) and the ESH protocol (European Society of Hypertension). In particular, the former requires a mean difference of 5 mmHg from the blood pressure measured using the auscultatory method, while the second requires that most of the tests give a result that differs of 5 mmHg at most from the measures reached by the reference auscultatory method.

The device matches these standards in the non-clinical field [73].

Another example is the Omron model, called the **HeartGuide**, the only model that

has received FDA approval until now. It measures blood pressure on the wrist continuously using tonometric technique [75].

Figure 3.5: HeartGuide smartwatch, Omron [20]

The signals are sent to the connected application that estimates the corresponding pressure value, as well as other vital parameters. The watch also has an accelerometer and it acquires the PPG signal as well as calculating the Heart Rate [20].

The HeartGuide watch processes the results in specific ranges:

- systolic pressure from 60 to 230 mmHg;
- diastolic pressure from 40 to 160 mmHg;
- heart rate range: 40-180 bpm;
- pressure accuracy: $\pm$ 3 mmHg of display reading;
- HR accuracy: $\pm$ 5 % of display reading.

Great interest has been shown recently in blood pressure measuring using the PTT or the PWV values. These promising techniques yet achieved FDA approval for the calculation of the pressure.

An example is the Heartisans model, the **Heartisans Blood** pressure watch. In addition to measuring the heart rate and to the monitoring of the physical activity, it uses an electrocardiographic and plethysmographic system to assess the changes that the pressure undergoes over time.

The watch requires a calibration, by means of an already validated device. In this way, the watch can estimate the variations that the systolic and diastolic pressure undergo over time through an estimate of the PTT value.

PTT value is evaluated through the plethysmographic sensor positioned on the body as well as through electrodes for electrocardiographic acquisitions. The device must be kept close to the chest for 20 seconds. The data packets are sent via Bluetooth synchronization to a custom application that allows processing.

Figure 3.6: Heartisans blood pressure watch

Another smartwatch is the CareUp, by Farasha. With the aim to find solutions that prevent cardiovascular problems, the French company produces small medical devices and it uses artificial intelligence algorithms [76]. The latest smartwatch produced consists of two green light PPG sensors: one positioned at the beak of the device so as to acquire the signal at the wrist, and one at the front to pick up the signal on the finger.

For the calculation of the SBP and DBP, the algorithm needs of:

- calculation of the delay between the two PPG signals;
- calculation of heart rate through the PPG detected on the finger;
- calibration parameters evaluated for each patient.

The results are compared with the results of the standard sphygmomanometer technique as shown in the table 3.1

	SBP	DBP
$\bar{e}$	-1.52	0.39
σ_e	9.45	4.93
p	0.6338	0.7249

Table 3.1: Mean error, standard deviation error and p-value of the results of the CareUp device

Since no significant differences were found, the watch was considered a valid alternative for measuring pressure [77].

Also Samsung has developed a wearable model, the Samsung Galaxy watch, which can give a continuous estimate of the blood pressure variation during the day and night. [78].

It is composed of accelerometers, barometers, gyroscopes, sensors for the measurement of heart rate as well as sensors used to collect the PPG signal. Samsung does not give other technical information about the technical functioning of the device [79].

In addition to the use of measuring devices, the development of the new technology has allowed the continuous monitoring of the blood pressure using smartphones and special processing applications. These techniques do not allow continuous monitoring, but are very comfortable and non-intrusive. This is possible by exploiting the sensors that common smartphones have. An example is the SISMO application [60].

Part II

Methodologies

Chapter 4

Hardware design

The aim of the STMicroelectronics is to create new devices for continuously monitoring the patient's health, without limiting the life of the user. This is the reason why STMicroelectronics created the *Bio2Bit NewMove* (B2BNM), designed with miniaturized dimensions.

It is a wearable and wireless electronic device, able to acquire costantly and transmit signals to an external device using the Bluetooth Low Energy connection.

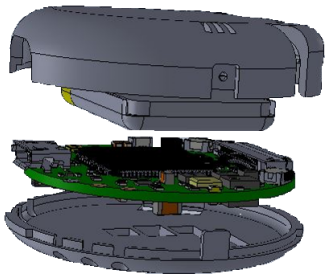

Figure 4.1: Representation of the B2BNM device.

The device has been developed to monitor the patient during the different phases of sleep as well as to assess any disorder. Due to its small size and large number of components, it can replace large and uncomfortable sensors which otherwise would positioned on the patient.

Combining the use of optical and environmental sensors, as well as algorithms under study, B2BNM is able to make continuous measurements of heart rate, PTT, to detect cardiac anomalies, to calculate the SpO_2 or the amount of glucose in the blood.

In figure 4.2 are shown the different features of the B2BNM, instead the device main features, as shown in 4.3, are described in the following list:

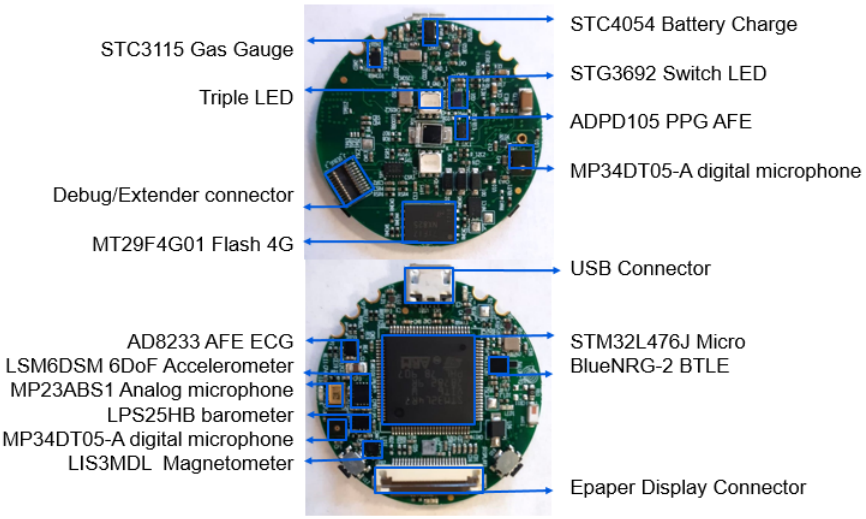

Figure 4.2: Representation of the inside B2BNM device.

- **STM32L4Rxx Microcontroller**. It is part of the STM32L4 microcontrollers family, which operate using the *Arm Cortex-M4 32-bit RISC core*, with a frequency of up to 120 MHz. The main components of the device are the fast 12-bit ADC and the two-channel DAC, allowing the comunication with both analog and digital interfaces. It is required a supply voltage in the range of $1.71V$ to $3.6V$ in addition to being timed by two external crystals oscillating in the range of 4 to $48MHz$.

- **Bluetooth Low energy BlueNRG-234**. It is a chip with a single mode system, i.e. standalone, powered by a low-power battery. The advantage of the connection with BLE compared to a normal Bluetooth connection is the saving of the module power, remaining in sleep mode constantly except during the connection. The BlueNRG-234 is able to be interface both analog sensors, using the 10-bit ADC, and digital sensors.

- **litium battery**. It provides the supply voltage of the device. A gas gauge control and evaluates the state of charge of the battery, estimating how much power it can still provide. Through an USB input, it is possible to interface the device with an external computer to supply the power battery, as well as to transfer data or charge the firmware.

- **LSM6DSM Inertial sensor**. It is a system containing a digital triaxial accelerometer and a 3D digital gyroscope enabling always-on low-power features. The main features are:

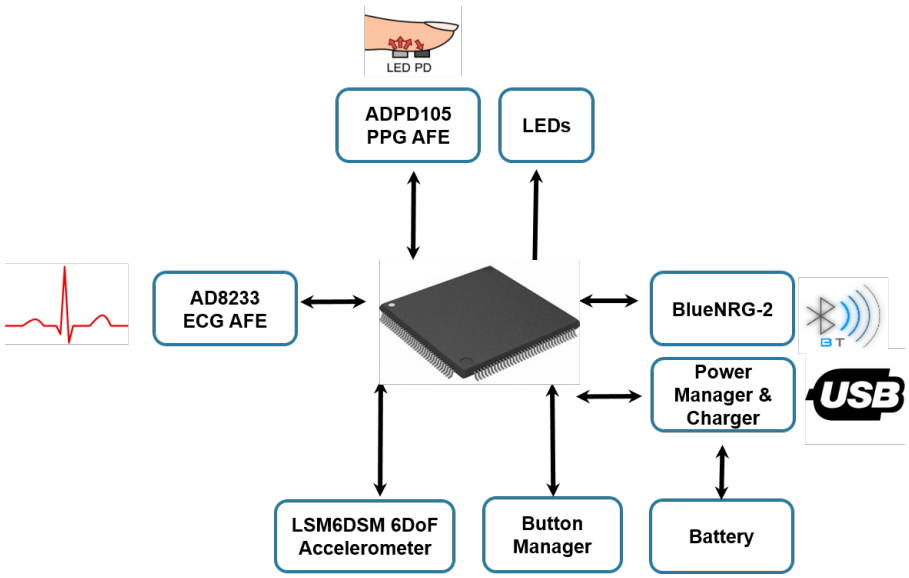

Figure 4.3: Schematic representation of the B2B-NM device main features

- power consumption: $0.4mA$ in combo normal mode and $0.65mA$ in combo high-performance mode;
- analog supply voltage: 1.71 V to 3.6 V;
- package size: 2.5 x 3 x 0.83 mm;
- fullscale: $\pm 2g$;
- sensitivity 0.061 $\frac{mg}{LSB}$.

- **Analog Devices AD8233 front end**. The chip integrates an entire signal conditioning system to obtain the *ECG signal*. Its analog architecture allows to extract, to amplify and to filter small bio-potentials deteriorated by motion artifacts. For this reason, in the cip there are two high pass filters combined with an instrumentation amplifier to increase the gain. Low-pass filters are inserted to eliminate other types of noise, such as the electronic one. Thanks to this analog front-end, it is possible to connect 2 or 3 electrodes to the analog-to-digital converter without further components and with an high level of quality and reliability. The main features are:
  - supply current: 50 μA;
  - single supply voltage: $1.7V$ to $3.5V$;
  - peak to peak voltage noise: $8.5\mu V$;
  - package size: 4 x 4 x 0.75 mm.

- **PLCC-6 package** of triple LEDs. It is a silicone resin package, with higher contrast by a black surface. The device consists of three LEDs with different colors, i.e. red, green and blue.

	RED	GREEN	BLUE
Wavelength (nm)	625	528	470
Operating temperature (C)	-40 to 110	-40 to 110	-40 to 110
Surge current (mA)	100	300	300
Reverse voltage (V)	12	5	5

Table 4.1: Parameters of the Triple LEDs

- **BPW34 Photodiode**. It detects light with a wavelength between 400 to 1100 nm. The device is covered by a plastic package. The characteristic parameters are:
  - operating temperature: -40 to 110 C;
  - reverse voltage: 32 V;
  - spectral sensitivity: 80 $\frac{NA}{Ix}$ (to room temperature);
- **ADPD105 Analog Devices**. It consists of a photometric front end capable of communicating with the LEDs, with a 14-bit ADC and a 20-bit accumulator. The task of the accumulator is to stimulate the LEDs to receive and measure the optical response in a range between 1,8 and 2 V. The system is able to detect the environment interference and reject it. It requires a supply voltage of 1.7V to 1.9V.

4.1 Body Area Network Setup

The aim of this project is to test the use of two devices in a Body Area Network (BAN) for the measurement of the PTT. Results are compared with those obtained through traditional techniques, i.e using a single device capable of acquiring both the ECG and PPG signal simultaneously.

For this reason, two B2BNMs positioned in two different parts of the body are used. In fact, the measurement of the PTT in a BAN requires the use of two devices located in two different positions. The method is based on the processing of ECG and PPG signals and requires the transmission of data to a base station using the BLE connection.

The first device, called in this work *wrist B2BNM*, was placed on the left wrist. The device and its case are kept fixed in the same position for the duration of the acquisition. For this reason, a silicone coating and an elastic band were also used to secure it, as shown

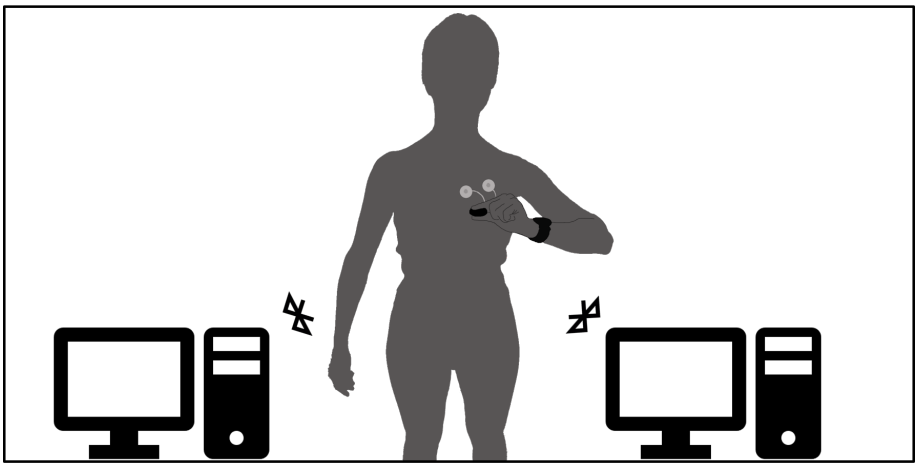

Figure 4.4: Body area network setup

in figure 4.5. The PPG sensor of the B2BNM with his green LED was used to acquire the PPG signal.

An accelerometric signal was also recorded using the accelerometer positioned in the B2BNM so as to have the reference axis Z agrees with that of the gravity acceleration.

The second device, called finger B2BNM, was used to acquire one lead ECG signal. The future development of the BAN expected the positioning of this second device, through an elastic band, on the thorax. During the test phase, however, a different configuration

Figure 4.5: Wrist B2BNM and his case

was used. Unlike the previous device, two cables were welded in order to allow, through the use of two disposable electrodes, the acquisition of the signal. The electrodes (Euro ECG electrodes, Fiab) consist of an Ag/AgCl sensor, solid gel and a stainless steel clip.

The device, on the other hand, was mainteined firm on the left hand of the patients in order to acquire the PPG signal on the finger. Also in this case, the signal was acquired using only the green LED. Unlike the previous case, the finger B2BNM was packed ex-

clusively with its ADS case, as shown in figure 4.6. In addition, another accelerometric signal was acquired.

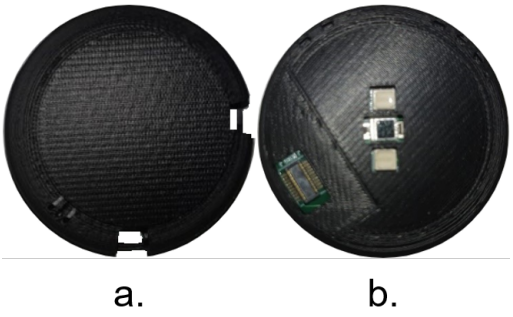

Figure 4.6: B2BNM with an ADS case

It was decided to proceed in this way, so as to acquire a second PPG signal with the same device as the ECG. It is a configuration that was adopted only to validate the results of the BAN and the alterations that the measurement of the PTT undergoes in this new system, compared to one already tested in several experimental works.

Each device communicates through a BLE connection with a reference computer. Therefore, the acquisition system consists of two *piconets*: the first piconet is constituted by a PC which acts as *master*, and by the finger B2BNM as *slave*.

The second piconet consists of a second computer, the master, and of the wrist B2BNM which acts as slave.

4.2 Graphical User Interface

Devices interface with computers using the Bio2BitWinApp. It is a graphical interface (GUI) that allows the user to connect and synchronize the computer with the desired device.

The application provides information about the charge status of the device, alerting the user when the available charge is low.

The acquisition parameters can be setted, i.e. the signals to acquire and the sampling frequency to use. The application is able to manage the incoming packets of the ECG signal up to 3 channels, 4 PPG signals, signals acquired with accelerometer, magnetometer and gyroscope.

With a button it can manage the start of the acquisition, the streaming display of the waveforms, as well as the interruption of the acquisition. The signals thus obtained, before being processed, were transformed into a readable format by the Matlab© software, used for the development of the code.

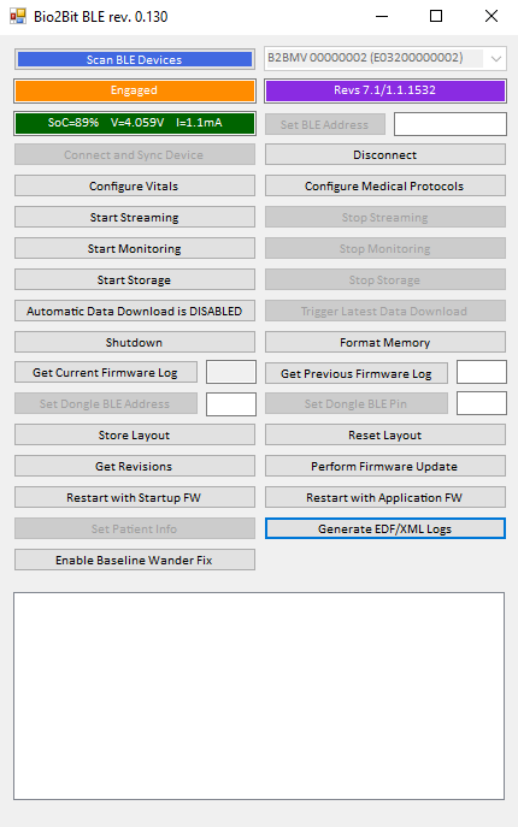

Figure 4.7: Bio2bitWinApp GUI

4.3 Test development

For the validation of the algorithm, the results obtained with the signals acquired from 8 subjects were analysed.

Signal acquisition lasts five minutes at most. During the acquisition, each computer was synchronized to the same time server, through the NTP communication (Network Time Protocol), so as to have a temporal reference between the two masters as similar as possible.

The NTP protocol regulates and enables the exchange of packets between the computer and the server used. Each of them contain information that allows to estimate and compensate systematic errors in the clock of the system hardware.

Moreover, the patient was allowed to adopt the most comfortable position and to make small movements, so as to test the algorithm from all points of view.

Chapter 5

The Algorithm Structure

The implemented algorithm consists of a preprocessing phase that follows the acquisition of the sample signal as well as its synchronization relative to a common timestamp.

The algorithm is made so as to process one sample at a time. Only the calculation of some parameters is made on group of samples, accumulated for 3 seconds each time.

So the algorithm provides the results almost in real time, with a short delay of about two seconds. In fact, the analysis of the signal is done as soon as the buffer, able to store the data for three seconds, is filled. After the first 3 seconds of acquisition, the samples corresponding to with the first two seconds stored are gradually updated with the new samples acquired. At the end of each data update, the buffer is processed.

The PTT calculation is carried out only for the acquired signal parts where the implemented Motion Detection and Noise Detection algorithms detect the absence of motion artifacts or noise. Both acquired PPG signals are processed in the same way. PTT is calculated with both finger PPG-ECG and wrist PPG-ECG signals.

In addition, the cardiac variability was estimated.

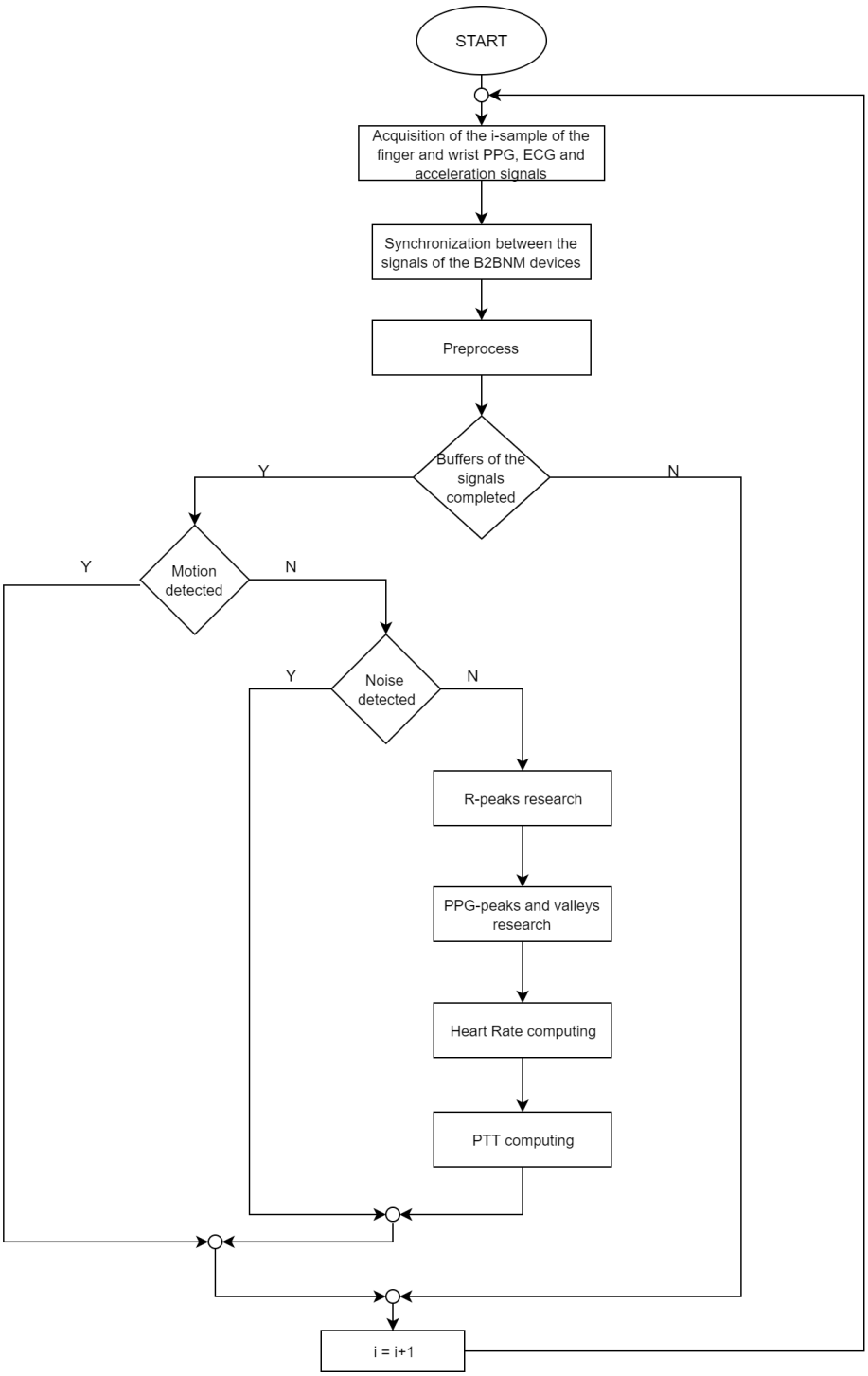

Figure 5.1: Block diagram of the algorithm

5.1 Synchronization

The synchronization process of the ECG and wrist PPG signals is divided into two phases:

- preliminary estimation of the time offset between the timestamps of the two devices;
- realigning of the timestamps. In this way, the p_i data packet of the finger B2BNM can be associated with the p_j data packet of the wrist B2BNM.

The first step is repeated for each acquisition, before starting signal processing.

Within a generic piconet, when the signal packets arrives to the master, it is associate with the timestamps that does not correspond with the instants of time in which the data is acquired. Indeed, adapting to the master receiving timestamps, to each signal corresponds the master arrival timestamps.

In this way, the time corresponding to each sample is delayed by Δt_{err}. This delay depends on the communication protocol between master and slave [80], in addition to the used type of device.

Generally, the aim of Bluetooth synchronization is to know the Δt_{err} of each master-slave connection, removing it.

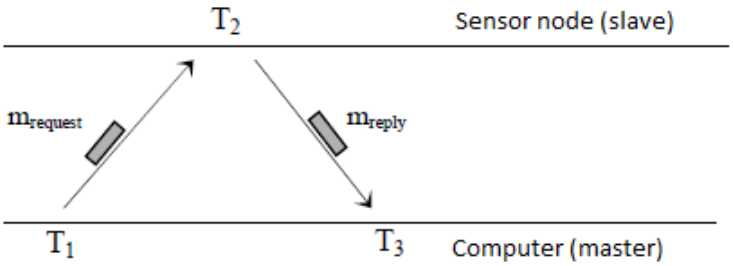

Figure 5.2: Representation of a message synchronization between master and slave [21]

Among the different synchronization protocols, initially it was decided to synchronize the two B2BNM using Cristian's algorithm, explained below.

The idea was to determine the offset between the clock of the master and the clock of the slave. In this way, the master, knowing its own timestamps can synchronize the two clocks.

As shown in figure 5.2, the master sends a $m_{request}$ message to the slave, on which is printed the timestamp T_1 of the time in which the message is sent. It is received at the time T_2 from the slave: it stores the timestamp T_2 in a new m_{replay} message. The m_{replay} message is sent by the slave and received by the master at the time T_3.

Considering the times T_1, T_3 defined by the master and T_2 defined by the slave, the total time (T_{round}) for the exchange of this messages is:

$$T_{round} = T_3 - T_1 \tag{5.1}$$

Moreover, assuming D_{min} as the lowest time delay of $m_{request}$ to move, then the real time T_2 can change between $(T_2 + D_{min})$ and $(T_2 + T_{round} - D_{min})$.

For this reason, the maximum error ϵ that can be made considering the times T_1, T_2 and T_3 is:

$$\epsilon = \pm\left(\frac{T_{round}}{2} - D_{min}\right) \tag{5.2}$$

With these assumptions, Cristian's theory considers that when the client asks the time to the server, this latter responds with its time t_{server}. The client synchronizes his clock adding a little delay to the server clock, as $(t_{server} + t_{\frac{round}{2}})$, where $t_{\frac{round}{2}}$ is the minimum delay between the time read T_1 and T_2. Therefore the offset O that the master adds to his timestamps is:

$$O = \frac{(T_1 - T_2 + T_3 - T_2)}{2} = T_1 - T_2 + \frac{(T_3 - T_1)}{2} \tag{5.3}$$

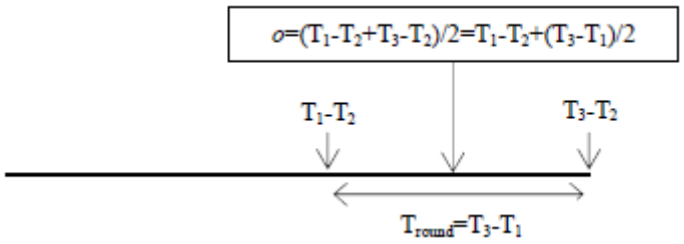

Figure 5.3: Representation of the round-trip time and slave's clock offset compared to the master one

The use of Cristian's algorithm involves several assumptions such as:

- to consider the transmission time of the messages $m_{request}$ and m_{reply} identical;
- to consider the time taken by each B2BNM to read the incoming message $m_{request}$ and to write the new time T_2 null.

Since high accuracy in offset estimation is necessary, it was decided to proceed differently. In this application, it is not relevant to know the absolute time in which the signal is acquired, but the difference between the offsets of the two piconets, i.e:

$$o = \Delta t_{err_i} - \Delta t_{err_j} \tag{5.4}$$

Adding this offset to the B2BNM timestamps, whose data transmission is slower, allows to have the same timestamps between the two B2BNMs, although not coincident with the exact time of signal collection.

A passive synchronization was made, without using the communication packets between the two devices connected in Bluetooth. The offset o was estimated analyzing the signals acquired [81]. Passive synchronization is advantageous because it does not require the use of any particular hardware or Bluetooth protocol. As long as it is applicable, it is necessary to observe events in the external environment that overlap the normal tracks of the sensors of the two B2BNMs in the same way.

The signal taken as reference is the accelerometric one of each B2BNM.

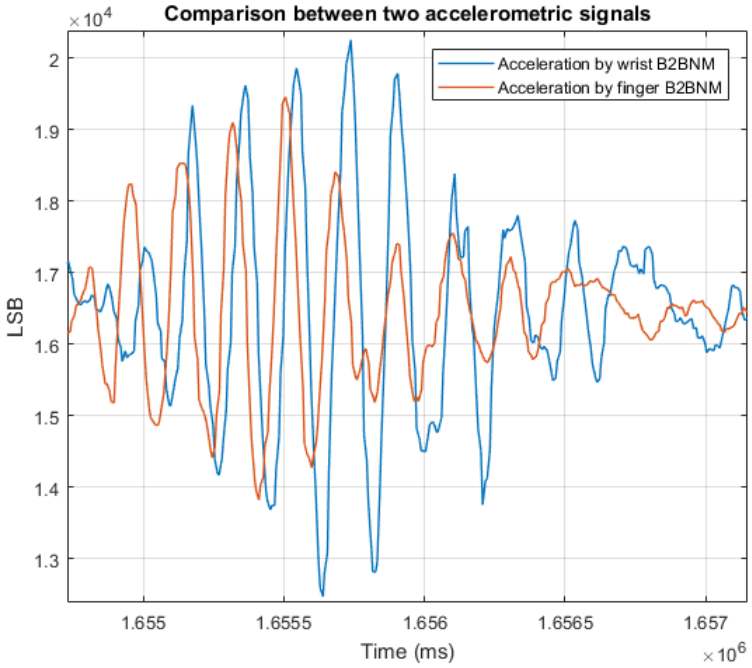

Figure 5.4: Representation of the two accelerometric signals acquired simultaneously by the two B2BNM

Since the accelerometer instantly converts the mechanical stimulus into the signal, it is expected that by generating a short and intense pulse on the device, it reacts with a rapid change in the acceleration, at the same time as the action is performed. Using two accelerometers synchronized with each other, the action must be displayed in the two tracks at the same instant of time.

Without synchronization, the overlap between the accelerometric traces is missing. These are translated between them. The only delay that causes the non-overlapping of the two tracks is caused by the Bluetooth communication and it coincides with the

difference o between the offsets produced by the two Bluetooth of the devices.

Compensating this offset, the B2BNMs timestemps do not coincide with the time instant in which the signals are acquired: the two timestamps are traslated in a different way from the originals one, but they are identicals to each other.

Figure 5.4 shows two signals acquired simultaneously with the accelerometers of the two B2BNM. As can be seen, the impulse produced by both devices changes the normal trend of the accelerometer trace, in absence of movement.

In this figure, it was decided to use the time reference axis in ms to minimize the approximations of subsequent measurements.

The delay between the two acquisition was estimated by calculating the average of the time interval between some corresponding peaks of the two accelerometric signals.

Since the sampling frequency set is 128 Hz, the maximum error that can be made in the study of the time offset is $\pm 15.6ms$, considering the Nyquist frequency.

For each acquisition, after evaluating the time offset, the signals are synchronized. The synchronization consists in the compensation of the time offset, i.e. in the sum of the offset to the timestamps of the B2BNM with a slower Bluetooth communication, as can be seen in figure 5.5.

5.2 Preprocessing

The acquired signals do not include only the component of the signal in the band of interest. Both the acquisitions of the ECG and PPG signals, as well as the accelerations, include components of noise and motion artifacts that degrade their quality, in addition to the information that can be obtained.

For this reason, a preprocessing algorithm was developed to remove signal components beyond the bands of interest.

The preprocess is divided into three phases:

- **filtering**;
- **removal of the transitory signal generated by the filter**;
- **removal of the time delay in the filtered signal**.

A FIR filter was implemented to filter the signal and to remove the components which degrade the information in the band of interest.

The FIR (Finite Duration Impulse Response) filter is a linear time-invariant system (LTI) consisting of a sequence of $N + 1$ coefficients and N order. Considering the raw sample $x(n)$, the filtered one $y(n)$ is obtained from the convolution sum equation with the

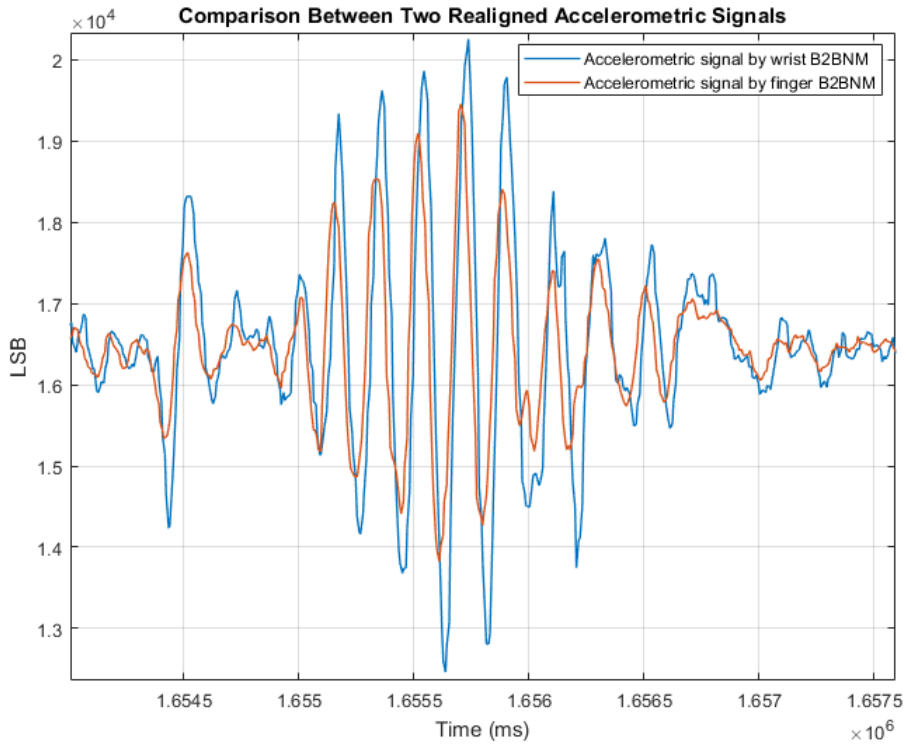

Figure 5.5: Representation of the two accelerometric realigned signals acquired simultaneously by the two B2BNM

transfer function of the filter h. Since the output depends only on the input signal, the FIR is a non recursive filter, as shown below:

$$y(n) = \sum_{k=0}^{N} h(k)x(n-k) \tag{5.5}$$

(5.6)

Each sample $y(n)$ of the filtered signal is obtained by considering $N+1$ multipliers, N adding blocks and N delay blocks, as shown in figure 5.6.

There are several reasons why it was chosen to work with the FIR filter rather than the IIR (Infinite Impulse Response) one.

Both types of filters delay the filtered signal in time with respect to the raw one, but the advantage of the FIR filter compared to the IIR one is its linear behavior, with a symmetrical or anti-symmetrical phase.

A linear phase filter is characterized by a phase that depends linearly on the frequency.

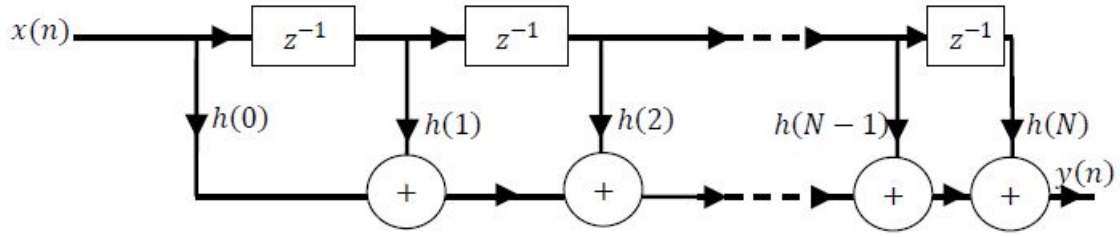

Figure 5.6: Flow graph of a linear-phase FIR filter [22]

Considering a FIR filter, its symmetrical impulse response $h(k)$ is:

$$h(k) = h(N-k) \tag{5.7}$$

where k is the position sample which varies from 0 to the order N. Its frequency response $H(f)$ is instead:

$$H(f) = \sum_{k=0}^{N} h(k)e^{-j2\pi fk} \tag{5.8}$$

$$H(f) = h(0) + h(1)e^{-j2\pi f} + ... + h(N-1)e^{-j2(N-1)\pi f} + h(N)e^{-j2N\pi f} = \tag{5.9}$$

$$= e^{-jN\pi f}\Big[h(N/2) + (h(0)e^{jN\pi f} + h(N)e^{-jN\pi f}) + (h(1)e^{j(N-2)\pi f} + \\ + h(N-1)e^{-j(N-2)\pi f}) + ...\Big]$$

Considering the symmetry of the filter transfer function, $h(0) = h(N)$ and $h(1) = h(N-1)$. For this reason the equation 5.9 can be written as:

$$H(f) = e^{-jN\pi f}\left[h(\frac{N}{2}) + 2h(0)\cos(N\pi f) + 2h(1)cos((N-2)\pi f)\right] = \tag{5.10}$$

$$= e^{-jN\pi f}\left[h(\frac{N}{2}) + \sum_{n=0}^{(N-1)/2} 2h(n)cos((N-2)\pi f)\right]$$

where the first term defines the filter phase response ϕ:

$$\phi(f) = \begin{cases} -N\pi f & if H_a(f) \geq 0 \\ -Nf + \pi & if H_a(f) < 0 \end{cases} \tag{5.11}$$

where H_a is the term in square brackets.

From equation 5.11, it can be seen that the filter phase response is a linear function of the frequency and N. In addition, with an anti-symmetrical filter the phase response is rotated of π, becoming negative.

Consequently, in the time domain the delay is equal to $\frac{N}{2}$ samples.

The IIR filters cause non-linear distortion in the signal phase. It generates a delay in the filtered signal which is different for each frequency component.

Although the problem can be solved applying forward and backward filter to eliminate any phase shift, the employment of the IIR filter is not recommended in real-time signal processing. The reason is that the computation time taken by a filter to perform a forward and backward filtering of the signal is greater, causing an excessive delay in the filtered signal.

The choice of an IIR filter is a valid compromise in off-line signal elaborations, since it can give a stable response even with a lower number of coefficients than the FIR filter. The advantages are both in the reduced computation time and in the reduced memory occupation.

Figure **??** shows the block diagram of the preprocessing phase, which follows the synchronization one. Each stage of the block is repeated for each sample of the acquired signal, considering for each type of signal (e.g ECG, PPG and acceleration) its own transfer function. Since the impulse response of the filter goes to zero only after exhausting the initial transient of N samples, each sample belonging to the first N filtered is not considered in the following steps.

Indeed, it is chosen to proceed with the removal of the delay produced by the filter in order to reduce the error that could be made for the estimation of the PTT at the end of the signal processing.

The filtered signal is gradually realigned with respect to its initial time reference: the first $\frac{N}{2}$ samples of the filtered signals are removed since they do not coincide with the firsts $\frac{N}{2}$ filtered samples of the raw signal.

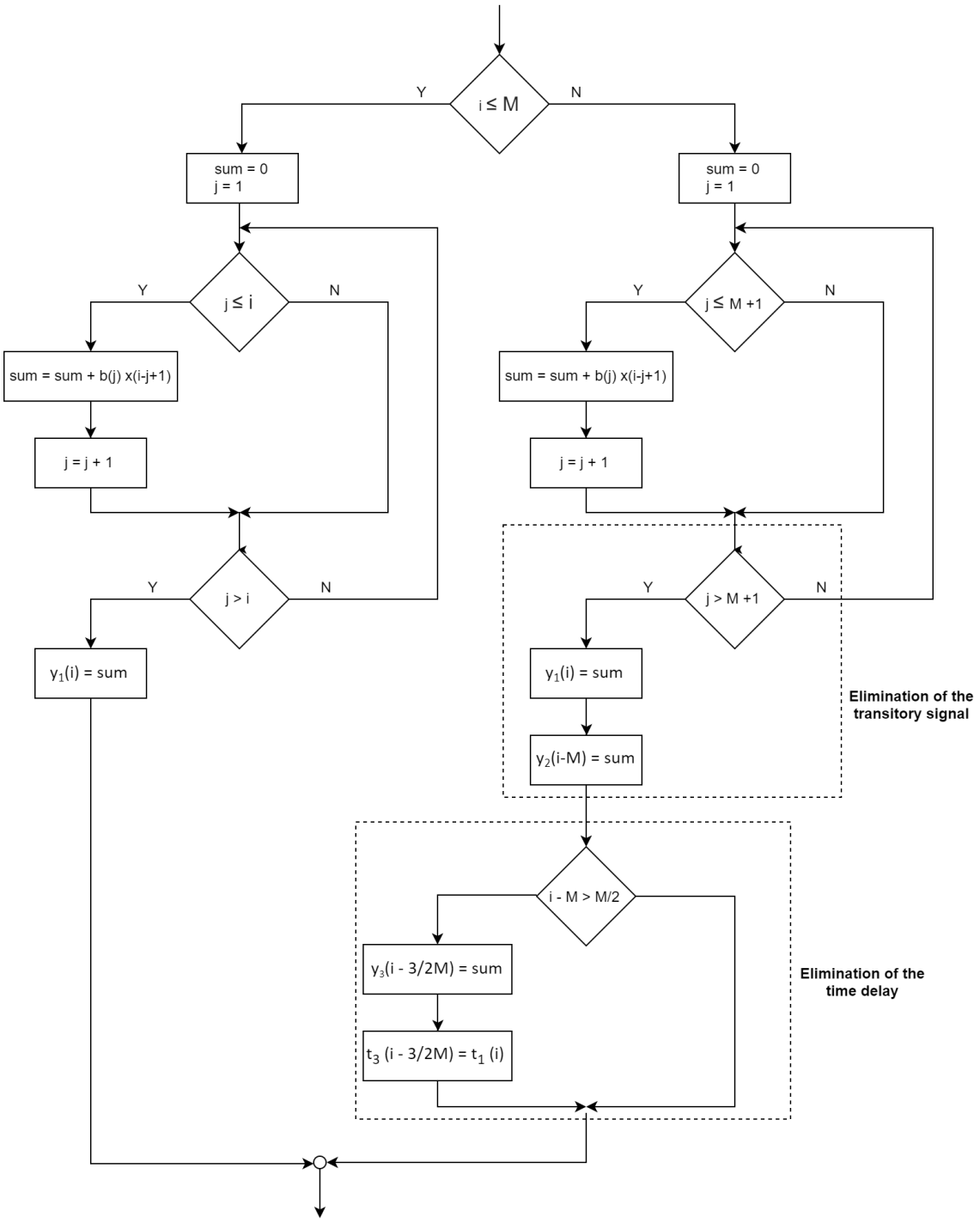

Figure 5.7: Block diagram of the pre-processing phase

5.2.1 PPG signal filtering

The presence of noise superimposed on to the PPG signal alters its morphology, being characterized by a low amplitude. The PPG signal band ranges from 0.01 Hz to almost 3 Hz [82].

Four distinct signal bands can be identified:

- **high frequencies** (0.15 Hz-0.5Hz), influenced by parasympathetic nervous system activity and by the respiration;
- **medium frequencies** (0.04 Hz-0.15Hz);
- **low frequencies** (0.01 Hz-0.04 Hz) influenced by the activity of the sympathetic and parasympathetic system;
- **heart rate** (0.5 Hz - 3 Hz).

Sources of noise degrading the PPG signal are:

- **electromagnetic interference**. The electronic instrumentation used to record the signal, such as cables and probes, generates an electromagnetic interference signal with a sinusoidal component at 50 Hz that overlaps the PPG signal [83]. It is generally removed with a low-pass filter;
- **movement artifact**. It is still a problem and it is hardly removed. It includes both the voluntary movement that the involuntary one, i.e. the movement caused by the sensor's poor adhesion to the tissues, altering the light detected [82]. This artifact has a frequency band from 0.05 Hz to 8 Hz, overlapping with that of the PPG signal.

  For this reason, its contribution cannot be removed with a common filter that excludes the components over the band of interest.

  Generally sophisticated techniques, such as the Adaptive filter or the Wavelet transform are employed.
- **baseline shift**. Components characterized by a frequency less than 0.4 Hz cause a slow change in the baseline. Since they give only information about temperature regulation, respiratory activity and nervous system activity, in this case they can be removed using an high pass filter [84].

To remove these components, it was decided to filter the PPG signal using a bandpass filter with cut-off frequencies of 0.5 Hz and 6 Hz, with a margin of 3Hz from the upper end of the maximum frequency of the PPG signal. The order of the filter has been chosen after several tests.

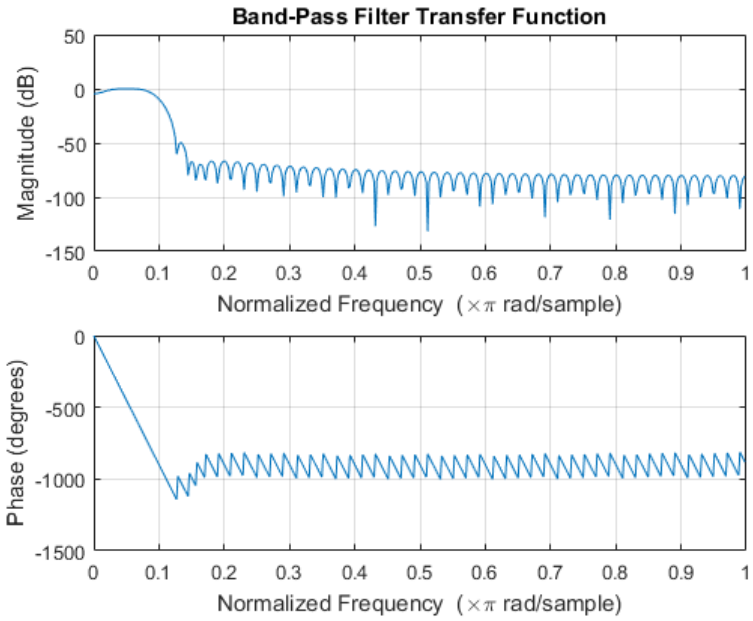

Figure 5.8: Band-Pass filter transfer function used for filtering the PPG signals

Ideally, a filter transfer function with vertical slopes in correspondence of the bandwith frequencies is desirable. In reality, a transfer function with high slope is acceptable.

In this case, the absence of the signal at frequencies lower than 0.5 Hz is expected, in reality it is tested that a FIR filter with moderate order is unable achieve this, having chosen stopband frequencies close to those of the bandwidth frequencies.

Through the Matlab Toolbox it has been estimated that 300 is the ideal order to remove most frequency components below 0.5 Hz. Given the high computation complexity of such a filter, the results of the PTT obtained by filtering the signal through filters with different order were compared.

Finally, it was evaluated that 100 is a good compromise between computational cost, RAM occupation in the microcontroller and results accuracy. In fact, the presence of the continuous component superimposed on the signal, besides adding an offset, does not alter its useful information.

In figure 5.9 the raw signal and the filtered one are shown. It was decided to represent the signal trend as a function of the samples. In this way, it is easy to appreciate the presence of the transient signal of 100 samples in the filtered signal, as well as the delay of 50 samples compared to the raw one.

In addition, in figure 5.14 the raw signal is shown compared to the filtered and realigned one. As well as to removing the delay introduced by the filter transfer function, the first 100 samples were removed in the filtered signal. In fact, the information carried out to

the first 100 samples, being distorted, is not useful for subsequent analysis.

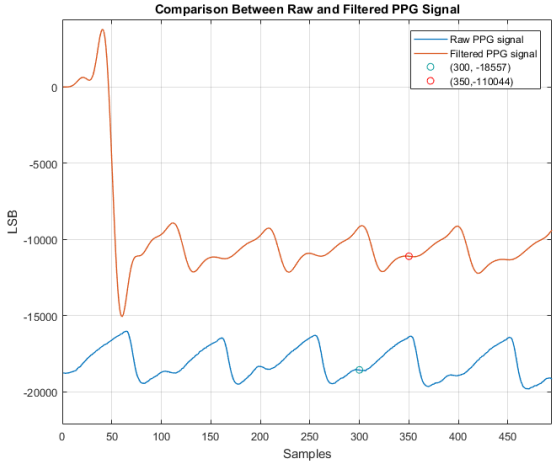

Figure 5.9: Representation of the raw and filtered delayed PPG signal

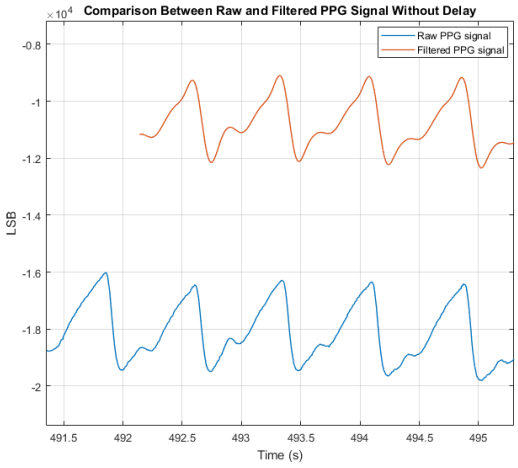

Figure 5.10: Representation of the raw and realigned filtered PPG signal

5.2.2 ECG signal filtering

The ECG signal consists of the superimposition of several waves with different frequencies [85]:

- **P wave** (0.67Hz - 5Hz);
- **T wave** (1 Hz - 7 Hz);
- **R wave** (5 Hz - 15 Hz).

Since in the implemented algorithm the ECG signal is used to detect only the R-peaks, it was decided to filter the signal using a bandpass filter with 5 Hz and 15 Hz as cut-off frequencies and order of 100.

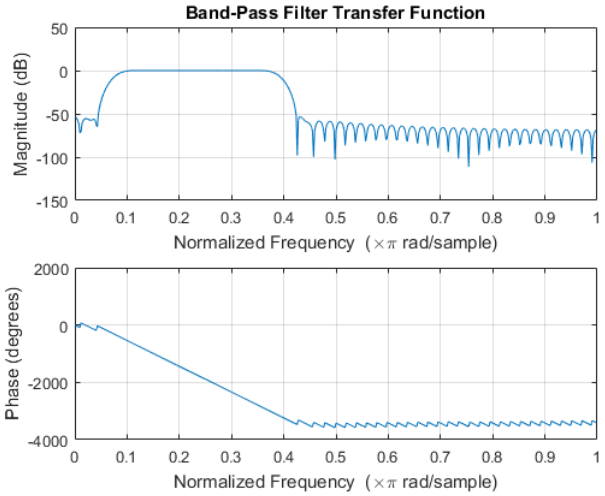

Figure 5.11: Band-Pass filter transfer function used for filtering the ECG signal

The noise sources that degrade the ECG signal are:

- **network interference**. It overlaps with sinusoidal trend at 50 Hz to the acquired signal. The amplitude of the electromagnetic sinusoid is generally equal to 50% of the peak-to-peak amplitude of the ECG signal, affecting the signal amplitude of about 25 mV. As for the previous signal, network interference can be removed with a low-pass filter [86];
- **muscle contraction**. It affects the quality of the ECG signal in a range between low frequencies and 10.000 Hz [86]. It is a source of noise which creates problems especially when the signal is acquired during physical exercise. Unlike other noise sources, it is a type of noise that has the same band as the PQRST complex. It cannot be removed with common filtering techniques, but techniques based on the morphology of the acquired signal are recommended [87].
- **baseline wander**. It is a noise generated at frequencies close to 0.5 Hz, which causes the shifting of the signal compared with the normal horizontal line. Generally, this artifact is caused by the patient's breathing. In addition, the high impedence between skin and electrode can also improve this arctefact. It can be removed through an high pass filter [87].

- **movement of the electrodes**, caused by the stretching of the skin that modifies the impedance between the skin and the electrode. This also occurs in the same band as the signal, from 1 to 10 Hz. This artifacts are characterized by wide waves that are often exchanged with the complex QRS. In this case, an adaptative filter can be implemented [87].

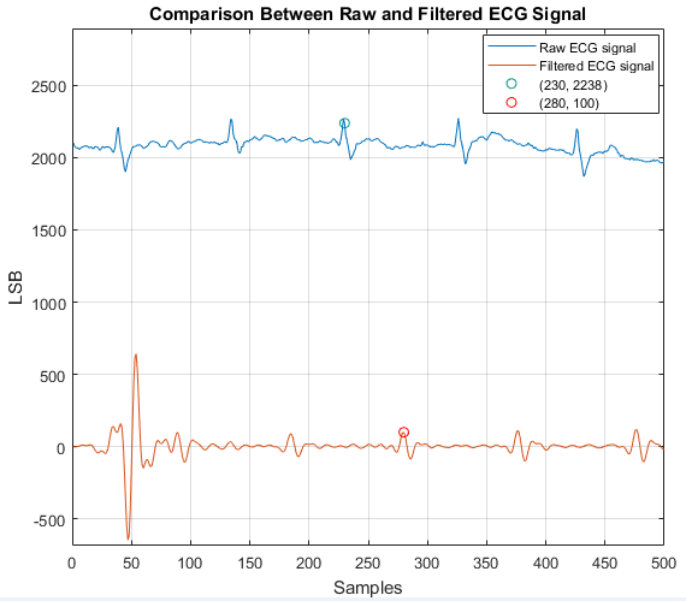

Figure 5.12: Representation of the raw and filtered delayed finger PPG signals

In figure 5.12 are shown the raw and the delayed and filtered ECG signals, with transients extending over 100 samples. In figure 5.13, the elimination of the delay and of the transient at the same samples are shown.

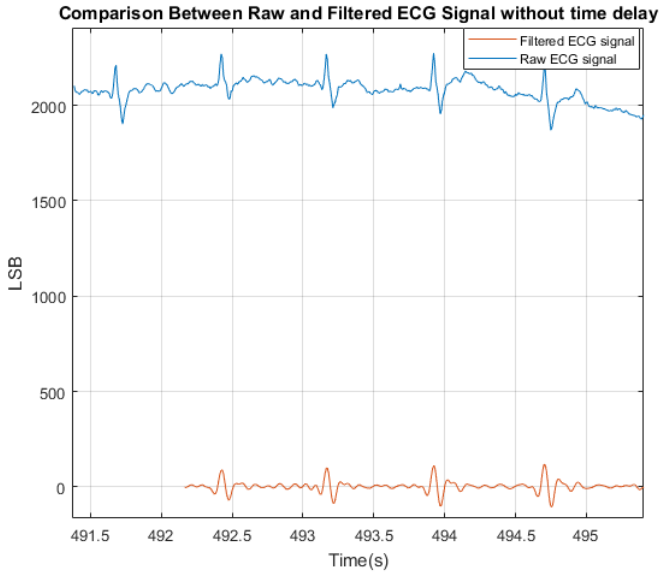

Figure 5.13: Representation of the raw and realigned filtered ECG signals

5.2.3 Accelerometric signal filtering

The accelerometric signal filtering was obtained employing a band-pass filter with 101 coefficients. The cut-off frequencies were chosen according to the analyses made on the

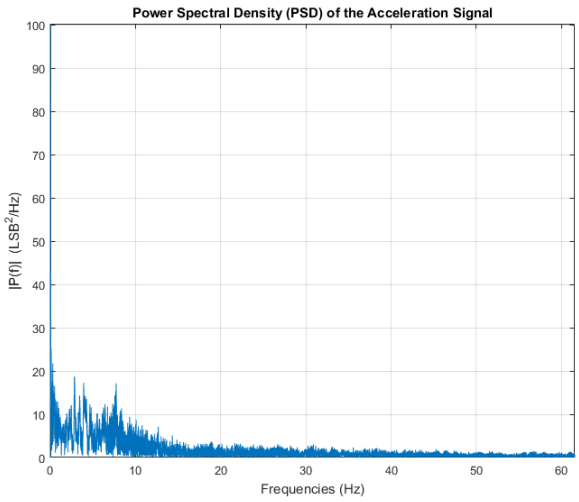

Figure 5.14: Power Spectral Density of the raw acceleration signal

power spectrum of the raw accelerometric signals. They were characterised by an higher spectral power in the frequency range from continuous to 15 Hz.

The chosen cut-off frequency also coincides with the upper end of the band-pass filter

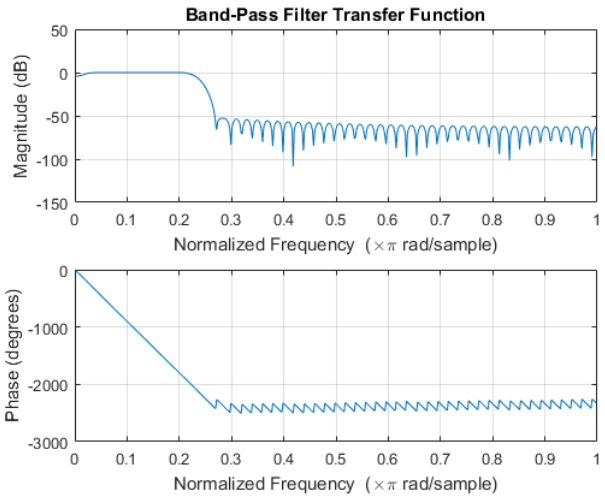

Figure 5.15: Band-Pass filter transfer function used for filtering the accelerometric signal

used for the ECG signal, so as to consider all the motion artifacts that could affect the acquired signals.

5.3 Motion detection

To avoid inaccurate results, causing false alarms, it was decided to calculate the parameters listed above only in absence of noise. There are two types of motion sources:

- patient or sensor movement, causing a change in the path of the light emitted and detected;
- variation in the internal arrangement of the tissues (e.g. due to the opening and closing of the hand as well as the movement of the fingers);

The first one can be easily detected by analyzing the accelerometric signal [88]. The second type, since it does not change the arrangement of the acceleration, can be hardly detected through the accelerometer [89].

In the first case, it was decided to acquire five accelerometric signals to analyze them.

The signal acquisition was initially done in steady state. Secondly, movements in both directions were introduced, as shown by the signal in figure 5.16.

For each accelerometric signal, obtained considering the contributions of the three axes (X, Y, Z), an index of statistical dispersion like the *root mean square* (RMS) was calculated.

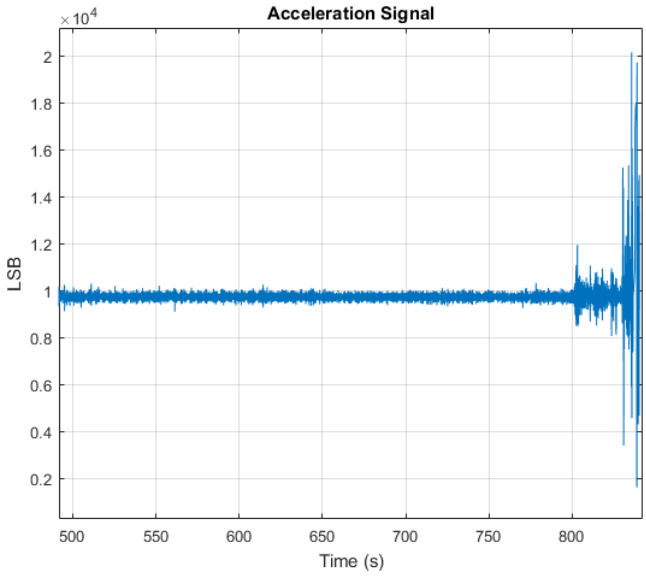

Figure 5.16: Example of acceleration signal acquired for the evaluation of the threshold of motion detection

The RMS value estimates the variability of the data compared to their average value. It gives information related to their dispersion. RMS value in steady state are compared with these in movement state.

A low RMS value represents the invariance of the position during the acquisition. A threshold close to the mean RMS of the signals in movement state is chosen.

Subject	RMS steady state	RMS motion state
1	9807.4	10129.1
2	9705.5	10106
3	9834.3	10316.1
4	9856.4	10216.9
5	9938.7	10523.4

Table 5.1: RMS values of the acceleration signals

In table 5.1, the RMS values in both configurations are shown. The value of 10100 was chosen.

If the acceleration RMS value of the buffer was less than the threshold chosen, the buffer was considered free of artifacts.

5.4 Noise detection

Unlike the previous case, the aim of the *noise detection algorithm* is to identify the presence of the noise on the signal, caused by artifacts undetected by the accelerometer. In this case it is chosen to proceed by calculating some parameters depending on the morphology of the signal waveform, in this case the PPG one. The parameters are the following:

- **kurtosis** (K), used to evaluate how the samples of the signal are distributed around the mean value. The distribution can be more or less flat, or with lot of peaks. K is defined as:

$$K = \frac{E(x-\mu)^4}{\sigma^4} \tag{5.12}$$

  where μ and σ are respectively the mean of the signal x and the standard deviation, instead E$(x-\mu)$ represents the expected value of the quantity $x-\mu$;

- **Shannon entropy** (Se) defines how much the probability density function of the signal deviates from the uniform distribution. It provides a measure of the uncertainty of the signal. Se is defined as:

$$Se = -\sum_{n=1}^{N} x[n]^2 \ln x[n]^2 \tag{5.13}$$

  where x is the signal and N the total number of samples on the signal;

- **Skewness** (S), whose value is used to get an idea of the symmetry of the distribution of PPG signal points. S is defined as:

$$S = \frac{1}{N}\sum_{i=1}^{N}(x_i - \frac{\mu_x}{\sigma})^3 \tag{5.14}$$

where μ_x is the empirical measure of the mean and σ the empirical value of the standard deviation x_i and N is the number of samples in the PPG signal.

As in the previus case, the thresholds were searched acquiring five PPG signals, in steady and noisy state. The values of K, S and Se were calculated in the two parts of the signal, as shown in table 5.2.

Subject	Se s.s	Se m.s	K s.s	K m.s	S s.s	S m.s
1	$4{\cdot}10^{+13}$	$1.54{\cdot}10^{+12}$	1.3	2.4	-0.19	0.8417
2	$1.34{\cdot}10^{+13}$	$1.07{\cdot}10^{+12}$	2.39	2.6259	-0.1995	0.6977
3	$8.59{\cdot}10^{+13}$	$1.48{\cdot}10^{+13}$	2.27	2.92	-0.1995	0.6977
4	$2.91{\cdot}10^{+13}$	$1.12{\cdot}10^{+12}$	2.49	1.86	-0.1162	0.1
5	$9.82{\cdot}10^{+12}$	$1.33{\cdot}10^{+9}$	2.106	2.96	-0.0334	0.6627

Table 5.2: Se, S and K values of the finger PPG signal in steady and motion state

The values shown in table 5.2 are relative to the analyses made on the finger, even if those obtained from the signal acquired on the wrist were of the same order of magnitude.

The idea was to compare the threshold values of S, Se and K for each PPG buffer to the corresponding threshold. In this way, the decision rules are evaluated.

Kurtosis decision rule states that:

$$DK_i = \begin{cases} 1 & if K_i \leq K_{Th} \\ 0 & if K_i \geq K_{Th} \end{cases}$$

Signals with a lower Kurtosis value than the threshold are considered free of artifacts, since they maintains an amplitude and a width more or less constant over time. If the estimated value exceeds the reference one, it means that the signal assumes an altered morphology compared to the normal one.

Shannon's entropy decision rule states that:

$$DSe_i = \begin{cases} 1 & if Se_i \geq Se_{Th} \\ 0 & if Se_i \leq Se_{Th} \end{cases}$$

The buffer of the PPG signal is corrupted by noise if its entropy is below the threshold. In fact, Se in information theory represents the amount of information carried by the signal. So the entropy is a measure of its complexity. In this case the obtained entropy values were negative. So their absolute value was considered.

Skewness decision rule states that:

$$DS_i = \begin{cases} 1 & if S_i \leq S_{Th} \\ 0 & if S_i \geq S_{Th} \end{cases}$$

in fact a high value of S in absolute value indicates the asymmetry of the signal, instead a value close to zero a more regular distribution around the central peak.

The idea was to consider the signal actually corrupted by noise if both decision rules

gave positive results [90]:

$$FD_i = \begin{cases} 1 & if DK_i + DSe_i + DS_i = 3 \\ 0 & if DK_i + DSe_i + DS_i \neq 3 \end{cases}$$

It was evaluated that even an ideal threshold of Se and S caused the exclusion from subsequent processing of PPG waves that had a correct morphology.

In order to avoid the exclusion of too many points, it was decided to take as reference only the value of K, whose chosen threshold was 3.5. In fact, in this way, the results obtained yielded a good compromise between correctly excluded and real peaks

5.5 R-Peaks research

As for the extraction of the R-peaks, it was implemented the algorithm that Pan and Tompkins proposed in 1985 for the detection of the QRS complex.

The algorithm is based on the analysis of the QRS complex slope, on their amplitude and duration.

A first preprocessing phase is employed to eliminate signal components that degrade the QRS complex.

Subsequently, values of the signal obtained at the previous step are compared with the chosen threshold, which is not constant for the whole signal but changes for each ECG signal buffer, adapting to specific values of each buffer [91].

The proposed algorithm differs from the Pan-Tomkins one as for the chosen mode of the threshold selection, having achieved satisfactory results.

The different phases of the preprocess are described below:

- **differentiation**. The first derivative of the signal is calculated to obtain information about the variation of the signal and about the slope of the rising and leading edges of the QRS complex [92];

- **squaring**. Each sample of the differentiated signal is squared, according to the following formula:

$$Y(mT) = [X(mT)]^2 \tag{5.15}$$

  where T is the sampling period, $Y(mT)$ is the sample squared and $X(mT)$ is the sample differentiated.

  This non-linear signal amplification allows to obtain only positive values. It gives more emphasis to signal components that have high frequency [93];

- **moving integration**. A moving average filter has been implemented, obtaining the following signal output:

$$Z(mT) = \frac{1}{M}[Y(mt - (M-1)T) + Y(mT - (M-2)T) + ... + Y(mT)] \quad (5.16)$$

where M is the order of the filter transfer function and $Z(mT)$ is the filter output.

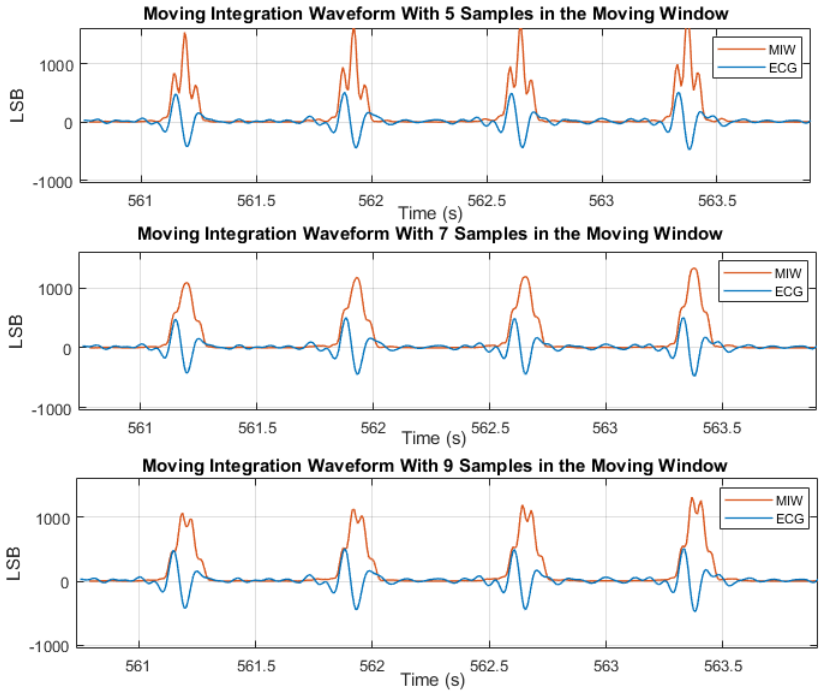

Figure 5.17: Representation of moving integration waveform (MIW) with different length of the moving window

Also in this case the time delay introduced by the filter is deleted. This integration step allows to obtain information about the waveform of the entire QRS complex: the moving average smoothes the signal, reducing the QRS complex peaks in a single one.

The choice of the M value influences the detection of the peaks: as shown in figure 5.17 high values of M are correlated with large integration windows that include not only the samples of the QRS complex but also those of the T wave. On the other hand, small values of M generate narrow windows, producing more peaks for each QRS complex. The value of M should be large enough to create windows that include the entire QRS complex, so that its extremes coincide with those of the integrated signal.

Several experimental tests were conducted, and finally, as shown in the figure 5.19, it was considered that better results were obtained using a 7 coefficient integration window.

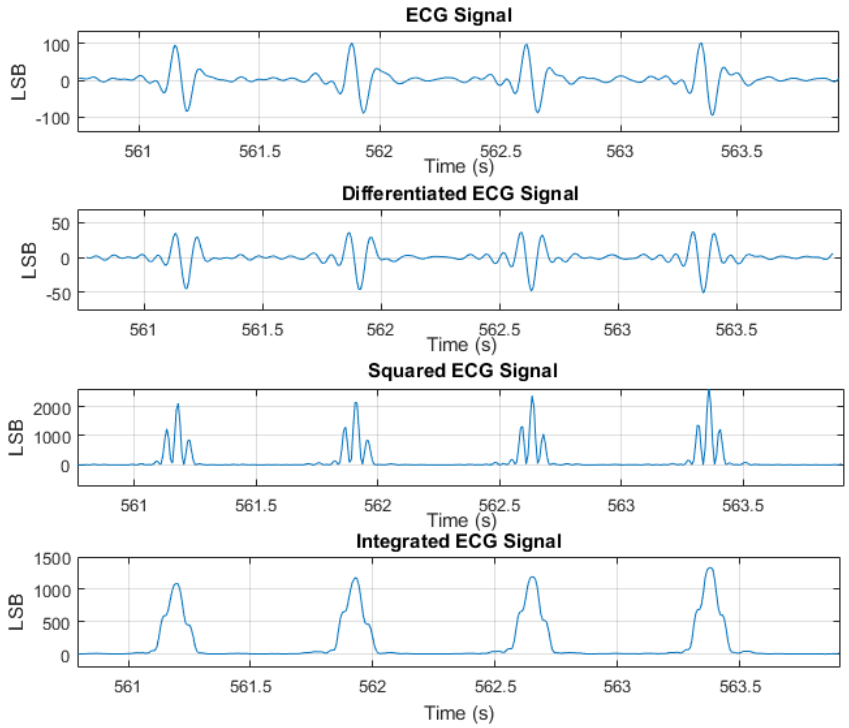

Figure 5.18: Representation of the preprocess phases for R-Peaks research

After the signal preprocessing phase, for each MIW rectangular windows are created, with a value different from 0 when the integrated signal has a value higher than the chosen threshold, 0 if lower. As shown in figure 5.19, the window created subtends the entire QRS complex rescaled with respect to its maximum value.

The threshold was chosen experimentally, after some tests, and corresponds to 10% of the maximum value of each ECG signal buffer, thus adapting to the variation that the signal undergoes over time.

In this way, the position of each R-peak corresponds to the position of the maximum value subtended to each window.

In figure 5.18 the different phases of the algorithm are shown.

Once the peaks in each buffer are selected, it is verified that each peak is at least 43 samples far from the previous one.

Since a sampling frequency of 128 Hz is chosen, the minimum distance chosen allows to have a maximum of 180 bmp, which is the physiological maximum value [94]. If this

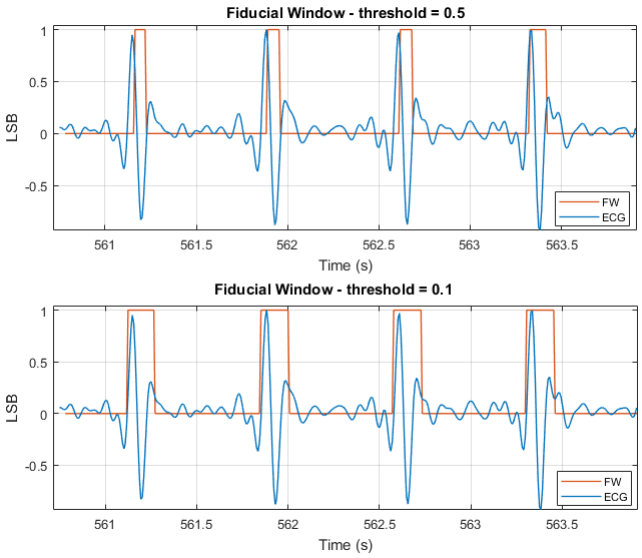

Figure 5.19: Representation of the fiducial window with differentes sizes

limit is not respected, the current peak is excluded.

5.6 PPG peaks and valley research

The algorithm of the PPG-peaks and valleys research is partly inspired by the one described in the work [95] and influenced by the study of the signal morphology. The same algorithm is used to detect the peaks and valleys of the finger and wrist PPG signals.

During the systolic phase, the amount of light that is transmitted is always lower than in diastolic phase. Therefore, the resulting wave is inverted with respect to the arterial pressure waveform. For a simple interpretation of the data, the acquired signal is generally inverted so as to consider the peak of the signal in corrispondence of the increase in blood pressure and blood flow. In this case it was decided to proceed with the non-inverted signal.

The two characteristic points of the signal are the follows:

- **PPG peaks**, corresponding to the beginning of the systolic part;
- **PPG valleys**, corresponding to the end of the systolic part.

The algorithm is not applied directly to the entire n-th buffer of the signal but it is repeated for each PPG buffer sample.

The first step allows to verify that the i-th sample of the buffer S_{PPG} is a valley: the

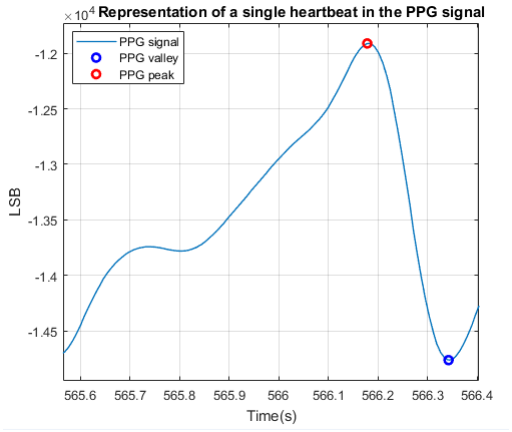

Figure 5.20: Representation of a single heartbeat in the PPG signal with his peak and valley

sample $S_{PPG}(i)$ is defined a valley $V(i)$ in the position i when:

$$S(i-1) > S(i) < S(i+1) \tag{5.17}$$

For each detected valley, it is verified whether there is at least one peak between the current valley and the previous one. A sample $S_{PPG}(i)$ is defined a peak $P(i)$ in the position i when:

$$S(i-1) < S(i) > S(i+1) \tag{5.18}$$

If several peaks are detected between two valleys, the one with the greatest amplitude in relation to the i-th valley is considered as the real peak. In this way the correct pair of points $P(i)$-$V(i)$ constitute the extremes of the systolic tract of the i-th heartbeat. For each pair of points $P(i)$-$V(i)$, the amplitude of the pulse wave is calculated as follow:

$$VPD(i) = max(||P(i)| - |V(i)||) \tag{5.19}$$

where VPD is the peak-minimum systolic amplitude. Subsequently a removal of false peaks and valleys was applied. For each pair of points $V(i)$-$P(i)$, the $VPD(i)$ is compared with the reference value, removing the i-th peak and valley if their amplitude is not equal or higher than the reference one.

This allows to eliminate false peaks and valleys easily detectable in presence of noise or of the dichrotic notch.

Since the VPD varies for each subject, it was decided to use a reference value which varies for each heartbeat. It is obtained by multiplying at the i-th heartbeat the VPD(i-1)

with a costant threshold. The threshold chosen is related to the morphology of the signal.

Physiologically, the morphology of the pressure wave is preserved over time, as also the properties of the tissues. For this reason, for each subject, the PPG signal has a morphology that does not change instantaneously over time, but gradually. With these considerations, for each pair of points $P(i)$-$V(i)$, the amplitude of the previous peak-valley $VPD(i-1)$ is taken as reference amplitude. In particular, the points detected are considered real peaks and valleys only if the i-th VPD is greater than the 50% of the previous VPD.

The % of the threshold was chosen experimentally. It was tested that smaller percentages increased the number of false peaks and valleys, especially in presence of the dichrotic notch. On the contrary, higher thresholds decreased the number of true peaks and valleys detected. The threshold of 50% is a valuable compromise between true and false detectable peaks.

The choice of the first reference value, at the beginning of the acquisition, is evaluated as the 50% of corresponding one with the maximum VPD between the first two pairs of points detected.

The algorithm also includes a re-calibration phase: if no peaks and valleys are recognized for a time interval established a priori, the threshold of the reference value is reduced to 30% until a new pair of true points are detected. The time interval chosen corresponds to the maximum physiological distance, which generates 30 bpm.

A further control allows to exclude the selected pairs of peaks and valleys distant from the previous one of a minimum time interval that allows to have a maximum of 180 bpm, respecting the physiological limits.

Another reference point was computed for each beat, that is the point to which corresponds the maximum slope of the systolic tract.

5.7 Heart Rate measurement

The heart rate is calculated using both ECG and PPG signals acquired. This is due to similarity between the point at the end of the sistolic phase of the PPG signal with the R-peak of the ECG one. As explained in Chapter 2, the heart rate can be calculated from the measurement of the distance in seconds between successive peaks (RRI). For this reason, the HR expressed in bpm has been calculated as follows [96]:

$$HR = \frac{60}{RRI} \tag{5.20}$$

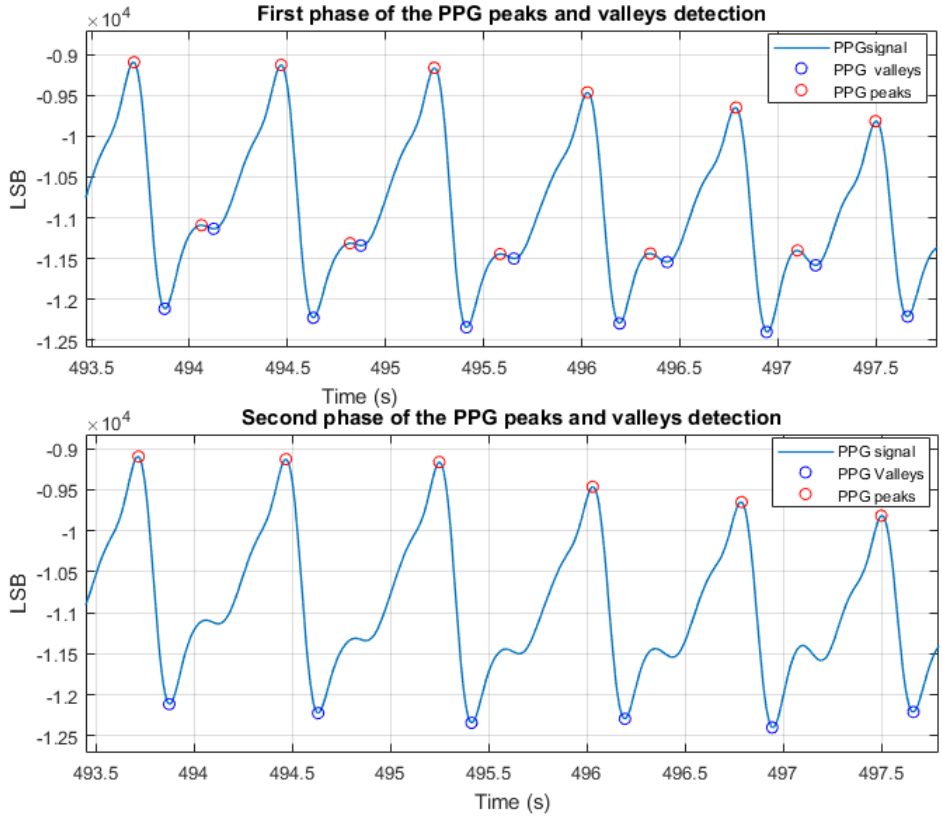

Figure 5.21: Representation of the detection of the PPG peaks and valleys detection in the two phases of the PPG peaks and valleys research algorithm

An alternative measurement is to count the number of signal peaks in 60 seconds [97]. In the same way, the HR is calculated in the PPG signal as follow:

$$HR = \frac{60}{PPI} \tag{5.21}$$

where PPI is the time distance between two peaks of the signal.

The RRI or PPI interval considered in the algorithm does not correspond with the i-th interval of the i-th peak of the signal, since the heart rate is processed every 3 seconds.

5.8 PTT computation

The objective of the algorithm is to calculate the PTT on the correctly detected pulse wave (PW) of the PPG signal. Therefore, the calculation of the PTT is preceded by a pre-processing phase called 'PW-filter'. Five criteria were drawn up and must be respected as long as the detected PW is not the result of an artifact and coincides with the same heartbeat as the i-th R-peak. Only if all the criteria are respected, then the calculation of

the i-th PTT is carried out.

The criteria applied are as follows:

- the i-th peak of the PW of the PPG signal is included between the i-th peak R and its next one, i.e.:

$$t_{R-peak}(i) < t_{PPG-peak}(i) < t_{R-peak}(i+1) \tag{5.22}$$

- the i-th valley of the PW of the PPG signal is included between the i-th peak R and the R peak i+1, i.e.:

$$t_{R-peak}(i) < t_{PPG-valley}(i) < t_{R-peak}(i+1) \tag{5.23}$$

- the i-th PPG-peak (corresponding to the beginning of the systolic phase) of the PW precedes the i-th PPG-valley (corresponding to the end of the systolic section)

$$t_{PPG-peak}(i) < t_{PPG-valley}(i) \tag{5.24}$$

- the maximum slope d of the systolic slope is positive, i.e.:

$$d_{max} > 0 \tag{5.25}$$

- the width of the point at the beginning of the systolic slope is greater than the one corresponding with the end of the systolic slope:

$$PPG_{peak} - PPG_{valley} > 0 \tag{5.26}$$

Assuming that the PEP interval is negligible, the PTT was calculated considering each R-peak of the ECG signal and three reference points in the PPG one. In literature, in fact, the points that are usually considered are the peaks of the PPG signal, the valleys, and the points with the maximum slope in the systolic phase. For this reason, it is decided to repeat the calculations considering both points. So the PTT was calculated in the following ways:

- distance between R-peak and PPG-valley corresponding to the same heartbeat;

$$fPTT(i) = t_{PPG-valley}(i) - t_{Rpeak}(i) \tag{5.27}$$

- distance between the R-peak and the PPG-peak of the same heartbeat;

$$pPTT(i) = t_{PPG-peak}(i) - t_{Rpeak}(i) \tag{5.28}$$

- distance between the R-peak and the steepest point of the systolic phase corresponding to the same heartbeat.

$$msPTT(i) = t_{PPG_{m.s}}(i) - t_{Rpeak}(i) \tag{5.29}$$

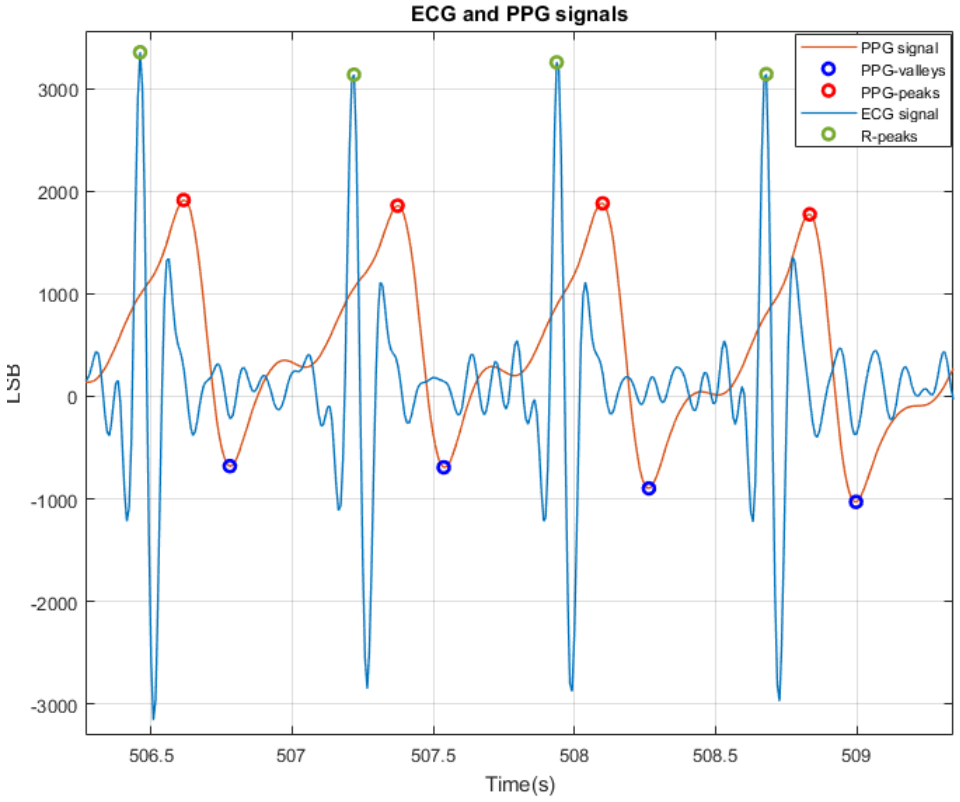

Figure 5.22: Representation of the ECG and PPG signals corresponding to the same heartbeats. The image is obtained resizing the two signals for better visualization.

If the criteria are not respected, it was decided to reconfirm the PTT value of the previous heartbeat. The same confirmation is maded if more than one PPG-peaks or valleys are detected between two R-peaks, since not significant variations in PTT are provided between consequtives heartbeats.

Part III

Results

Chapter 6

Results

The algorithm was tested by comparing the results of the signals acquired on 8 patients.

For each acquisition, a statistical study was carried out, in order to define an overall performance of the implemented algorithm.

6.1 Synchronization

As explained in the previous chapter, the synchronization of the BAN devices was done by comparing the position of correspondent points for the two accelerometric signal. In particular, it was decided to evaluate the offset considering for each acquisition the mean distant time of more corresponding points.

By averaging the time offset among several corresponding points, it is tried to reduce the weight of this error. In table 6.1 are shown the offsets obtained for each acquisition. In particular, they were added to the signals acquired by the B2BNM on the finger.

Subject	Offset (ms)
1	2031.50
2	2022.67
3	-2414.33
4	6949.00
5	-3221.00
6	7696.00
7	1974.50
8	6701.50

Table 6.1: Results of the synchronization offset

6.2 Peaks research validation

Since the detection of the peaks greatly influences the course of the following results, it was decided to proceed by calculating for each acquisition, the confusion matrix relative to the point that the algorithm was able to detect.

Since an already validated algorithm was not used, the confusion matrix was obtained through a visual inspection of each signal. Samples were classified as true negatives (TN), false negatives (FN), true positives (TP) and false positives (FP).

To evaluate the performance of the algorithm, a static test was conducted, by calculating various statistical indices:

- **Sensitivity** (SE), i.e. the ability of the test to identify true peaks. Corresponds to the proportion of real peaks identified as such. It was calculated as:

$$Sensitivity = \frac{TP}{TP + FN} \tag{6.1}$$

- **Specificity** (SP), i.e. the ability of the algorithm to identify samples that are not peaks. It corresponds to the proportion of true non-peaks identified as such. It is calculated as:

$$Specificity = \frac{TN}{TN + FP} \tag{6.2}$$

- **Predictive value of the positive test** (PPV), i.e. the probability that a peak identified by the test is a true peak. It is calculated as:

$$PPV = \frac{TP}{TP + FP} \tag{6.3}$$

- **Predictive value of the negative test** (PNV), i.e. the probability that a non-peak is really recognized in this way. It is calculated as:

$$PNV = \frac{TN}{TN + FN} \tag{6.4}$$

The results of R-peaks and PPG-peaks validation are shown respectively in figure 6.1, 6.2 and 6.3

The same parameters were not evaluated for the detection of valleys in the PPG signals, due to the difficult detection by means of visual inspection.

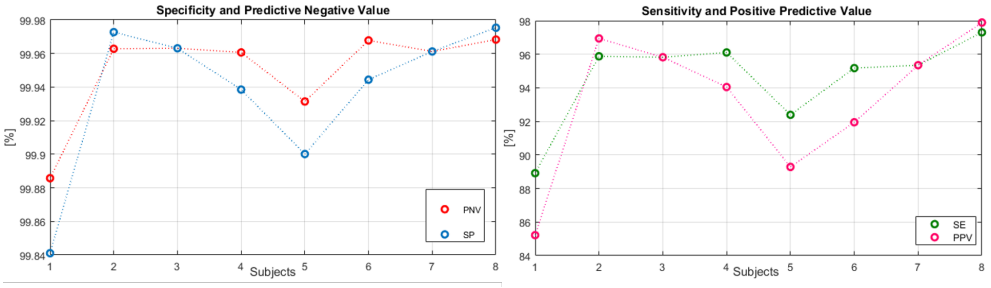

Figure 6.1: Statistical parameters of the R-peaks algorithm

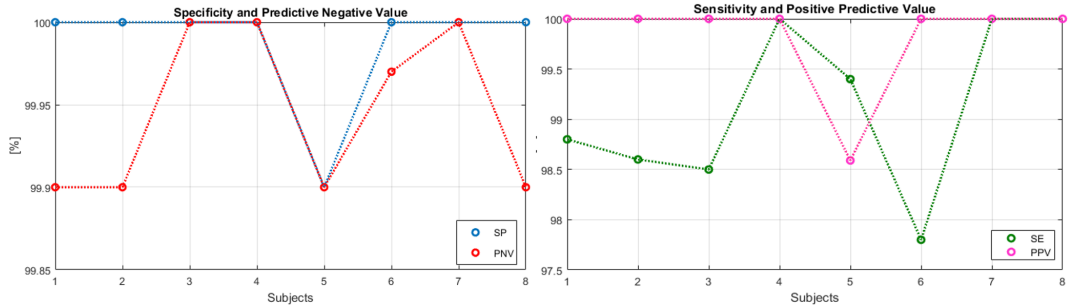

Figure 6.2: Statistical parameters of the finger PPG-peaks algorithm

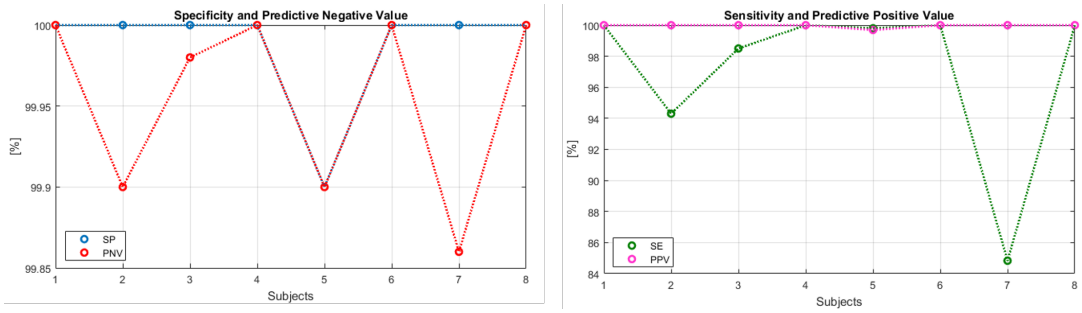

Figure 6.3: Statistical parameters of the wrist PPG-peaks algorithm

6.3 Heart Rate validation

The heart rate algorithm was validated by comparing the heart rate trends of wrist PPG, finger PPG and ECG signals among them. Since it was not used any reference device or algorithm, it was decided to calculate some parameters of statistical distribution, rather than the exact error value and accuracy of the algorithm. So, the analysed parameters are:

- **covariance**;

- **Pearson correlation coefficient**.

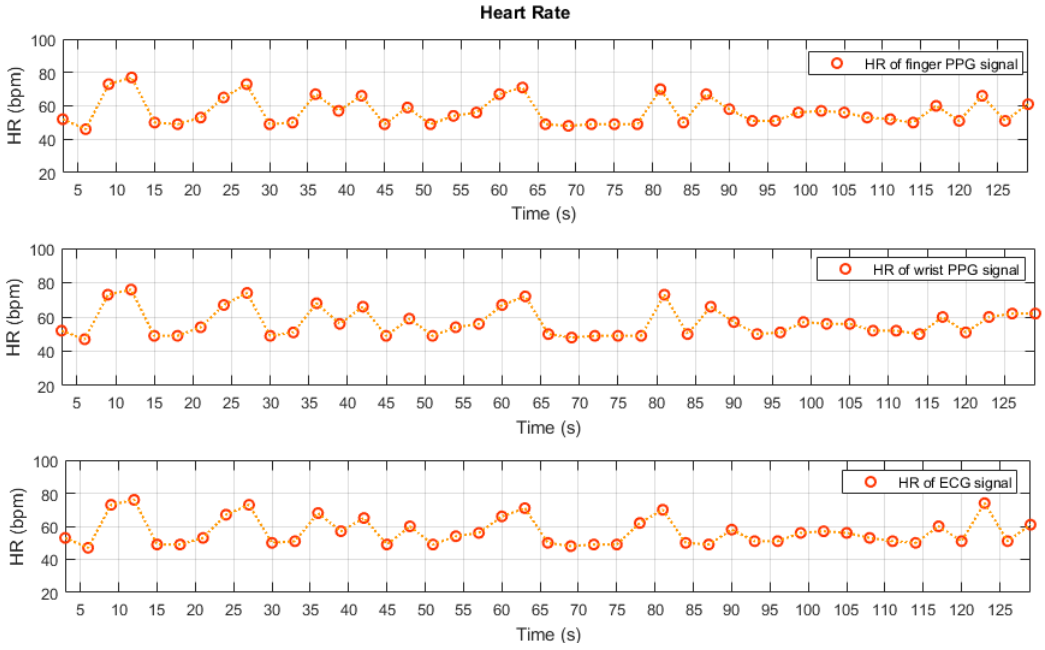

Figure 6.4: Representation of HR with ECG, wrist PPG and finger PPG signals

Analytically, considered two random variables X and Y, its *covariance* show how two variables change together: in particular, the covariance is positive if X and Y move in the same direction, i.e. they undergo oscillations in agreement. So, it is negative when two variables X and Y undergo discordant oscillations. There is no covariance if they change independently from each other, in this case the value of the covariance is 0. It is computated as:

$$Cov(X,Y) = \frac{1}{N}\sum_{i=1}^{N}(x_i - \bar{X})(y_i - \bar{Y}) \tag{6.5}$$

where x_i and y_i are the i-th values of X and Y, instead $\bar{X}$ and $\bar{Y}$ are the mean of X and Y respectively.

Pearson's correlation coefficient (r) measures the degree of agreement or disagreement between two data sets. It defines how the variables are linearly correlated and how strong their relationship is [98]. It is defined as:

$$\rho(X,Y) = \frac{1}{N-1}\sum_{i=1}^{N}\frac{(x_i - \bar{X})}{\sigma_X}\frac{(y_i - \bar{Y})}{\sigma_Y} \tag{6.6}$$

where σ_x and σ_y are the standard deviations of X and Y the signals respectively.

The r coefficient varies between -1 and 1. If R is equal to 1, it means that the two

	Wrist PPG		Finger PPG		ECG	
Subj.	Mean std	Range	Mean std	Range	Mean std	Range
1	67+7.5	48 to 80	68+9.1	48 to 112	67+8.3	49 to 119
2	57+8.4	46 to 77	57+8.5	47 to 76	76+8.5	47 to 67
3	62+2.3	59 to 67	65+5.6	58 to 83	62+2.1	59 to 67
4	67+2.8	62 to 75	68+3.0	62 to 77	68+8.7	62 to 132
5	70+11.9	61 to 153	67+2.6	62 to 75	68+7.5	62 to 132
6	79+4.8	66 to 88	79+5.0	65 to 88	78+9.4	65 to 152
7	74+3.9	68 to 84	71+11.5	35 to 82	73+4.3	64 to 88
8	81+4.9	71 to 94	81+5.0	69 to 94	82+12	42 to 148

Table 6.2: Mean, standard deviation and range of both ECG, finger and wrist PPG Heart Rate results

set of variables change perfectly together, while it is equal to -1 if the two data move in opposite directions. If the coefficient is equal to 0, then they move in random directions.

It was decided to use both parameters in combination. Indeed, the covariance value only defines if the signals vary together and in which direction, but it does not define its degree of correlation and how much the change of the signal influences the other one [99].

In particular, the results are computed for each subject considering all the combinations among the ECG, finger and wrist PPG signals. In figure 6.5 and 6.6, the performance of the covariance and Pearson Correlation Coefficient are shown.

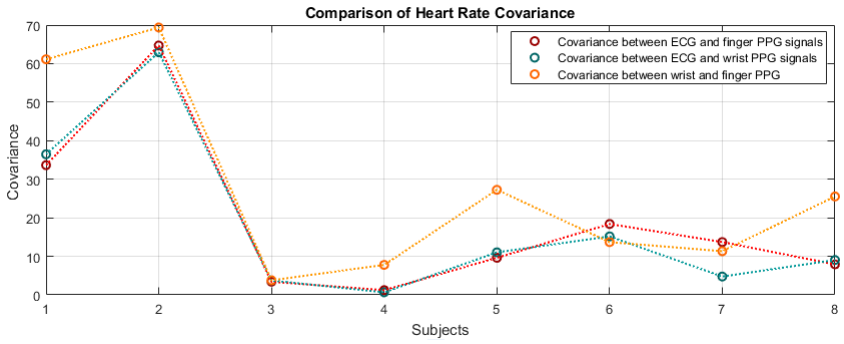

Figure 6.5: Representation of the HR covariance trend of the Heart rate

The trend of the correlation coefficient is rather variable among the eight acquisitions. In both cases, as shown by the sign of covariance, the three measurements are correlated with each other in a directly proportional way.

Generally, better results were obtained from the correlation of the HR computed with the finger and wrist PPG signals.

In fact, as shown with the specificity values of the R-peaks research algorithm, the

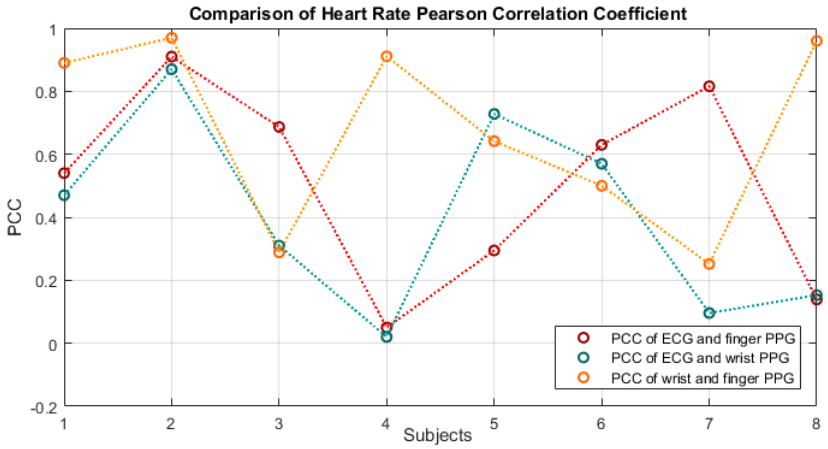

Figure 6.6: Representation of the HR Pearson correlation coefficients

presence of false detected R-peaks distort the HR measurements.
Others indices were evaluated for the finger and wrist PPG signals. Considering the anatomy of the two points of acquisition, the smaller amount of tissues overlapped in areas such as the finger, causes less alteration in the path of the light emitted by the PPG sensor, so less degradation of the acquired signal.

For this reason, even if the signal acquired in the two zones is generated in the same way, it is highlighted a non-uniformity quality between the wrist and finger PPG signals.

With the sensitivity and specificity values shown above, it can be prove that the heart rate obtained with the PPG finger signal is more accurate than the one of the wrist. For this reason, it was decided to calculate the error of the HR values considering the finger PPG signal as reference, as well as the accuracy of the results. The *error* was computed as:

$$e_i\ [\%] = \left(\frac{|y_i - x_i|}{y_i}\right) \cdot 100 \tag{6.7}$$

where y_i is i-th the sample of the reference signal, in this case the finger one, meanwhile x_i is the i-th sample of the wrist PPG signal. The *mean absolute error* is calculated as:

$$MAE\ [\%] = \frac{1}{N}\sum_{i=1}^{N} e_i \tag{6.8}$$

where N is the number of total errors calculated.

In the same way, the accuracy of the HR results was calculated. The accuracy quantifies the correspondence between the data in question, i.e the heart rate obtained with the wrist

PPG signal, compared to the reference, in this case the finger one. It was computed as:

$$ACC\ [\%] = \frac{1}{N}\sum_{j=1}^{N}\frac{|y_i - |y_i - x_i||}{y_i} \cdot 100 \tag{6.9}$$

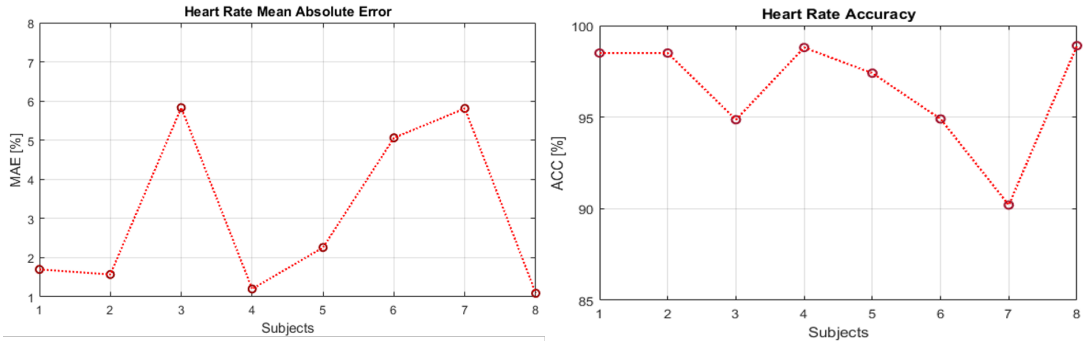

Figure 6.7: Representation of the accuracy and mean absolute error of finger and wrist HR

As done in various scientific works in literature, it was decided to complete the analysis with the Bland-Altman plot [97]. In figure 6.8 and 6.9, the plots obtained for each acquisition are shown.

The Bland-Altman plot is a dispersion graph used to compare two quantities of the same nature, as in this case. It does not give statistical values as solved, but by comparing the distribution of points in the plan it is possible to draw conclusions on the comparability of the two measures. The diagram was computed in Matlab © reporting:

- the difference of the two measures on the y-axis. In this case it was considered the wrist HR menus the finger HR;
- the arithmetic mean of the two measures on the x-axis.

Three horizontal lines are also plotted:

- one obtained from the average of the differences;
- two lateral lines obtained considering the average $\pm 1.96SD$. They represent the limit of the confidence interval.

As can be seen from the B-A plots, the two HR estimates differ on average by 3 bmp at most, with differences close to 0 in many acquisitions.

Generally, for the acquisitions with significant correlations, it is noticed that the trend of the points moves around the difference average line, in orange. In these cases, in fact,

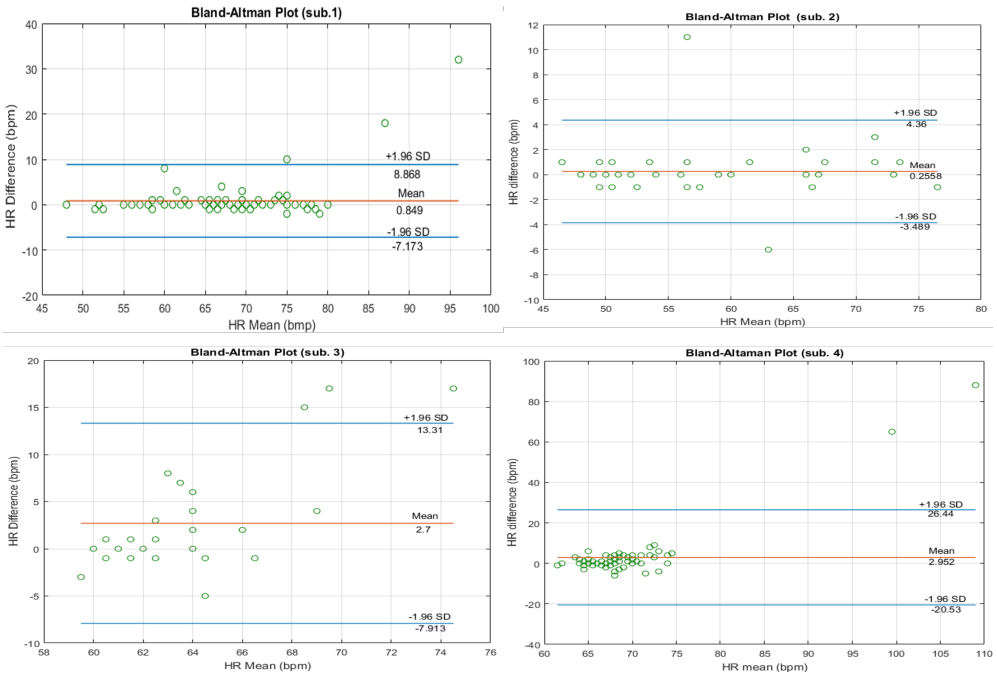

Figure 6.8: Bland-Altman Plot of wrist and finger HR results (acquisitions 1-2-3-4)

even if the confidence interval has more or less wide margins, generally the points do not appear distributed in the plan in a disorderly manner.

Moreover, at most 3 points are outliers. For acquisitions with low correlation coefficient, such as 4, 5 and 8, there is a disorganized distribution around the mean line.

However, the number of outliers remains limited. Moreover, in the acquisition 5 and 8, the points are arranged in a symmetrical way, therefore the error committed in the estimation in this case is not a random error but a systemic one.

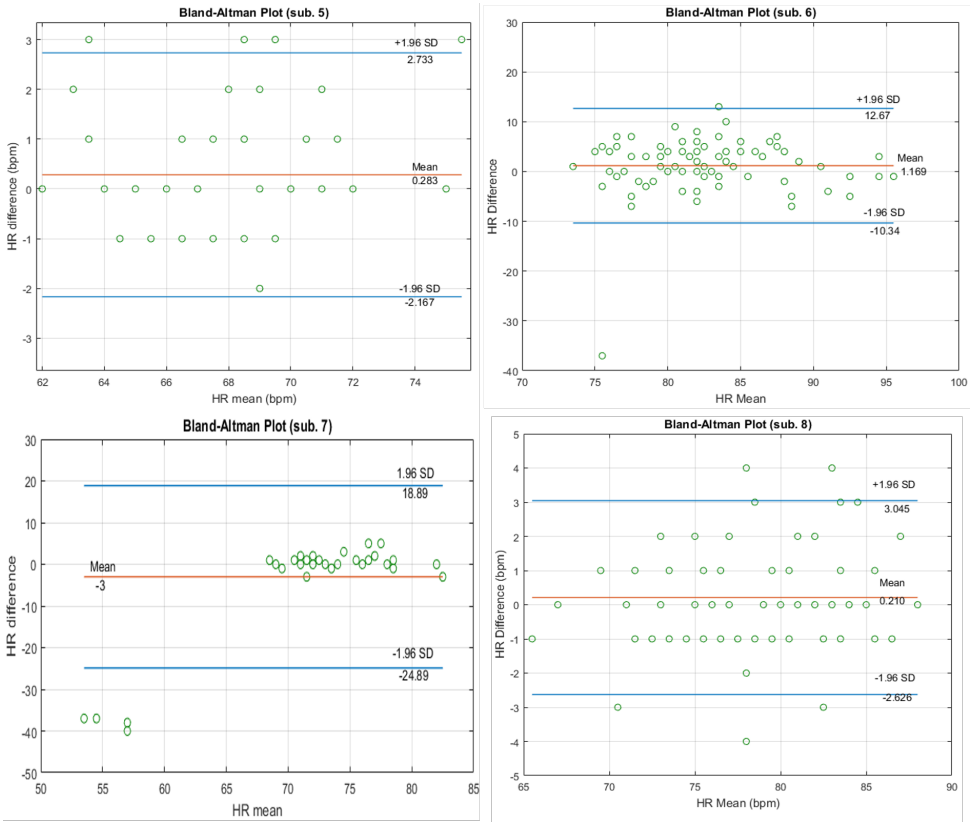

Figure 6.9: Bland-Altman Plot of wrist and finger HR results (acquisitions 5-6-7-8)

6.4 Pulse transit Time Validation

In order to proceed with the PTT validation of the BAN, the PTT values obtained using only one B2BNM device are taken as reference values. The choice is justifiable for several reasons.

The ECG and finger PPG signals of reference are acquired from a single device and sent via Bluetooth to a single computer. For this reason, the data are referred to instant times that do not correspond to the acquisition instant times. In fact, an offset, corresponding to the time it takes for Bluetooth to exchange data, is added to the latter. Working with a single device, the offset is identical for the two signals, so the estimate of the PTT is not altered by any synchronization delay.

Furthermore, others motivation are considered. As demonstrated above, the specificity of the finger PPG peaks research algorithm is higher than the obtained one with the wrist PPG signal.

This allows to consider the finger PPG signal as a good candidate with which to compare the results. Moreover, considering human physiology, to a pressure pulse wave

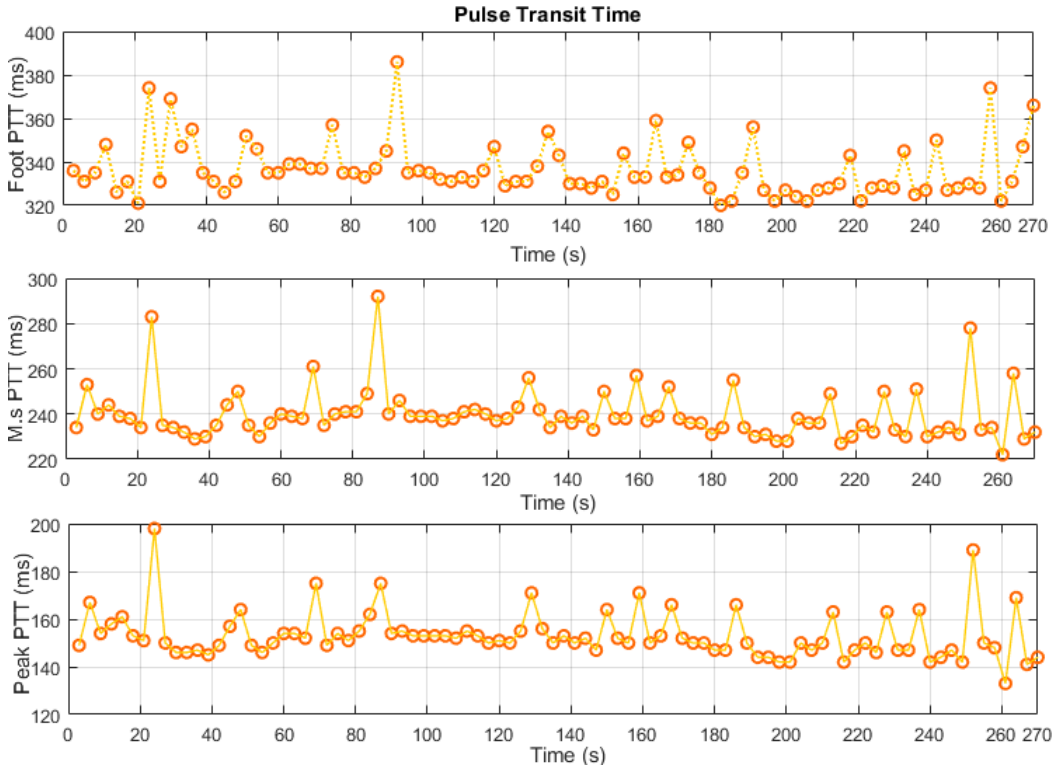

Figure 6.10: Comparison of peak, foot and maximum slope finger PTT

on the finger corresponds one on the wrist, in previous instant. For this reason, a lack of pressure pulse wave in the wrist is related to a limited quality of the signal.

PTT validation consists of two steps:

- validation of the three methods of the PTT computation;
- validation of the BAN-PTT.

Having used three different reference points on the PPG signal, as shown in figure 6.10, in the first step of the validation, the results obtained with both methods are compared. In table 6.3 the mean, standard deviation and range values are shown.

To study the reliability of the results, it was decided to do a statistical analysis. In particular, more attention was focused on the study of the dispersion and variability of the data, assessing its adequacy in comparison with the predicted trend influenced by the physiological cours.

As shown in figure 6.11, the variance of each acquisition is computed, for both of the approches.

The *variance* is a statistical indicator that identifies the dispersion of the X variable

	Foot fPTT (ms)		Middle ffPTT (ms)		Peak fPTT (ms)	
Subj.	Mean ± std	Range	Mean ± std	Range	Mean ± std	Range
1	349 ± 38.3	266 to 507	240 ± 13.2	182 to 262	155 ± 12.7	117 to 208
2	374 ± 46.2	267 to 531	234 ± 13.1	155 to 268	150 ± 10.4	98 to 182
3	520 ± 66.5	193 to 623	224 ± 18.9	73 to 253	139 ± 12.9	44 to 119
4	479 ± 27.4	393 to 550	304 ± 10.8	237 to 321	220 ± 9.4	167 to 238
5	361 ± 24.0	276 to 427	263 ± 16.9	170 to 306	176 ± 13.0	112 to 210
6	391 ± 27.2	321 to 550	280 ± 14.2	212 to 306	162 ± 13.9	126 to 218
7	366 ± 17.7	296 to 401	257 ± 12.9	203 to 271	170 ± 12.6	124 to 183
8	336 ± 12.5	320 to 386	240 ± 11.3	222 to 292	153 ± 9.9	133 to 198

Table 6.3: Mean,standard deviation and range of PTT computed in three different way with ECG and finger PPG signal

values around its mean value. Small values of variance indicate a limited variation of the values in comparison to the average one. It is calculated as follows:

$$V = \frac{1}{N-1} \sum_{i=1}^{N} |X_i - \mu|^2 \tag{6.10}$$

where N is the number of samples in X and $\mu = \frac{1}{N} \sum_{i=1}^{N} X_i$.

Since changes in PTT over time occur slowly, it is expected to have small PTT variations in acquisitions of up to 5 minutes.

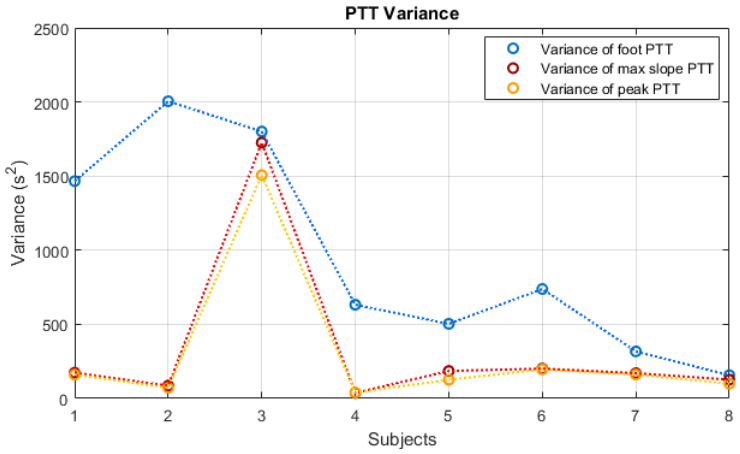

Figure 6.11: Comparison of peak, foot and maximum slope finger PTT variance

As shown in figure 6.11, the PTT values obtained by considering the foot as the reference point in the PPG signal have greater variability. This is influenced by the signal quality. As shown above, detection of the valley in the PPG signal is not always easy to calculate. In some cases, in fact, the algorithm has not detected correctly all the valleys

	Foot wPTT (ms)		Middle wPTT (ms)		Peak wPTT (ms)	
Subj.	Mean ± std	Range	Mean ± std	Range	Mean ± std	Range
1	461 ± 56.0	329 to 634	274 ± 13.0	208 to 321	189 ± 12.3	145 to 242
2	520 ± 66.5	193 to 623	224 ± 18.9	73 to 253	139 ± 12.9	44 to 119
3	520 ± 66.5	193 to 623	223 ± 18.9	73 to 253	139 ± 12.9	44 to 119
4	579 ± 43.8	469 to 734	354 ± 13	269 to 369	265 ± 12.6	193 to 281
5	516 ± 86.9	105 to 712	296 ± 25.5	68 to 328	199 ± 20.2	46 to 228
6	527 ± 62.9	434 to 703	344 ± 17.9	270 to 373	255 ± 18.1	185 to 281
7	571 ± 40.9	478 to 661	321 ± 14.1	284 to 359	217 ± 13.6	164 to 236
8	517 ± 69.5	388 to 674	308 ± 17.7	231 to 375	217 ± 13.7	147 to 242

Table 6.4: Mean and standard deviation of peak, foot and maximum slope PTT obtained with two synchronized devices

and in others they are not detected. The error is generated by the presence of the low frequency components, below 0.5 Hz. In fact, in some cases the bandpass filter was not able to remove them, as shown in figure 6.12.

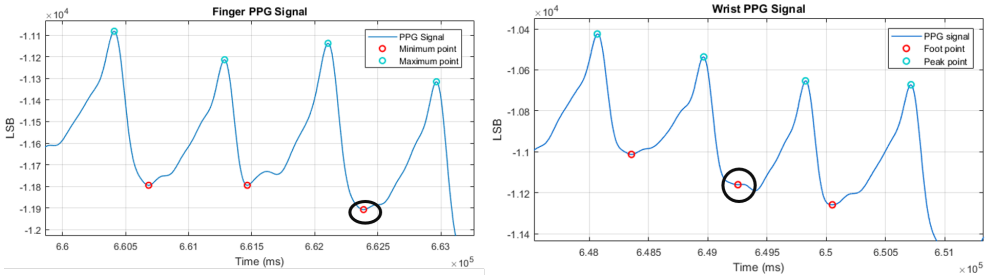

Figure 6.12: Representation of detected uncertain PPG feet

The PTT computed with the other two methods gave better results. In fact, the PPG peaks, as shown with the sensitivity and specificity values, were detected more reliably. Moreover, the amplitude of the low frequency components compared to the PPG peaks is negligible, facilitating the capability detection.

Small variability was obtained with the calculation of the PTT through the maximum slope point of the systolic phase.

These points were detected by differentiating the systolic part of the signal. This differentiation process consists of a high pass filtering effect on the signal, removing the remaining low frequency components. In this way, the steepest points in the rising edge were detected correctly with a higher probability.

As shown in table 6.4 and in figure 6.13, the same variance trend is obtained with the PTT results of the BAN. In figure 6.14 it is also shown the trend of the BAN-PTT.

For this reason, it was decided to proceed with the evaluation of the results using the

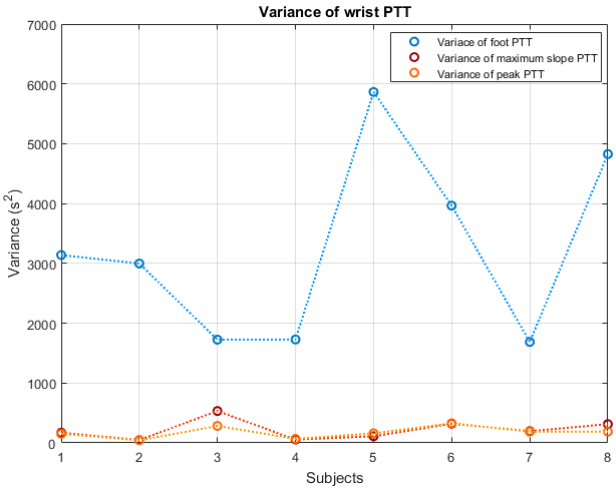

Figure 6.13: Comparison of peak, foot and maximum slope wrist PTT variance

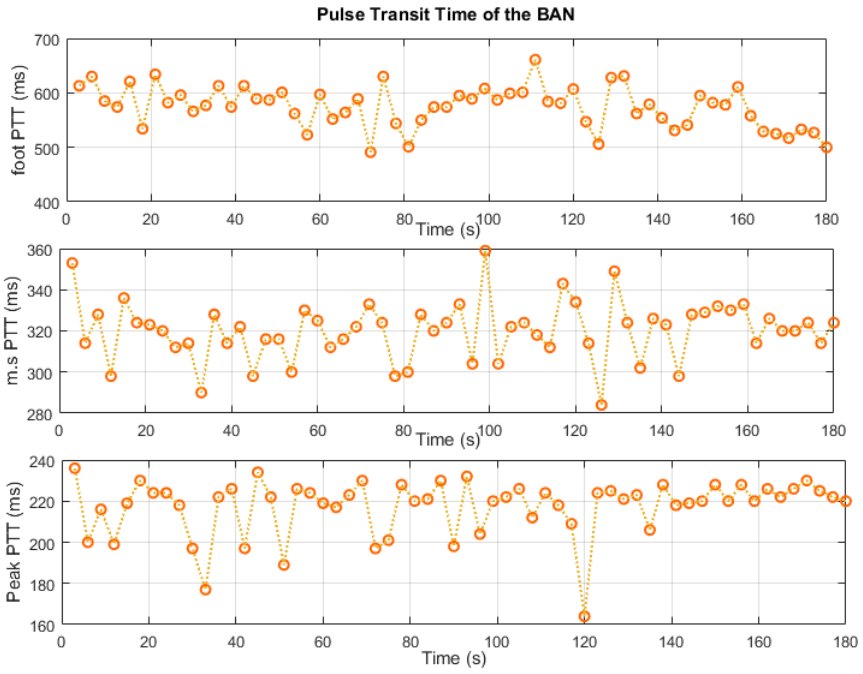

Figure 6.14: Trend of BAN PTT for each type PTT calculated

last two techniques described.

In the second step of the PTT validation, PTT values of the BAN are compared with the ones of reference. The used reference is therefore not accurate on to 100%.

After visually inspection, it was highlighted that the only incorrect PTT values obtained using a single device, are related to the incorrect detection of some R-peaks.

In fact, the majority of the finger PPG peaks were correctly detected. So the incorrect PTT values related to the false R peak generates same errors both on the estimate of the wrist PTT and on the finger one. So in this way, the two measurements are comparable.

Also in this case, it was decided not to calculate the error and accuracy of the algorithm since the values estimates by the BAN and the reference device are not the same. Due to their anatomical arrangement with respect to the heart, the peak of the signal detected on the finger is always delayed compared to the one on the wrist.

For this reason, also in this case, a statistical analysis was made to study the distribution of the data. In fact, it is expected that the two PTTs differ in an amount that is almost constant throughout the acquisition, i.e generated exclusively by the time taken by the blood flow to move from the wrist to the finger.

The covariance and the Pearson correlation coefficient between the reference PTT values and the BAN ones are computed. In figure 6.15 are shown the respective trends calculated for each acquisition.

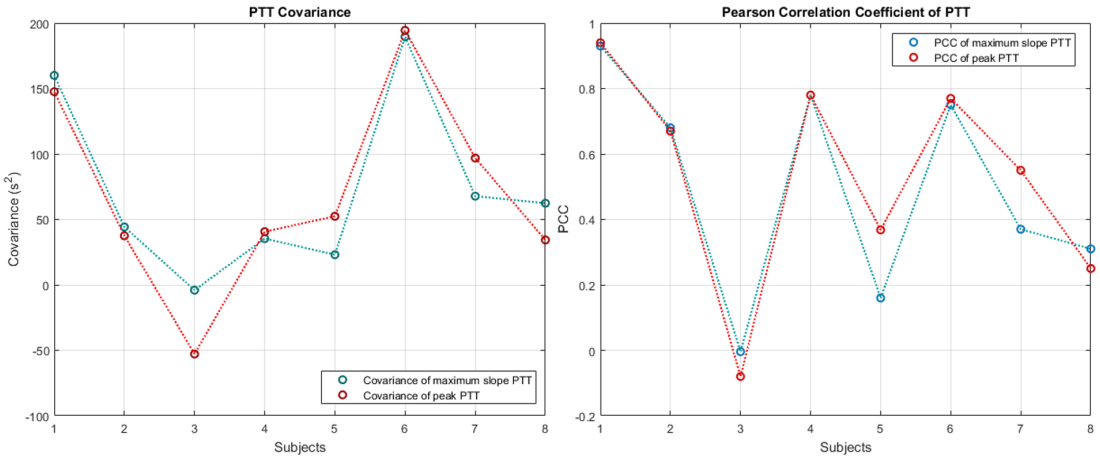

Figure 6.15: Covariance and Pearson Correlation Coefficient trend of the reference and BAN PTT

Positive covariance values are reasonable as two directly proportional values are compared. In particular, it should be noted that only for some acquisitions the correlation assume satisfactory values, close to 1.

For others, on the other hand, the correlation coefficient have decreased, up to become negative for the third acquisition.

Table 6.5 shows the mean, standard deviation and range values of the difference between BAN-PTT and the reference one. Both techniques (peak PTT and maximum slope PTT) give comparable results.

Also in this case, in addition to the correlation test made using the Pearson coefficient, the data were compared with each other through the Bland-Altman plot, in order to visually assess the agreement between the two measurements [100].

In this case, the BA plot disadvantage is the absence of a "Gold Standard" as referance. So the results are compared with imperfect other. Same situations have already been addressed in literature, such as in [101].

Subject	Mean ± std pPTT (ms)	Mean ± std msPTT (ms)
1	35 ± 4.9	34 ± 4.2
2	-10 ± 6.8	14 ± -6.4
3	70 ± 47.6	55 ± 43.5
4	50 ± 4.7	45 ± 5.1
5	33 ± 15.8	24 ± 13.5
6	65 ± 11.9	63 ± 11.6
7	63 ± 15.2	47 ± 12
8	69 ± 17.8	64 ± 14.8

Table 6.5: Mean and standard deviation of the difference between wrist and finger PTT

For this reason, the BA plot was not studied to evaluate the algorithm error, but to verify how the difference between the PTT measurements varies along the acquisition.

The scatter plot was also used in order to detect the linear relationship between the data. So the reference PTT values are shown on the x-axis, instead of those estimated on the y-axis.

The graphs obtained for each acquisition are shown in figures 6.16, 6.17 and 6.18.

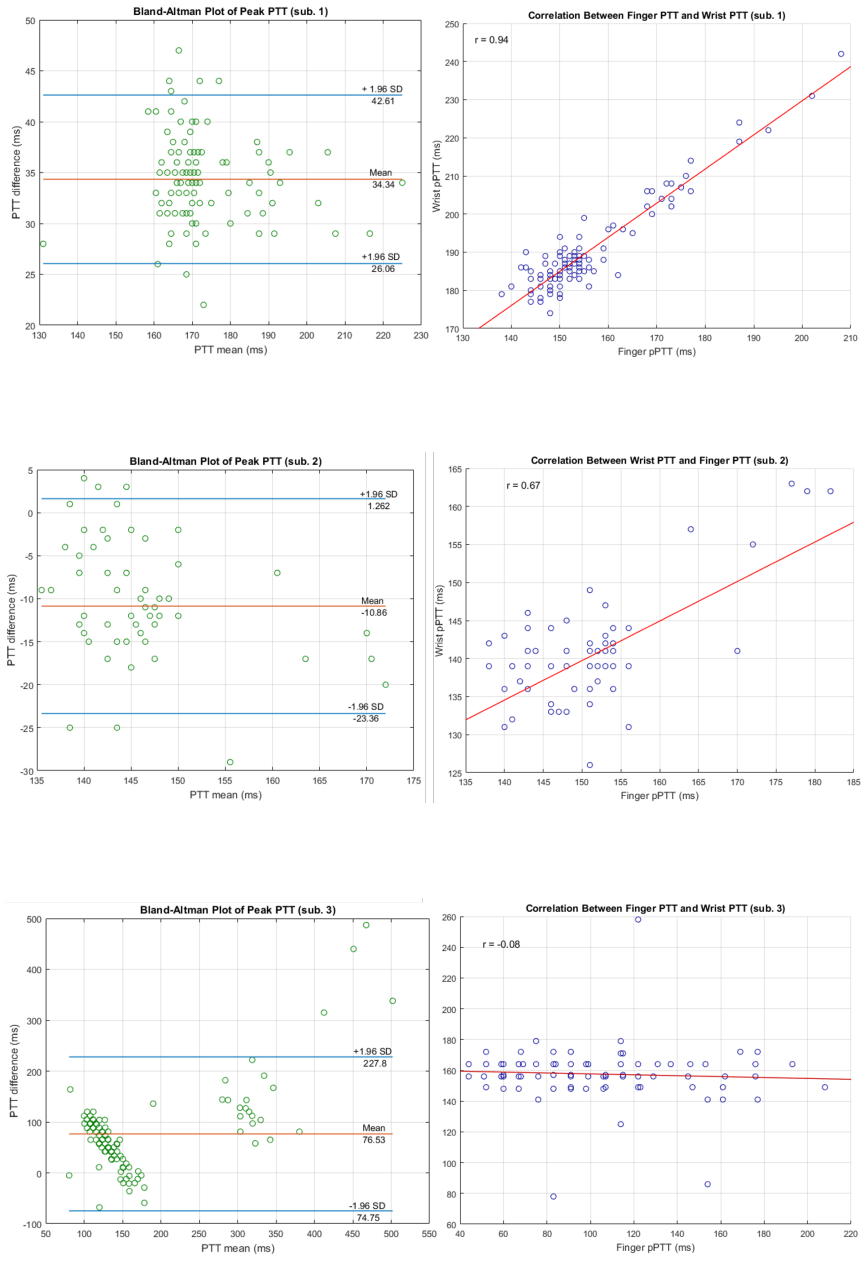

Figure 6.16: Scatter Plot and Bland-Altman Plot of the acquisition n.1-2-3

With the BA and scatter plots can be observed the non-uniformity of the data correlations. Moreover, the Bland-Altman indicator appears more effective because even in cases of good correlation, a distribution of points with non-costant difference is shown.

In particular, for high values of r (>0.9), as in the acquisition 1, a lineary correlation between the data in the scatter plot is evident: the correlation tends to decrease for high values of PTT.

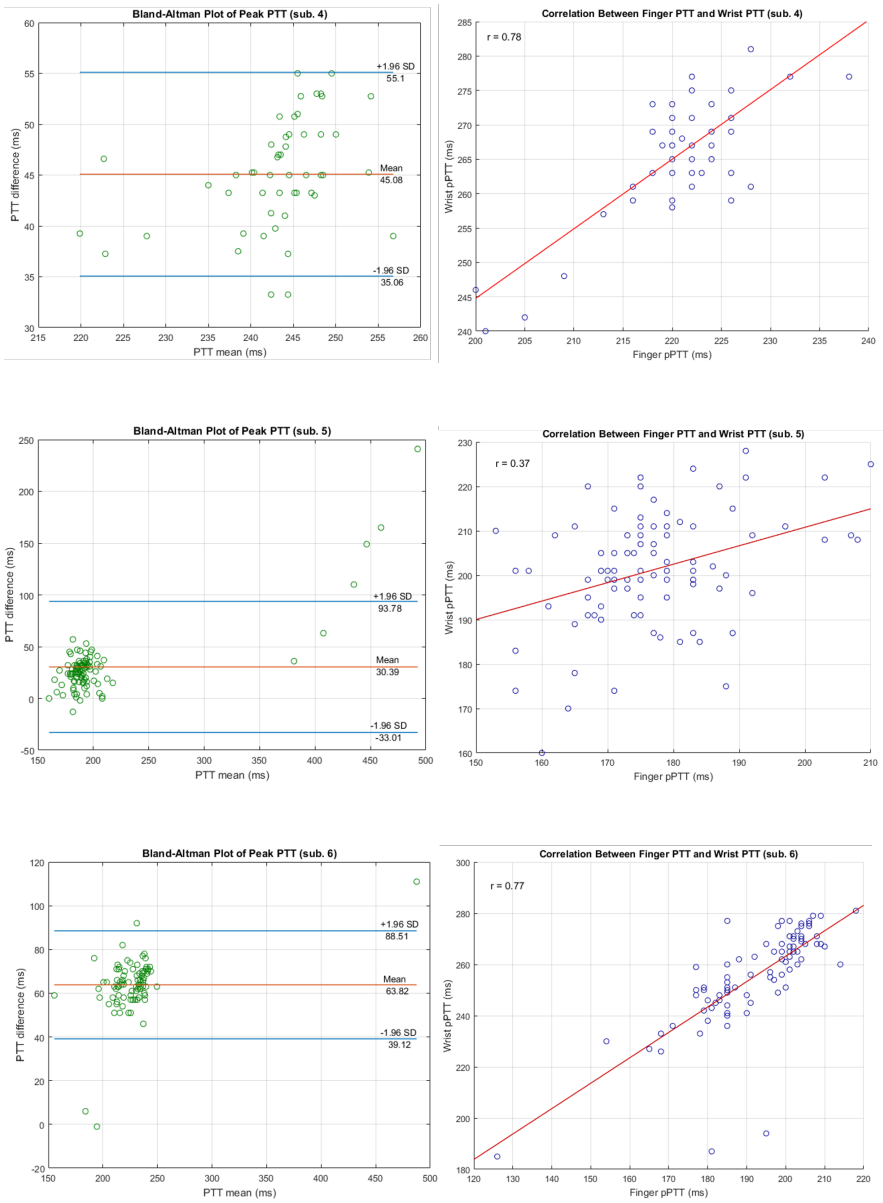

Figure 6.17: Scatter Plot and Bland-Altman Plot of the acquisition n.4-5-6

In this case, by comparing the corresponding Bland-Altman diagram, the points move mainly within the confidence interval. Some outliers exceed the possible range of values. Moreover, the points are distributed symmetrically around the mean: the errors have a distribution that is not random, but systematic in absolute value, so the two methods provide different measurements, as expected, but not randomly variable.

In acquisitions with significant correlation coefficient (0.7-0.9) [102] it is observed a lower reproducibility of the difference, in fact the points move away from the mean value

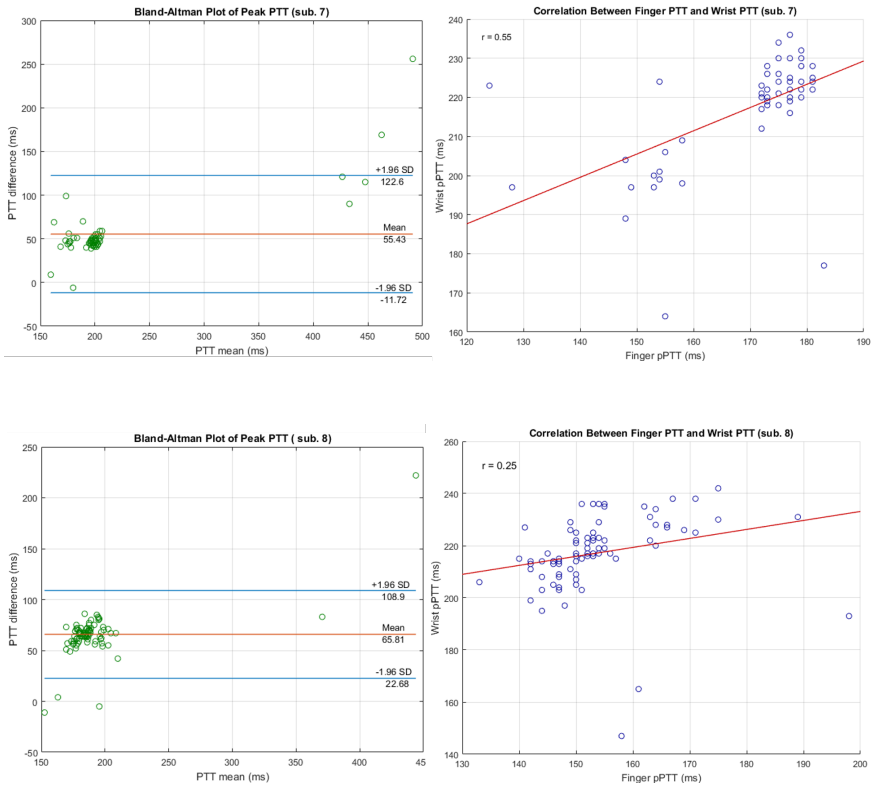

Figure 6.18: Scatter Plot and Bland-Altman Plot of the acquisition n.7-8

in a random way. This implies that the variance of the signal samples does not assume a constant value inside it. In these conditions, on the other hand, in the scatter plot the points are not exactly arranged close to the best-fit line. However, the points still move within the confidence interval.

For correlation values below 0.7, the points of the BA plot are agglomerated in a restricted region but in a completely random way around the best-fits line.

In any case, the range of values of the confidence interval, with or without good correlation, does not comply with the expected results.

Part IV

Conclusions

Chapter 7

Conclusions

In recent years, there has been a rapid increase in the development of intelligent wearable systems, i.e. wearable devices modelled around the human body with the aim of make the technology as usable and less invasive as possible. Integrated with telemedicine systems, these mini-devices allow both continuous monitoring of the patient and also a constant communication with medical staff, useful to keep under control the onset of diseases.

A promising approach is the use of the devices within a Body Area Network, which consists of the use of multiple devices located in strategic parts of the patient's body. Using wireless connections, the devices are able to acquire signals from several parts of the body at the same time and to communicate with each others. Without constraining the patient's life, they provide measurements with the same accuracy of the old cumbersome devices.

The aim of the STMicroelectronics is to test the new device, the Bio2Bit New Move, which can provide feedback on patient health monitoring. Inserted within a BAN, the B2BNM is able to communicate via Bluetooth Low Energy with other devices in real time.

The purpose of this work is to test the reliability of the PTT measured using two B2BNMs within the BAN, comparing the results with the obtained one with a single device.

The algorithm was developed in order to synchronize the BAN devices and to calculate the PTT through the ECG signal and the wrist PPG one. Being a preliminary study, the analysis was made only in steady state conditions.

Among the three implemented PTT techniques, more stable results were obtained by the *maximum slope-PTT* and *peak-PTT*, even if the first gives results comparable to the literary studies one. In fact, the negligible influence of the low-frequency components in these cases promotes high specificity value in the PPG-peaks research.

Instead of the traditional synchronization techniques, it was used an innovative approach based on the temporal comparison of the acceleration components, corresponding to similar actions on different signals.

Evaluating the time delay introduced by the Bluetooth connections, the two signals were synchronized with respect to a common time reference.

The technique used has many advantages. The first one is the possibility to synchronize more devices at the same time reference, without produce any time error for each device, which would generate a not negligible error inside the BAN . It also requires a minimum setup, consisting of two accelerometric signals which feel the same event in the same way. Therefore, any modification to the firmware is necessary. It is also a simple, inexpensive computationally process, so the synchronization can be repeated frequently during analysis, keeping devices accurately synchronized with each other.

The only disadvantage is the high precision required in the signal acquisition. In fact, since the motion frequencies can be detected up to a frequency of 1KHz, it is advisable to use a high sampling frequency, which cannot be used by all devices.

Since a sampling frequency of 128 Hz was used, synchronization errors of up to 15 ms were expected. The error, however, in the pre-processing phase, was considered negligible as it was included in the PTT acceptable error, which is 20 ms at most, as shown in literature study. In addition, if the offset is calculated using a multipoint averaging process, the influence of the error decreases.

The reliability of the results was evaluated by comparing, in both cases, the PTT values with the reference ones, showed in literature studies. The obtained values of finger PTT have an average value of 244 $\pm$14 ms referred to the PPG point of systolic maximum slope, comparables with the ones of Kortekaas study (271 $\pm$ 28) [103].

Therefore, the algorithm of the PTT calculation gave satisfactory results. The same can be observed for the wrist PTT values, which average value is 293 $\pm$ 17 ms compared to some scientific works with an average of 266 ms.

Although the PTT ranges are satisfactory, the difference between finger and wrist PTT is not exactly within the expected values range. Through an in-depth analysis, it was remarked the variation of the sampling frequency signal along the course of the acquisition, caused by the loss of signal packets during the Bluetooth data exchange.

It concerns a frequent error when using wireless connections. Missing the signal coverage, Handoffs are generated, i.e. operations which guarantee the continuity of the connection, finding a new connection in new networks. The passage of the network, even if done in a shortest time possible, causes a loss of signal packets. The variation of the sampling frequency of the received signal, oscillating between 90 and 200 Hz randomly, besides causing the loss of useful signal samples, has not allowed an accurate synchronization between

the BAN devices. The reasons are as follows:

- with lower sampling frequency than expected, as demonstrated above, the error in the PTT estimation goes beyond the permissible range;
- random loss of samples causes oversynchronization between signal parts without delay, if acceleration reference points was identified in parts with a lower sampling rate than expected.

For this reason, even if the difference between the finger and wrist PTT average values oscillates in the range of possible values, which is at most equal to 80 ms according to some literature works, the overcompensation of the offset has caused an excessive temporal translation of the wrist PPG signal compared to the finger one.

Furthermore, only a visual inspection to compare the corresponding parts of the acceleration signals is inaccuracies.

The variable sampling frequency of the signal has considerably decreased the specificity of the algorithm for the detection of the R-peaks. In fact, by implementing the Pan-Tomkins algorithm, thresholds were chosen, based on the width of the QRS complex. The variability of the number of samples between the QRS complex has increased the number of false detected peaks.

The problem consequently influenced the results of the ECG Heart Rate. On the contrary, satisfactory results were obtained by comparing the wrist and finger PPG HR, for which an average error of 3% and an accuracy of 96.5% were obtained.

7.1 Future works

Algorithm improvements can be proposed as future work, such as:

- compensation of the lost signal packets, resampling the intervals with different sampling frequency from the desired one;
- implementation of the adaptive filtering to enable reliable data analysis even during motion phases;
- usage of other signal sensors, such as gyroscope or red LED light to accurately detect noise and motion;
- automates the synchronization algorithm using cross-correlation between the accelerometer signals. Cross-correlation, rather than visual inspection, assess the correlation degree between two time signals series. In this way, it can be study the portions of signals corresponding to the same actions in a more accuratele way. In

fact, since the same action can have different repercussions on the signals, an estimate that takes into account the trend of a large number of samples rather than singular points appears more reliable.

Bibliography

[1] E. Jovanov, A. Milenkovic, C. Otto, and P. C. De Groen, "A wireless body area network of intelligent motion sensors for computer assisted physical rehabilitation," *Journal of NeuroEngineering and rehabilitation*, vol. 2, no. 1, p. 6, 2005.

[2] Mammalian heart and blood vessels. [Online]. Available: https://courses.lumenlearning.com/os-biology/chapter/mammalian-heart-and-blood-vessels/

[3] How does the blood circulatory system work? [Online]. Available: https://www.informedhealth.org/how-does-the-blood-circulatory-system-work.2097.en.html

[4] S. Vandeput, "Heart rate variability: linear and nonlinear analysis with applications in human physiology," 2010.

[5] A. E. Draghici and J. A. Taylor, "The physiological basis and measurement of heart rate variability in humans," *Journal of Physiological Anthropology*, vol. 35, no. 1, p. 22, 2016.

[6] Arterial blood pressure. [Online]. Available: https://www.cvphysiology.com/Blood%20Pressure/BP002

[7] Image: Types of reflection. [Online]. Available: https://www.sciencelearn.org.nz/images/45-types-of-reflection

[8] A. V. Moço, S. Stuijk, and G. de Haan, "New insights into the origin of remote ppg signals in visible light and infrared," *Scientific reports*, vol. 8, no. 1, p. 8501, 2018.

[9] J. Allen, "Photoplethysmography and its application in clinical physiological measurement," *Physiological measurement*, vol. 28, no. 3, p. R1, 2007.

[10] T. Tamura, Y. Maeda, M. Sekine, and M. Yoshida, "Wearable photoplethysmographic sensorsâpast and present," *Electronics*, vol. 3, no. 2, pp. 282–302, 2014.

[11] G. Joseph, A. Joseph, G. Titus, R. M. Thomas, and D. Jose, "Photoplethysmogram (ppg) signal analysis and wavelet de-noising," in *2014 Annual International*

Conference on Emerging Research Areas: Magnetics, Machines and Drives (AICERA/iCMMD). IEEE, 2014, pp. 1–5.

[12] S. Laurent, J. Cockcroft, L. Van Bortel, P. Boutouyrie, C. Giannattasio, D. Hayoz, B. Pannier, C. Vlachopoulos, I. Wilkinson, and H. Struijker-Boudier, "Expert consensus document on arterial stiffness: methodological issues and clinical applications," *European heart journal*, vol. 27, no. 21, pp. 2588–2605, 2006.

[13] G. Martínez, N. Howard, D. Abbott, K. Lim, R. Ward, and M. Elgendi, "Can photoplethysmography replace arterial blood pressure in the assessment of blood pressure?" *Journal of clinical medicine*, vol. 7, no. 10, p. 316, 2018.

[14] M. Gao, N. B. Olivier, and R. Mukkamala, "Comparison of noninvasive pulse transit time estimates as markers of blood pressure using invasive pulse transit time measurements as a reference," *Physiological reports*, vol. 4, no. 10, p. e12768, 2016.

[15] J. L. Moraes, M. X. Rocha, G. G. Vasconcelos, J. E. Vasconcelos Filho, V. H. C. De Albuquerque, and A. R. Alexandria, "Advances in photopletysmography signal analysis for biomedical applications," *Sensors*, vol. 18, no. 6, p. 1894, 2018.

[16] S. i Carós and J. Maria, "Continuous non-invasive blood pressure estimation," Ph.D. dissertation, ETH Zurich, 2011.

[17] Sfigmomanometro: Cos'Ã¨? a cosa serve? tipologie e modo d'uso. [Online]. Available: https://www.my-personaltrainer.it/benessere/sfigmomanometro.html

[18] C. M. Ehrenfeld J., *Noninvasive Arterial Pressure Monitoring*. Springer, 2014.

[19] Healthstats. [Online]. Available: https://www.healthstats.com/abpm

[20] Omron, heartguide. [Online]. Available: https://omronhealthcare.com/products/heartguide-wearable-blood-pressure-monitor-bp8000m/

[21] J. Wåhslén, I. Orhan, and T. Lindh, "Local time synchronization in bluetooth piconets for data fusion using mobile phones," in *2011 International Conference on Body Sensor Networks*. IEEE, 2011, pp. 133–138.

[22] H. H. Al-Ani, "Group delay reduction methods in fir digital filters," Master's thesis, Eastern Mediterranean University (EMU)-Doğu Akdeniz Üniversitesi (DAÜ), 2013.

[23] R. Asmar, "Pression artérielle. régulation et épidémiologie. mesures et valeurs normales," *Néphrologie & thérapeutique*, vol. 3, no. 4, pp. 163–184, 2007.

[24] M. della Salute, "Telemedicina, linee di indirizzo nazionali," 2017.

[25] W. Raghupathi and V. Raghupathi, "An empirical study of chronic diseases in the united states: a visual analytics approach to public health," *International journal of environmental research and public health*, vol. 15, no. 3, p. 431, 2018.

[26] X. Ding, B. P. Yan, Y.-T. Zhang, J. Liu, N. Zhao, and H. K. Tsang, "Pulse transit time based continuous cuffless blood pressure estimation: A new extension and a comprehensive evaluation," *Scientific reports*, vol. 7, no. 1, p. 11554, 2017.

[27] W. H. Organization, I. S. of Hypertension Writing Group *et al.*, "2003 world health organization (who)/international society of hypertension (ish) statement on management of hypertension," *Journal of hypertension*, vol. 21, no. 11, pp. 1983–1992, 2003.

[28] P. Bonato, "Wearable sensors/systems and their impact on biomedical engineering," *IEEE Engineering in Medicine and Biology Magazine*, vol. 22, no. 3, pp. 18–20, 2003.

[29] Pulse transit time (ptt), pulse wave velocity (pwv) and pulse wave amplitude (pwa). [Online]. Available: https://www.biopac.com/application/plethysmography/advanced-feature/pulse-transit-time-ptt-and-relative-bp-measurement/

[30] P. A. Obrist, K. C. Light, J. A. McCubbin, J. S. Hutcheson, and J. L. Hoffer, "Pulse transit time: Relationship to blood pressure," *Behavior Research Methods & Instrumentation*, vol. 10, no. 5, pp. 623–626, 1978.

[31] H. Akhlaghi and H. Asadi, *Essentials of telemedicine and telecare.* Chichester Wiley, 2002.

[32] Y. Zhang, N. Ansari, and H. Tsunoda, "Wireless telemedicine services over integrated ieee 802.11/wlan and ieee 802.16/wimax networks," *IEEE Wireless Communications*, vol. 17, no. 1, pp. 30–36, 2010.

[33] H. Ng, M. Sim, C. M. Tan, and C. Wong, "Wireless technologies for telemedicine," *BT Technology Journal*, vol. 24, no. 2, pp. 130–137, 2006.

[34] D. Girola, *Cardiologia & fitness.* Alea, 1999.

[35] How does the blood circulatory system work? [Online]. Available: https://www.ncbi.nlm.nih.gov/books/NBK279250/?report=classic

[36] N. J. Ashley EA, *Cardiology Explained.* London Remedica, 2004.

[37] L. Biel, O. Pettersson, L. Philipson, and P. Wide, "Ecg analysis: a new approach in human identification," *IEEE Transactions on Instrumentation and Measurement*, vol. 50, no. 3, pp. 808–812, 2001.

[38] M. Y. Rudenko, O. K. Voronova, and V. A. Zernov, "Ecg periodic table: a new ecg classification based on heart cycle phase analysis," *Cardiometry*, no. 2, p. 19, 2013.

[39] What is blood pressure and how is it measured? [Online]. Available: https://www.ncbi.nlm.nih.gov/books/NBK279251/

[40] Physiology, central venous pressure. [Online]. Available: https://www.ncbi.nlm.nih.gov/books/NBK519493/

[41] Zanichelli, *Scienze integrate*. Franco Lucisano Editore, 2010.

[42] P. Salvi, *Onde di polso*. Springer, 2012.

[43] Arterial and aortic pulse pressure. [Online]. Available: https://www.cvphysiology.com/Blood%20Pressure/BP003.htm

[44] G. Fortino and V. Giampà, "Ppg-based methods for non invasive and continuous blood pressure measurement: an overview and development issues in body sensor networks," in *2010 IEEE International Workshop on Medical Measurements and Applications*. IEEE, 2010, pp. 10–13.

[45] Y. Sun and N. Thakor, "Photoplethysmography revisited: from contact to noncontact, from point to imaging," *IEEE Transactions on Biomedical Engineering*, vol. 63, no. 3, pp. 463–477, 2015.

[46] A. Gorczewska, "Influence of sensor design and optical properties of tissue on the photoplethysmographic signal," 2015.

[47] M. J. Hayes, "Artefact reduction in photoplethysmography," 2019.

[48] N. Daimiwal and M. Sundhararajan, "Non invasive measurement and analysis of cardiac output for different age group using ppg sensor," *International Journal of Computer Applications*, vol. 975, p. 8887.

[49] W. Cui, L. E. Ostrander, and B. Y. Lee, "In vivo reflectance of blood and tissue as a function of light wavelength," *IEEE transactions on biomedical engineering*, vol. 37, no. 6, pp. 632–639, 1990.

[50] R. Gonzalez, A. Manzo, J. Delgado, J. Padilla, B. Trénor, and J. Saiz, "A computer based photoplethysmographic vascular analyzer through derivatives," in *2008 Computers in Cardiology*. IEEE, 2008, pp. 177–180.

[51] J. Lee, K. Matsumura, K.-i. Yamakoshi, P. Rolfe, S. Tanaka, and T. Yamakoshi, "Comparison between red, green and blue light reflection photoplethysmography for heart rate monitoring during motion," in *2013 35th annual international conference of the IEEE engineering in medicine and biology society (EMBC)*. IEEE, 2013, pp. 1724–1727.

[52] D. McDuff, S. Gontarek, and R. W. Picard, "Remote detection of photoplethysmographic systolic and diastolic peaks using a digital camera," *IEEE Transactions on Biomedical Engineering*, vol. 61, no. 12, pp. 2948–2954, 2014.

[53] H. Sharma, "Heart rate extraction from ppg signals using variational mode decomposition," *Biocybernetics and Biomedical Engineering*, vol. 39, no. 1, pp. 75–86, 2019.

[54] R. Payne, C. Symeonides, D. Webb, and S. Maxwell, "Pulse transit time measured from the ecg: an unreliable marker of beat-to-beat blood pressure," *Journal of Applied Physiology*, vol. 100, no. 1, pp. 136–141, 2006.

[55] V. Jadav and H. Sitapra, "A novel approach for designing of pulse transit time measurement device for physiological applications," *J. Inf*, vol. 2, pp. 779–782, 2013.

[56] M. Nadin, *Anticipation and medicine*. Springer, 2017.

[57] Q. Zhang, D. Zhou, and X. Zeng, "Highly wearable cuff-less blood pressure and heart rate monitoring with single-arm electrocardiogram and photoplethysmogram signals," p. 23, 2017.

[58] J. M. Huttunen, L. Kärkkäinen, and H. Lindholm, "Pulse transit time estimation of aortic pulse wave velocity and blood pressure using machine learning and simulated training data," *PLoS computational biology*, vol. 15, no. 8, p. e1007259, 2019.

[59] M. Sharma, K. Barbosa, V. Ho, D. Griggs, T. Ghirmai, S. K. Krishnan, T. K. Hsiai, J.-C. Chiao, and H. Cao, "Cuff-less and continuous blood pressure monitoring: a methodological review," *Technologies*, vol. 5, no. 2, p. 21, 2017.

[60] S. Mazaheri and E. Zahedi, "A comparative review of blood pressure measurement methods using pulse wave velocity," in *2014 IEEE International Conference on Smart Instrumentation, Measurement and Applications (ICSIMA)*. IEEE, 2014, pp. 1–5.

[61] A. Z. Sameen, R. Jaafar, E. Zahedi, and G. Being, "A novel waveform mirroring technique for systolic blood pressure estimation from anacrotic photoplethysmogram," *Journal of Engineering Science and Technology*, vol. 13, no. 10, pp. 3252–3262, 2018.

[62] R. Wang, W. Jia, Z.-H. Mao, R. J. Sclabassi, and M. Sun, "Cuff-free blood pressure estimation using pulse transit time and heart rate," in *2014 12th international conference on signal processing (ICSP)*. IEEE, 2014, pp. 115–118.

[63] N. Hollister, "Special edition intensive care medicine."

[64] D. Sahu and M. Bhaskaran, "Palpatory method of measuring diastolic blood pressure," *Journal of anaesthesiology, clinical pharmacology*, vol. 26, no. 4, p. 528, 2010.

[65] S. Cagliano, U. P. Soccorso, O. S. Paolo, P. Russo, E. Sgamma, and P. A. R. Civitavecchia, "Il punto su."

[66] L. Pilotto, "Percorso diagnostico dei pazienti ipertesi. misurazione della pressione arteriosa: metodi e strumenti," *Ital Heart J*, vol. 1, no. 5, pp. 32–35, 2000.

[67] M. Forouzanfar, H. R. Dajani, V. Z. Groza, M. Bolic, S. Rajan, and I. Batkin, "Oscillometric blood pressure estimation: past, present, and future," *IEEE reviews in biomedical engineering*, vol. 8, pp. 44–63, 2015.

[68] C. F. Babbs, "Oscillometric measurement of systolic and diastolic blood pressures validated in a physiologic mathematical model," *Biomedical engineering online*, vol. 11, no. 1, p. 56, 2012.

[69] T. Sato, M. Nishinaga, A. Kawamoto, T. Ozawa, and H. Takatsuji, "Accuracy of a continuous blood pressure monitor based on arterial tonometry." *Hypertension*, vol. 21, no. 6_pt_1, pp. 866–874, 1993.

[70] T. W. Kurtz, K. A. Griffin, A. K. Bidani, R. L. Davisson, and J. E. Hall, "Recommendations for blood pressure measurement in humans and experimental animals: part 2: blood pressure measurement in experimental animals: a statement for professionals from the subcommittee of professional and public education of the american heart association council on high blood pressure research," *Hypertension*, vol. 45, no. 2, pp. 299–310, 2005.

[71] D. Chemla and B. Lamia, "Monitorage hémodynamique non-invasif en réanimation: intérêt potentiel de la tonométrie artérielle," *Réanimation*, vol. 18, no. 3, pp. 197–200, 2009.

[72] J. Truijen, J. J. van Lieshout, W. A. Wesselink, and B. E. Westerhof, "Noninvasive continuous hemodynamic monitoring," *Journal of clinical monitoring and computing*, vol. 26, no. 4, pp. 267–278, 2012.

[73] D. M. Bard, J. I. Joseph, and N. van Helmond, "Cuff-less methods for blood pressure telemonitoring," *Frontiers in cardiovascular medicine*, vol. 6, 2019.

[74] D. Nair, S. Tan, H. Gan, S. Lim, J. Tan, M. Zhu, H. Gao, N. Chua, W. Peh, and K. Mak, "The use of ambulatory tonometric radial arterial wave capture to measure ambulatory blood pressure: the validation of a novel wrist-bound device in adults," *Journal of human hypertension*, vol. 22, no. 3, p. 220, 2008.

[75] J. Cho, "Current status and prospects of health-related sensing technology in wearable devices," *Journal of Healthcare Engineering*, vol. 2019, 2019.

[76] Farasha care. [Online]. Available: https://ico.farasha.care

[77] R. Lazazzera, Y. Belhaj, and G. Carrault, "A new wearable device for blood pressure estimation using photoplethysmogram," *Sensors*, vol. 19, no. 11, p. 2557, 2019.

[78] M.-C. Cho, "Clinical significance and therapeutic implication of nocturnal hypertension: Relationship between nighttime blood pressure and quality of sleep," *Korean circulation journal*, vol. 49, no. 9, pp. 818–828, 2019.

[79] Samsung watch active. [Online]. Available: https://www.samsung.com/it/wearables/galaxy-watch-active-r500/SM-R500NZSAITV/

[80] J. Wåhslén, I. Orhan, T. Lindh, and M. Eriksson, "A novel approach to multi-sensor data synchronisation using mobile phones," *International Journal of Autonomous and Adaptive Communications Systems*, vol. 6, no. 3, pp. 289–303, 2013.

[81] L. Fridman, D. E. Brown, W. Angell, I. Abdić, B. Reimer, and H. Y. Noh, "Automated synchronization of driving data using vibration and steering events," *Pattern Recognition Letters*, vol. 75, pp. 9–15, 2016.

[82] J.-W. Lee and J.-H. Nam, "Design of filter to reject motion artifacts of ppg signal by using two photosensors," *Journal of information and communication convergence engineering*, vol. 10, no. 1, pp. 91–95, 2012.

[83] M. Elgendi, "On the analysis of fingertip photoplethysmogram signals," *Current cardiology reviews*, vol. 8, no. 1, pp. 14–25, 2012.

[84] A. K. Bhoi, S. Sarkar, P. Mishra, and G. Savita, "Pre-processing of ppg signal with performance based methods," *International Journal of Computer Application*, vol. 4, no. 2, pp. 251–256, 2012.

[85] T. Nguyen, X. Qin, A. Dinh, and F. Bui, "Low resource complexity r-peak detection based on triangle template matching and moving average filter," *Sensors*, vol. 19, no. 18, p. 3997, 2019.

[86] V. Singh, S. Kaur, and A. Gupta, "Comparative study of ecg signal denoising and r-peak registration methods," 2014.

[87] J. Kameenoff, "Signal processing techniques for removing noise from ecg signals," *Biomedical Engineering and Research*, vol. 1, no. 1, p. 1, 2017.

[88] S. A. Santos, B. Venema, and S. Leonhardt, "Accelerometer-assisted ppg measurement during physical exercise using the lavimo sensor system," *Acta Polytechnica*, vol. 52, no. 5, 2012.

[89] Y. Zhang, S. Song, R. Vullings, D. Biswas, N. Simões-Capela, N. Van Helleputte, C. Van Hoof, and W. Groenendaal, "Motion artifact reduction for wrist-worn photoplethysmograph sensors based on different wavelengths," *Sensors*, vol. 19, no. 3, p. 673, 2019.

[90] N. Selvaraj, Y. Mendelson, K. H. Shelley, D. G. Silverman, and K. H. Chon, "Statistical approach for the detection of motion/noise artifacts in photoplethysmogram," in *2011 Annual International Conference of the IEEE Engineering in Medicine and Biology Society*. IEEE, 2011, pp. 4972–4975.

[91] Q. Qin, J. Li, Y. Yue, and C. Liu, "An adaptive and time-efficient ecg r-peak detection algorithm," *Journal of healthcare engineering*, vol. 2017, 2017.

[92] K. Bawa and P. Sabherwal, "R-peak detection by modified pan-tompkins algorithm," *International Journal of Advancements in Research & Technology*, vol. 3, no. 5, pp. 30–33, 2014.

[93] J. Pan and W. J. Tompkins, "A real-time qrs detection algorithm," *IEEE Trans. Biomed. Eng*, vol. 32, no. 3, pp. 230–236, 1985.

[94] J. D. Harry and R. Freeman, "Determining heart-rate variability: Comparing methodologies using computer simulations," *Muscle & Nerve: Official Journal of the American Association of Electrodiagnostic Medicine*, vol. 16, no. 3, pp. 267–277, 1993.

[95] S. Kuntamalla and L. R. G. Reddy, "An efficient and automatic systolic peak detection algorithm for photoplethysmographic signals," *International Journal of Computer Applications*, vol. 97, no. 19, 2014.

[96] M. T. I. Papon, I. Ahmad, N. Saquib, and A. Rahman, "Non-invasive heart rate measuring smartphone applications using on-board cameras: A short survey," in *2015 International Conference on Networking Systems and Security (NSysS)*. IEEE, 2015, pp. 1–6.

[97] B. Askarian, K. Jung, and J. W. Chong, "Monitoring of heart rate from photoplethysmographic signals using a samsung galaxy note8 in underwater environments," *Sensors*, vol. 19, no. 13, p. 2846, 2019.

[98] A. Bánhalmi, J. Borbás, M. Fidrich, V. Bilicki, Z. Gingl, and L. Rudas, "Analysis of a pulse rate variability measurement using a smartphone camera," *Journal of healthcare engineering*, vol. 2018, 2018.

[99] W.-H. Lin, D. Wu, C. Li, H. Zhang, and Y.-T. Zhang, "Comparison of heart rate variability from ppg with that from ecg," in *The International Conference on Health Informatics*. Springer, 2014, pp. 213–215.

[100] M. H. van Velzen, R. J. Stolker, A. J. Loeve, S. P. Niehof, and E. G. Mik, "Comparison between pulse wave velocities measured using complior and measured using biopac," *Journal of clinical monitoring and computing*, vol. 33, no. 2, pp. 241–247, 2019.

[101] H. Gesche, D. Grosskurth, G. Küchler, and A. Patzak, "Continuous blood pressure measurement by using the pulse transit time: comparison to a cuff-based method," *European journal of applied physiology*, vol. 112, no. 1, pp. 309–315, 2012.

[102] M. U. R. Naidu, B. M. Reddy, S. Yashmaina, A. N. Patnaik, and P. U. Rani, "Validity and reproducibility of arterial pulse wave velocity measurement using new device with oscillometric technique: a pilot study," *Biomedical engineering online*, vol. 4, no. 1, p. 49, 2005.

[103] M. C. Kortekaas, M. H. van Velzen, F. Grüne, S. P. Niehof, R. J. Stolker, and F. J. Huygen, "Small intra-individual variability of the pre-ejection period justifies the use of pulse transit time as approximation of the vascular transit," *PloS one*, vol. 13, no. 10, p. e0204105, 2018.